

26785

National Library  
of CanadaBibliothèque nationale  
du CanadaCANADIAN THESES  
ON MICROFICHETHÈSES CANADIENNES  
SUR MICROFICHE

NAME OF AUTHOR/NOM DE L'AUTEUR WILLIAM DAVID HUME

TITLE OF THESIS/TITRE DE LA THÈSE DEVELOPMENT OF A QUASI-GEOSTROPHIC  
PREDICTION MODEL FOR WEATHER SYSTEMS  
OVER WESTERN CANADA

UNIVERSITY/UNIVERSITÉ ALBERTA

DEGREE FOR WHICH THESIS WAS PRESENTED/  
GRADE POUR LEQUEL CETTE THÈSE FUT PRÉSENTÉE M. Sc.

YEAR THIS DEGREE CONFERRED/ANNÉE D'OBTENTION DE CE GRADE 1975

NAME OF SUPERVISOR/NOM DU DIRECTEUR DE THÈSE EDWARD P. LOZOWSKI (P.H.D.)

Permission is hereby granted to the NATIONAL LIBRARY OF  
CANADA to microfilm this thesis and to lend or sell copies  
of the film.

L'autorisation est, par la présente, accordée à la BIBLIOTHÈ-  
QUE NATIONALE DU CANADA de microfilmer cette thèse et  
de prêter ou de vendre des exemplaires du film.

The author reserves other publication rights, and neither the  
thesis nor extensive extracts from it may be printed or other-  
wise reproduced without the author's written permission.

L'auteur se réserve les autres droits de publication; ni la  
thèse ni de longs extraits de celle-ci ne doivent être imprimés  
ou autrement reproduits sans l'autorisation écrite de l'auteur.

DATED/DATE July 16/1975 SIGNED/SIGNÉ Bill Hume

PERMANENT ADDRESS/RÉSIDENCE FIXE 11633-125 St  
EDMONTON ALBERTA  
T5M0N5

THE UNIVERSITY OF ALBERTA

DEVELOPMENT OF A QUASI-GEOSTROPHIC PREDICTION MODEL  
FOR WEATHER SYSTEMS OVER WESTERN CANADA

by



WILLIAM DAVID HUME

A THESIS

SUBMITTED TO THE FACULTY OF GRADUATE STUDIES AND RESEARCH  
IN PARTIAL PULFILMENT OF THE REQUIREMENTS FOR THE DEGREE OF  
MASTER OF SCIENCE  
IN  
METEOROLOGY

DEPARTMENT OF GEOGRAPHY

EDMONTON, ALBERTA

FALL, 1975

THE UNIVERSITY OF ALBERTA  
FACULTY OF GRADUATE STUDIES AND RESEARCH

The undersigned certify that they have read, and recommend to the Faculty of Graduate Studies and Research, for acceptance, a thesis entitled "Development of a Quasi-Geostrophic Prediction Model for Weather Systems Over Western Canada," submitted by William David Hume in partial fulfilment of the requirements for the degree of Master of Science in Meteorology.

*Edward R. Ross*  
.....  
Supervisor

*— 1 —*  
.....

*Kurt R. Hay*  
.....

Date *July 3 1975*  
.....

DEDICATION

For Judith



## ABSTRACT

In this study, a numerical weather prediction model is developed and tested on some selected synoptic situations over Western Canada. A four-level model of the atmosphere is formulated in which a prediction is obtained by numerical solution of the quasi-geostrophic omega and vorticity equations. The horizontal grid (with a grid point spacing of 200 km) encompasses Western Canada and parts of the Northwest Territories, the Yukon, Alaska, the Eastern Pacific Ocean and the northwestern United States. The Adams-Bashforth time stepping scheme with a time increment of  $1\frac{1}{2}$  hour is employed to achieve the forecast. Three synoptic situations were chosen in which the western Cordillera of North America appeared to have some influence on the development and movement of cyclones in Western Canada. In data sparse areas of the grid, bogus data are generated in an attempt to provide an accurate analysis for initialization of the forecasts.

The study focuses on the importance of different formulations of the lower boundary condition in the numerical model. Terrain elevations at each grid point are obtained from topographic charts, while frictional drag coefficients are interpolated to the grid from Cressman's

(1960) data. Several lower boundary conditions which have been employed in other numerical models are compared with each other. The relative accuracies of the 12 hour forecasts are obtained through the calculation of root-mean-square errors between the forecast and the observed geopotential height fields.

The testing shows that frictionally-induced vertical motion at the lower boundary is as important as orographic lift and subsidence in accurate prediction of lee cyclogenesis. The best forecasts were achieved if a slightly smoothed terrain was employed and the vertical velocity at the lower boundary was assumed to originate at the terrain surface rather than at the 1000 mb surface. If the 850 mb geostrophic wind rather than a geostrophic wind at terrain height was employed in calculations of frictional and orographic components of the vertical velocity in the planetary boundary layer, a more accurate forecast was achieved.

In conclusion, the four-level quasi-geostrophic model with a suitable lower boundary condition shows skill in short term weather prediction over Western Canada.

## ACKNOWLEDGEMENTS

I wish to express my thanks to the many people and organizations who made completion of this study possible.

For his helpful guidance in the latter term of this study, I wish to thank Dr. Edward P. Lozowski. A special note of thanks is also due Dr. Madhav L. Khandekar who provided the initial impetus in the formulation of the problem. I also thank Dr. Keith D. Hage and Dr. Stan Cabay who served on my examining committee in addition to Dr. Lozowski who acted as chairman.

I gratefully acknowledge the Division of Meteorology, for providing the funding for the extensive computing which this study entailed. The helpful advice offered by the staff and many of my fellow students in the Division of Meteorology is also sincerely appreciated. The excellent photo-reduction of the many diagrams was the responsibility of Mr. J. Chesterman.

This study was conducted while I was on Educational Leave from the Atmospheric Environment Service, Environment Canada.

# TABLE OF CONTENTS

	Page
DEDICATION	iv
ABSTRACT	v
ACKNOWLEDGMENT	vii-
TABLE OF CONTENTS	viii
LIST OF TABLES	xi
LIST OF FIGURES	xii
CHAPTER	
I INTRODUCTION	1
1.1 Preliminary Comments	1
1.2 Studies of Lee Cyclogenesis and Numerical Modeling	2
1.3 Outline of This Study	5
II THE MODEL	6
2.1 The Prediction Equation	6
2.2 The Diagnostic Omega Equation	8
2.3 The Horizontal Grid	9
2.4 The Vertical Representation	11
2.5 The Lower Boundary Condition	13
III DATA ACQUISITION AND ANALYSIS	20
3.1 Upper Air Data	20
3.2 Surface Data	22

	Page
3.3 The Objective Analysis	26
3.4 The Static Stability Parameter	28
IV NUMERICAL PROCEDURES	31
4.1 Horizontal Finite-Difference Operators	31
4.2 The Vertical Derivatives	36
4.3 The Time Step	38
4.4 Solution of the Differential Equations	43
4.5 The Forecast	50
V RESULTS AND DISCUSSION	52
5.1 Preliminary Comments	52
5.2 Testing of Numerical Procedures	53
5.3 Case 1: January 5, 1972	56
5.4 Comparison of Several Forecast Runs: Case 1	63
5.4.1 Smoothing of Topography: Runs 1A, 1B, 1C	63
5.4.2 Friction and Topography: Runs 2A, 2B, 2C	73
5.4.3 Small Frictional Vertical Velocity: Run 3	84
5.4.4 The 850 mb Wind in PBL Computations: Run 4	87
5.5 Case 2: March 5, 1972	90
5.6 Case 3: April 27, 1972	97
5.7 Systematic Errors in the Model	104

VI	SUMMARY AND CONCLUSIONS	109
	BIBLIOGRAPHY	113
APPENDIX A	The Aitken Polynomial	117
APPENDIX B	Spatial Smoothing	121

# LIST OF TABLES

Table		Page
1	Surface regimes and drag coefficients	25
2	The static stability parameter	30
3	Statistics of Case 1, Run 1	67
4	Statistics of Case 1, Run 2	74
5	Statistics of Case 1, Run 3	86
6	Statistics of Case 1, Run 4	89
7	Statistics of Case 2	96
8	Statistics of Case 3	102

# LIST OF FIGURES

Figure		Page
1	The horizontal grid area	10
2	The vertical structure of the model atmosphere	12
3	Relationship between the geostrophic wind and the wind in the PBL	17
4	Pressure at terrain height	23
5	Cressman drag coefficients	24
6	Horizontal grid point structure	32
7	Comparison of centered-difference and Adams-Bashforth time step procedures	44
8	Initial analysis at 850, and 500 mb for Case 1	57
9	Initial surface analysis for Case 1	58
10	Verification analysis at 850 and 500 mb for Case 1	60
11	Verification surface analysis for Case 1	62
12	Smoothed pressure at terrain height	65
13	12 hour forecast at 850 mb for Runs 1A and 1B	66
14	Same as Figure 13 but at 500 mb	68
15	Same as Figure 13 but at the surface	70
16	12 hour forecast at 850 mb and surface for Run 1C	72
17	Same as Figure 16 but for Run 2A	75



Figure		Page
18	Initial vertical velocity fields at the surface and at 600 mb for Run 2B	77
19	12 hour forecast at 850 mb and the surface for Run 2B	78
20	Same as Figure 18 but for Run 2C	80
21	Same as Figure 19 but for Run 2C	82
22	12 hour forecast at 850 mb and at the surface for Run 3	85
23	Same as Figure 22 but for Run 4	88
24	Initial analysis at 850 and 500 mb for Case 2	91
25	Verification analysis at 850 and 500 mb for Case 2	93
26	850 mb forecasts for Case 2	94
27	500 mb forecast for Case 2, Run 1	96
28	Initial analysis at 850 and 500 mb for Case 3	98
29	Verification analysis at 850 and 500 mb for Case 3	99
30	850 mb forecasts for Case 3	101
31	500 mb forecast for Case 3, Run 1	102

## CHAPTER I

### INTRODUCTION

#### 1.1 Preliminary Comments

Numerical prediction of meteorological systems on the synoptic scale has achieved a high degree of sophistication over the past two decades, and many of the physical processes which govern atmospheric motions have been included in the numerical models. Only limited success has been achieved in the simulation of the cyclogenesis observed in the lee of major mountain ranges, although most models are able at least to predict the gross characteristics of this phenomenon. Since advances in computer technology have allowed the direct solution of the primitive equations of motion, most attention has recently focused on primitive equation models. However such models, while logically quite straight-forward, tend to be difficult to implement because of their sensitivity to the initialization of the data. As

well they require a large amount of computing to achieve a forecast.

A numerical model based on the system of filtered geostrophic equations is somewhat less stringent in its requirements because gravity oscillations present in the primitive equations models have no solution in the geostrophic formulation. Although the geostrophic assumption is a powerful constraint between the horizontal wind and the pressure gradient, especially near the surface of the earth, successful duplication of synoptic scale motion using the geostrophically filtered system of equations has been achieved for many years. In this study, a geostrophic model with four levels in the vertical is developed and tested on an area encompassing Western Canada, including parts of the Northwest Territories, the Yukon, Alaska, the Eastern Pacific Ocean as well as the northwestern United States. The purpose of this study is to assess the influence of the lower boundary condition of the numerical model in the prediction of weather systems in Western Canada, especially in relation to the simulation of the lee cyclogenesis process.

## 1.2 Studies of Lee Cyclogenesis and Numerical Modeling

Since it is through the vertical velocity that atmospheric potential energy is converted into kinetic energy (Lorenz, 1955), many diagnostic studies have examined

the vertical velocity or omega fields ( $\omega = \frac{dp}{dt}$ ) at the surface of the earth as well as at levels well above orographic features. In an early study, Newton (1956) calculated vertical velocities using the adiabatic assumption. He indicated that the horizontal variation of frictional drag at the surface may be of primary importance in the initial low-level lee cyclogenesis.

Diagnostic studies using the quasi-geostrophic omega equation have been employed to study the role of the vertical velocity field in the mechanism of circulation change in the lower to middle troposphere. Haltiner, Clarke and Lawniczak (1963) and Stuart (1964) utilized omega equations to evaluate the  $\omega$  fields, and to estimate the relative magnitudes of terms in the vorticity equation responsible for the development of baroclinic waves. In a later study, Schram (1974) showed that with certain lower boundary conditions, areas of vorticity production were well correlated with favored areas of lee cyclogenesis in Western Canada.

Actual numerical prediction using the quasi-geostrophic filtered equations has been extensively developed, but few studies have focused on the lower boundary condition and especially on the lee cyclogenesis problem. Many models formulated for prediction on limited area grids have included crude parameterizations of the processes within the atmospheric boundary layer at the surface of the earth. The

early two-level model of Thompson and Gates (1956) included only the large scale ascent of air over orographic features. The incorporation of a representative lower boundary condition in numerical models was discussed by Sawyer (1959). His derivation of frictional effects was based on the theory of the flow in the planetary boundary layer as well as on synoptic experience. The two-level model of Greystone (1962) was tested on fifty different synoptic cases over the north Atlantic and Europe. Only a small change in forecast error was noted when forecasts employing a sophisticated lower boundary were compared with those employing no orographic or frictional influence.

Most filtered equation models have made use of the drag coefficients tabulated by Cressman (1960) for the entire northern hemisphere. As well, the highly smoothed orography of the northern hemisphere provided by Berkofsky and Bertoni (1955) is generally employed in prediction models such as those of Cressman (1963) and Danard (1966). More recent work with the primitive equations has allowed the incorporation of more sophisticated boundary layer models into the large scale predictions. The primitive equation model employed by Egger (1972, 1974) was used to simulate the flow in the vicinity of the high mountains of Europe and North America, while Danard (1971) studied the formulation of frictional effects in the boundary layer of his primitive equation model.

### 1.3 Outline of This Study

In this study, a four-level model is developed employing the quasi-geostrophic system of equations to obtain short range (12 hour) prediction of weather systems over Western Canada. Testing of the model was conducted on three cases in which some degree of lee cyclogenesis was observed to occur within the short prediction period.

The emphasis in the study is on the formulation of a lower boundary condition for the numerical model which permits the most accurate prediction of the motion and development of weather systems in the vicinity of the Canadian Rocky Mountains. Six different parameterizations of the lower boundary condition are tested. Quantitative comparisons of the forecasts are obtained through calculation of the root-mean-square errors between forecast and observed (or verification) geopotential fields.

In Chapter II the quasi-geostrophic system of prediction equations and the details of the model atmosphere are briefly described. Chapter III describes the data extraction and analysis procedure, while the numerical techniques employed in the model are presented in Chapter IV. The results of the testing of the three cases are detailed in Chapter V, and in Chapter VI a brief summary and the conclusions of the study are presented.

## CHAPTER II

### THE MODEL

#### 2.1 The Prediction Equation

The prediction equation used in this study is an approximation to the complete vorticity equation which, when written in a coordinate system with pressure  $p$  along the vertical axis  $\hat{k}$ , is:

$$\frac{\partial \zeta}{\partial t} + \bar{\nabla} \cdot \nabla(\zeta + f) - (\zeta + f) \frac{\partial \omega}{\partial p} + \omega \frac{\partial \zeta}{\partial p} + \hat{k} \cdot \nabla \omega \times \frac{\partial \bar{\nabla}}{\partial p} = 0 \quad (2.1)$$

In this equation,  $\zeta$  is the vertical component of the relative vorticity,  $f$  the Coriolis parameter,  $\bar{\nabla}$  the horizontal wind,  $\omega = \frac{dp}{dt}$  the vertical velocity in pressure coordinates, and  $\nabla$  the horizontal gradient operator.

While studies by Stuart (1964) and Schram (1974) have shown that the last term on the left-hand-side of equation (2.1) may on occasion be of some importance, it is generally

7

ignored in numerical prediction models. The analysis of Wiin-Nielsen (1959) has shown that if this twisting term is ignored, the vertical advection term,  $\omega \frac{\partial \zeta}{\partial p}$ , should also be ignored since the two tend to compensate each other. As well, he indicates that if the divergence term  $(\zeta+f) \frac{\partial \omega}{\partial p}$ , is retained, the absolute vorticity,  $\zeta + f$ , should be replaced by a constant in this term only. All of these modifications are necessary because the integral of the complete vorticity equation over a closed surface is zero. Hence any simplification to the vorticity equation should attempt to retain this property.

With these simplifications, the resulting quasi-geostrophic vorticity equation is:

$$\frac{\partial \zeta_g}{\partial t} = -\vec{\nabla}_g \cdot \nabla(\zeta_g + f) + \bar{f} \frac{\partial \omega}{\partial p} \quad (2.2)$$

where  $\bar{f}$  is the average value of the Coriolis parameter over the region of interest. The horizontal wind has been replaced by the non-divergent geostrophic wind:

$$\vec{\nabla}_g = g/\bar{f} \hat{k} \times \nabla Z \quad (2.3)$$

and the relative vorticity by its geostrophic counterpart:

$$\zeta_g = g/\bar{f} \nabla^2 Z \quad (2.4)$$

In these equations,  $Z$  is the height of an isobaric surface



in geopotential meters ( gpm ) and  $g$  is the gravitational acceleration (assumed constant) . Using the standard definitions of the Laplacian and Jacobian operators, the quasi-geostrophic vorticity equation may now be written:

$$\frac{\partial}{\partial t} (\nabla^2 Z) = \nabla^2 \left( \frac{\partial Z}{\partial t} \right) = -J(Z, \zeta_g + f) + \bar{f}^2 \frac{\partial \omega}{\partial p} \quad (2.5)$$

## 2.2 The Diagnostic Omega Equation

In order to derive a diagnostic equation for omega, use is made of the quasi-geostrophic thermodynamic equation in the pressure coordinate system:

$$g \frac{\partial}{\partial t} \left( \frac{\partial Z}{\partial p} \right) + g \frac{\partial^2}{\partial f} J(Z, \frac{\partial Z}{\partial p}) + \sigma \omega = 0 \quad (2.6)$$

In this equation,  $\sigma = -\frac{\alpha}{\Theta} \frac{\partial \Theta}{\partial p}$  is a static stability parameter where  $\alpha$  is the specific volume of the air and  $\Theta$  the potential temperature. The static stability is permitted to be a function of pressure only in this version of the thermodynamic equation, for if  $\sigma$  were spatially variable, it may be shown (Haltiner 1971, pp 73-74) that global integral constraints on the thermodynamic equation would be violated. With the generally stable atmospheric stratifications of winter months in high latitudes,  $\sigma$  is a positive number, and is evaluated as indicated in Chapter IV.

The time-derivatives in equations (2.5) and (2.6) may be eliminated by operating on the former with  $\frac{\partial}{\partial p}$  and on the latter with  $\nabla^2$  and subtracting, yielding the quasi-geostrophic omega equation:

$$\sigma \nabla^2 \omega + \bar{f}^2 \frac{\partial^2 \omega}{\partial p^2} = g \frac{\partial}{\partial p} J(Z, \zeta_g + f) - g^2 / \bar{f} J(Z, \frac{\partial Z}{\partial p}) \quad (2.7)$$

From this equation it may be observed which atmospheric conditions tend to give rise to negative  $\omega$  (ascent). With warm advection into an area  $J(Z, \frac{\partial Z}{\partial p})$  is positive and thus  $\omega$  is negative. On the other hand subsidence will be associated with cold advection. If vorticity advection increases with height, then  $\frac{\partial}{\partial p} J(Z, \zeta_g + f)$  is positive and ascent will be initiated. Thus in a situation with a short wave propagating in a westerly flow, an area of ascent will be located between the trough and the downstream ridge.

Equations (2.5) and (2.7) are a closed set for  $\omega$  and  $\frac{\partial Z}{\partial t}$  and are solved sequentially using numerical techniques. The approximation of these equations by finite-difference analogues and the method of solution will be described in Chapter IV.

### 2.3 The Horizontal Grid

In the horizontal, atmospheric parameters are represented on a grid of points over the area indicated in Figure 1. The grid is so oriented that the prime region of

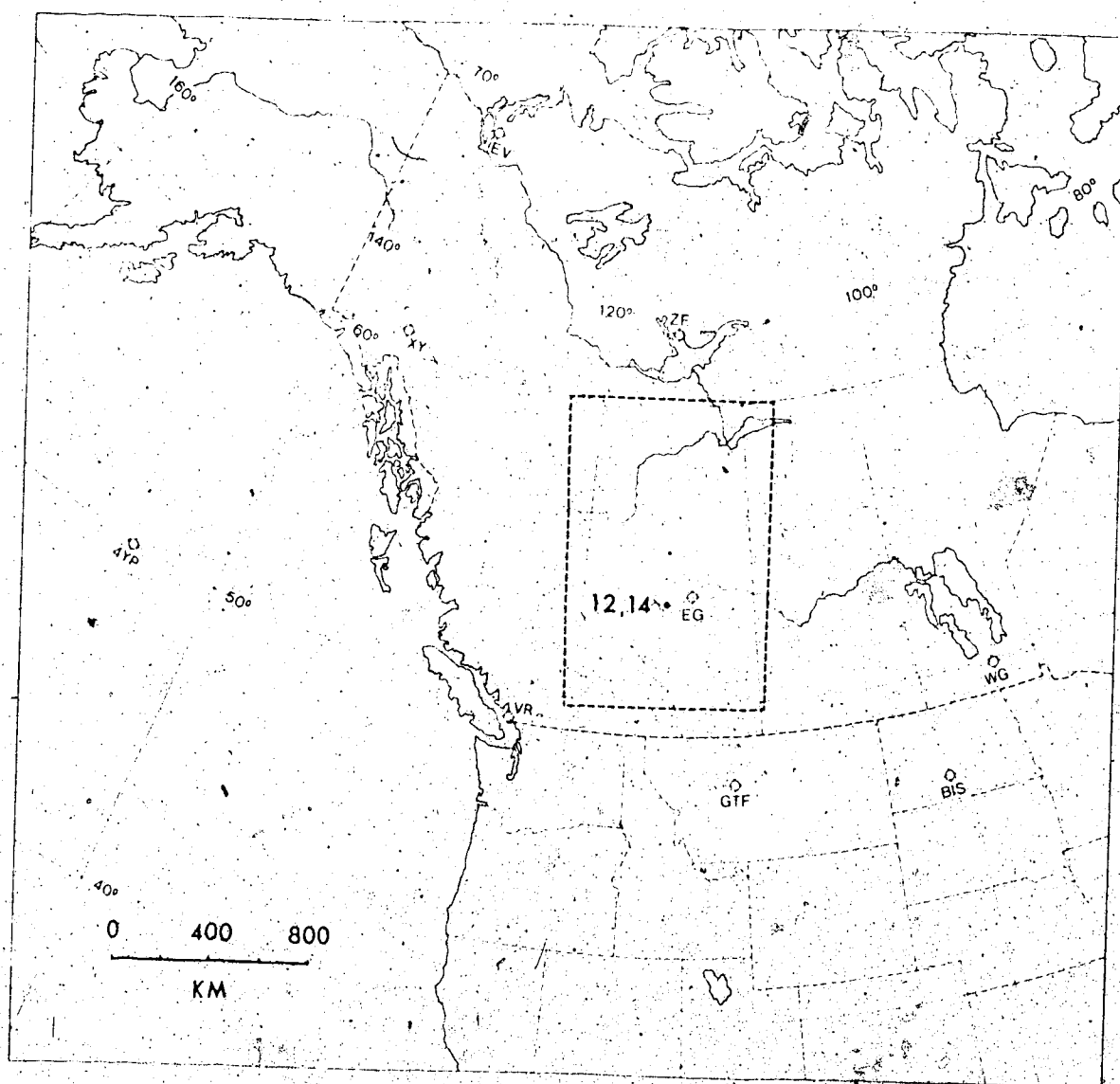


Figure 1. The areal extent of the horizontal grid. Grid point 12,14 lies to the west of Edmonton, Alberta. The scale indicated is the grid point spacing true at 60° N. The area outlined is that for which root-mean-errors were calculated.

interest is located near the center of the area, with the Rocky Mountain chain essentially bisecting the area. The grid itself is a matrix of 21 rows and 23 columns and the grid element is a square on a polar stereographic projection. The grid interval is 200 kilometers (km), true at latitude  $60^\circ$  north while elsewhere on the grid, the spacing  $d_{ij}$  is given by:

$$d_{ij} = \frac{D}{m_{ij}} \quad (2.8)$$

where  $D$  is 200 km and  $m$  the map scale factor defined by:

$$m_{ij} = \frac{1 + \sin 60^\circ}{1 + \sin \phi_{ij}} \quad (2.9)$$

In this equation  $\phi_{ij}$  is the latitude of grid point  $i, j$ .

#### 2.4 The Vertical Representation

In the vertical, the model atmosphere has five layers separated by the four primary isobaric surfaces: 300, 500, 700 and 850 millibars (mb) which coincide with the standard levels at which data are measured in the real atmosphere. The input of data is at the four primary levels and the omega equation is solved at the intermediate levels, 400, 600 and 775 mb, subject to the vertical boundary conditions that  $\omega = 0$  at 200 mb and  $\omega = \omega_g$  at the lower boundary. A schematic vertical cross-section of the model atmosphere is illustrated in Figure 2.

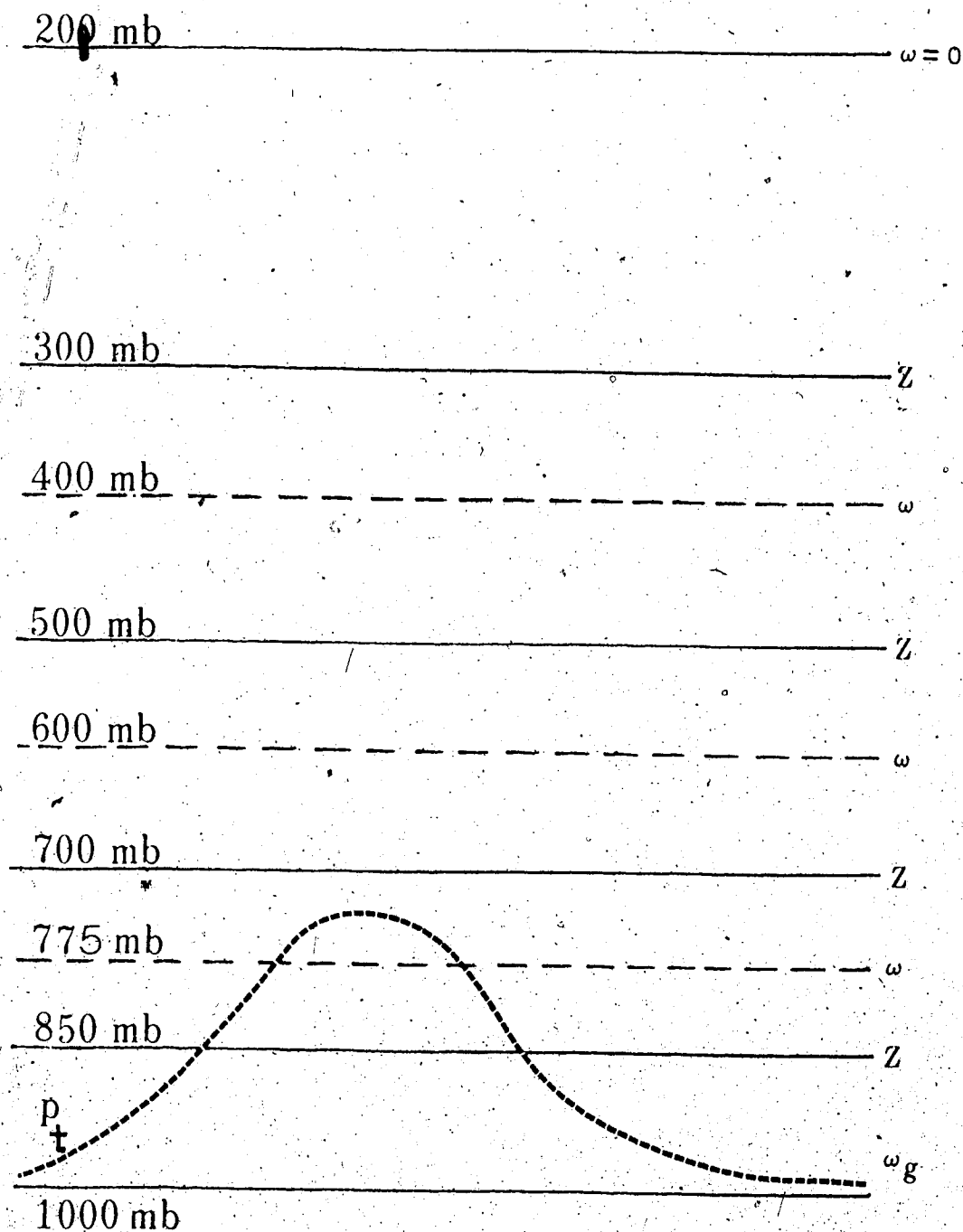


Figure 2. The vertical structure of the model atmosphere using pressure as the vertical coordinate. The vorticity equation is solved at levels labelled  $Z^*$ , and the omega equation at levels labelled  $\omega$ . The vertical velocity at the lower boundary originates either at 1000 mb or at the terrain pressure surface  $p_t$ .

## 2.5 The Lower Boundary Condition

The lower boundary in the model is the terrain surface, and the lower boundary condition is therefore the specification of omega at this surface. The vertical velocity has two components in the model which are determined respectively by: a) the earth's topography, and b) the friction in the surface boundary layer.

### a) The Orographic Vertical Velocity

Haltiner (1971) gives an expression for the orographic component of the vertical velocity in the form:

$$\omega_t = g \rho_t \vec{V}_t \cdot \nabla H_t(x, y) \quad (2.10)$$

where  $H_t$  is the height of the terrain above sea level and  $\rho_t$  and  $\vec{V}_t$  are respectively the atmospheric density and the horizontal wind velocity at terrain height. Converting to pressure coordinates, this expression reduces to:

$$\omega_t = \vec{V}_t \cdot \nabla P_t \quad (2.11)$$

where  $P_t$  is the pressure at terrain height. In the model,  $P_t$  is evaluated to be the pressure at a height  $H_t$  in the U. S. Standard Atmosphere. In principle, it should be possible to estimate terrain pressure from actual atmospheric conditions aloft, but such a refinement was not

believed to be necessary, since the gradient of terrain pressure rather than its absolute value is of importance in equation (2.11). In the vicinity of a mountain, the synoptic pressure gradient will be very much smaller than the variation of pressure with height. Thus the additional computational complications required to forecast terrain pressures are not justified by the very small percentage changes anticipated in  $\omega_t$ . The details regarding the determination of  $H_t$  and  $\bar{V}_t$  will be discussed in Chapters III and IV.

#### b) The Frictional Vertical Velocity

The frictionally-induced vertical velocity at the top of the boundary layer is determined in the model by a parameterization of the ageostrophic mass transport in the planetary boundary layer (PBL). The equation relating the horizontal divergence and the turbulent Reynolds shear stress in the PBL may be written (following Haltiner, 1971) as:

$$-\nabla \cdot \vec{V} = \frac{\partial \omega}{\partial p} = g/f \frac{\partial}{\partial p} \left( \frac{\partial \tau_{zy}}{\partial x} - \frac{\partial \tau_{zx}}{\partial y} \right) \quad (2.12)$$

where  $\tau_{zx}$  and  $\tau_{zy}$  are the horizontal shear stress components in the x and y directions respectively due to the vertical wind shear. These are assumed to vanish at the top of the PBL. If this equation is integrated from the bottom to the top of the PBL, the resulting expression for the

frictionally-induced vertical velocity component  $\omega_f$  at the top of the PBL is:

$$\omega_f = g/\bar{f} \left( \frac{\partial \tau_{zy}}{\partial x} - \frac{\partial \tau_{zx}}{\partial y} \right)_{\text{TOP}} \quad (2.13)$$

The surface stress  $\vec{\tau}$  is assumed, in this model, to be proportional to the square of the wind speed  $\vec{V}_0$  at a height of ten meters (anemometer level) according to the relationship:

$$\vec{\tau} = \rho_t C_d \vec{V}_0 |\vec{V}_0| \quad (2.14)$$

The drag coefficient  $C_d$  depends on the roughness of the underlying surface, while  $\rho_t$  is the air density at terrain height  $H_t$ . As with the pressure, the density at terrain height is given the value corresponding to that in the U. S. Standard Atmosphere. Thus the frictional vertical velocity is now written:

$$\omega_f = g/\bar{f} \left[ \frac{\partial}{\partial y} (\rho_t C_d u_0 |\vec{V}_0|) - \frac{\partial}{\partial x} (\rho_t C_d v_0 |\vec{V}_0|) \right] \quad (2.15)$$

where  $u_0$  and  $v_0$  are respectively the x- and y-components of the horizontal wind.

There are several methods by which  $\vec{V}_0$  may be estimated. Some quasi-geostrophic models use the value of  $\vec{V}_g$  at a level near terrain height. Danard (1966) for



example used the 850 mb geostrophic wind. Some models use the geostrophic 1000 mb wind forecast by the model while others employ a wind which is extrapolated to terrain height from the flow at higher levels (e.g. Cressman, 1963). In the model used in the current study, experiments were conducted using the 850 mb geostrophic wind, as well as, a geostrophic wind extrapolated to terrain height by means of the Aitken polynomial which is described in Appendix A.

The geostrophic wind  $\vec{V}_{g0}$  may be further modified in the calculation of the vertical velocity  $\omega_f$ . Following Sawyer (1959), Greystone (1962) and Haltiner (1971), a representative value for  $\vec{V}_0$  may be considered to be smaller by a fraction  $r$ , than the magnitude of the geostrophic wind  $\vec{V}_{g0}$  at the top of the planetary boundary layer. This wind may also be turned through some angle  $\alpha$  from the direction of  $\vec{V}_{g0}$ . Making these assumptions, it may be shown from a consideration of Figure 3 that:

$$\begin{aligned} u_0 &= r (u_{g0} \cos \alpha - v_{g0} \sin \alpha) \\ v_0 &= r (v_{g0} \cos \alpha + u_{g0} \sin \alpha) \end{aligned} \quad (2.16)$$

where  $u_{g0}$  and  $v_{g0}$  are respectively the x- and y-components of the geostrophic wind  $\vec{V}_{g0}$ . Substituting into equation (2.15), the complete expression for the frictionally-induced vertical velocity at the top of the boundary layer becomes:

$$\begin{aligned} \omega_f &= g/f \left[ \frac{\partial}{\partial y} \left\{ \rho_t C_d r^2 (v_{g0} \cos \alpha + u_{g0} \sin \alpha) |\vec{V}_{g0}| \right\} \right. \\ &\quad \left. - \frac{\partial}{\partial x} \left\{ \rho_t C_d r^2 (u_{g0} \cos \alpha - v_{g0} \sin \alpha) |\vec{V}_{g0}| \right\} \right] \end{aligned} \quad (2.17)$$

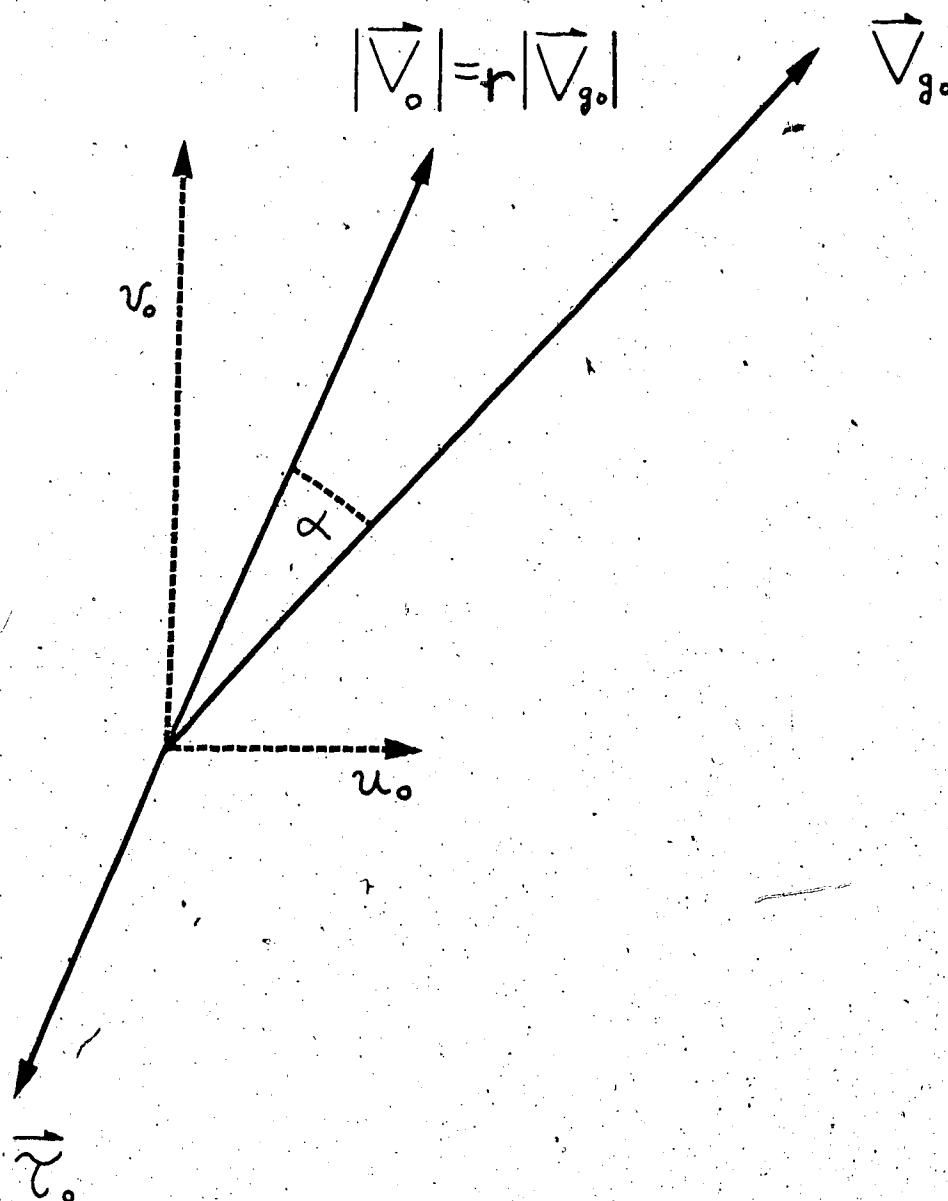


Figure 3. The relationship between the geostrophic wind vector  $\vec{V}_g$  at the top of the planetary boundary layer, the surface stress and the resultant wind vector  $\vec{V}_0$  at anemometer level employed in the calculation of the frictionally-induced vertical velocity at the top of the PBL.

Both the reduction factor  $r$  and the turning angle  $\alpha$  are dependent on the nature of the underlying surface. Sawyer (1959) suggests that  $\alpha$  may vary from  $6^\circ$  over the sea to  $30^\circ$  over land and to  $35^\circ$  over mountainous areas. Greystone (1962), in his two-level model, considered values for  $\alpha$  of  $3^\circ$  to  $6^\circ$  over the sea and  $30^\circ$  elsewhere.

The value of  $r$  used in Greystone's model was .35 over land and .85 over the sea, while the drag coefficient had one constant value over land and another value over the sea. In the models of Cressman (1960, 1963), Danard (1966) and many others, the drag coefficients were variable in space, with a maximum value over mountain ridges and a smaller constant value over the sea surfaces and flat land. The drag coefficients used in the current study are the empirical values calculated by Cressman (1960), which are modified by the inclusion of a variable  $r$  and  $\alpha$  as indicated in equation (2.17). The justification for such a modification is that we are attempting to determine the parameterization of the lower boundary condition which best simulates atmospheric development near the mountains. A discussion of the different combinations of the parameters used at the lower boundary will be given in Chapter V.

While  $\omega_f$  is assumed to originate at the top of the PBL, in most filtered equation models with a pressure coordinate system, the thickness of this layer is ignored in comparison with the thickness of the next layer above.

Thus, in these models  $\omega_f$  is considered to originate at terrain height. If the thickness of the PBL were taken into account, there would be two options available: the PBL thickness could be specified as constant in time and variable in space, or a predictive equation for this layer could be specified. The first option is equivalent to a modification of the terrain height field which does not seem justified because of the smoothed topography already present in the model. The second option is difficult to employ in a filtered model, although it is more amenable to inclusion in a primitive equation model using the sigma pressure coordinate system.

Thus in filtered models, both  $\omega_f$  and  $\omega_t$  are assumed to originate at terrain height  $H_t$  (and hence  $P_t$ ). An even more crude assumption often used for convenience is that the terrain-induced vertical velocity originates at some lower pressure surface, for example the 1000 millibar surface. Such an assumption allows a simpler representation of vertical derivatives near the lower boundary. A full description of the different boundary conditions tested in the model will be presented in Chapter V.

## CHAPTER III

### DATA ACQUISITION AND ANALYSIS

#### 3.1 Upper Air Data

For two of the three cases chosen for study (January 5 and March 5, 1972), the upper air data were extracted from the Northern Hemispheric Data Tabulations, (NHDT), available from the National Climatic Center in Asheville, North Carolina, U.S.A. These data were in the form of radiosonde reports from which the temperature, wind, and geopotential height at the four primary levels were coded on cards. For about 85 upper air stations lying on or near the grid, the above data were extracted for both the initial time and for the verification time, 12 hours later. In the third case (April 27, 1974), the data were obtained from the records of the Canadian Meteorological Center (CMC) at Dorval, Québec. This data was made available in magnetic tape form, and consisted of the output of the CMC objective analysis

program on the 381 km hexagonal grid used in the hemispheric numerical weather prediction model run by CMC.

With the radiosonde data available at standard upper air stations only, a large area of the grid is not covered with observations in the first two cases. These data sparse areas over the Eastern Pacific Ocean are especially troublesome when attempting objective analysis, because the computer program described in Section 3.3 will extrapolate unrealistic flow patterns and gradients into these areas. Consequently, bogus data must be generated. A sufficient density of bogus data points were selected so that no grid point was further than 2 or 3 grid intervals from any bogus data point. Geopotential heights, calculated geostrophic winds and temperatures were then estimated at these points from the CMC objective analysis available in map form. Since these maps are based on an analysis with a much more extensive data base than that available in this study, a consistent and reasonably accurate analysis should thereby be possible in the data sparse areas of this study. No testing of alternate bogussing techniques was undertaken.

Since no 300 mb maps were available, it was necessary to extrapolate the 300 mb bogus data from that at 700 and 500 mb. For this purpose a simple equation was obtained by integration of the hydrostatic equation from 700 and 500 mb to the 300 mb pressure surface. The resulting equation is:

$$Z_3 = \{Z_5 + 7.57(T_5 - T_7) - 0.6Z_7\} / 0.398 \quad (3.1)$$

where  $Z_7$ ,  $Z_5$  and  $Z_3$  are the geopotential heights in meters at 700, 500 and 300 mb respectively, and  $T_7$  and  $T_5$  are the temperatures in degrees Celsius at 700 and 500 mb. This equation was tested at radiosonde stations in the vicinity of the data sparse area, and a representative correction value was determined based on the mean difference between the reported and extrapolated 300 mb height at these stations. This corrected extrapolation equation was then used to generate 300 mb heights over the Eastern Pacific portion of the grid.

### 3.2 Surface Data

The terrain heights used in the model were those extracted by Schram (1974). The objective technique for obtaining these heights at grid points consisted in determining the average terrain height within a circle of radius 100 km around each grid point using 1:1,000,000 World Aeronautical Charts. In the current model, this terrain height field is converted to pressure in the U.S. Standard Atmosphere (Hess, 1959) by making use of the formula

$$P_t = 1013.25 [1 - (0.0065/288) H_t]^{5.257}$$

A similar formula was used to determine the atmospheric density at terrain height. Figure 4 depicts the terrain pressure field used in

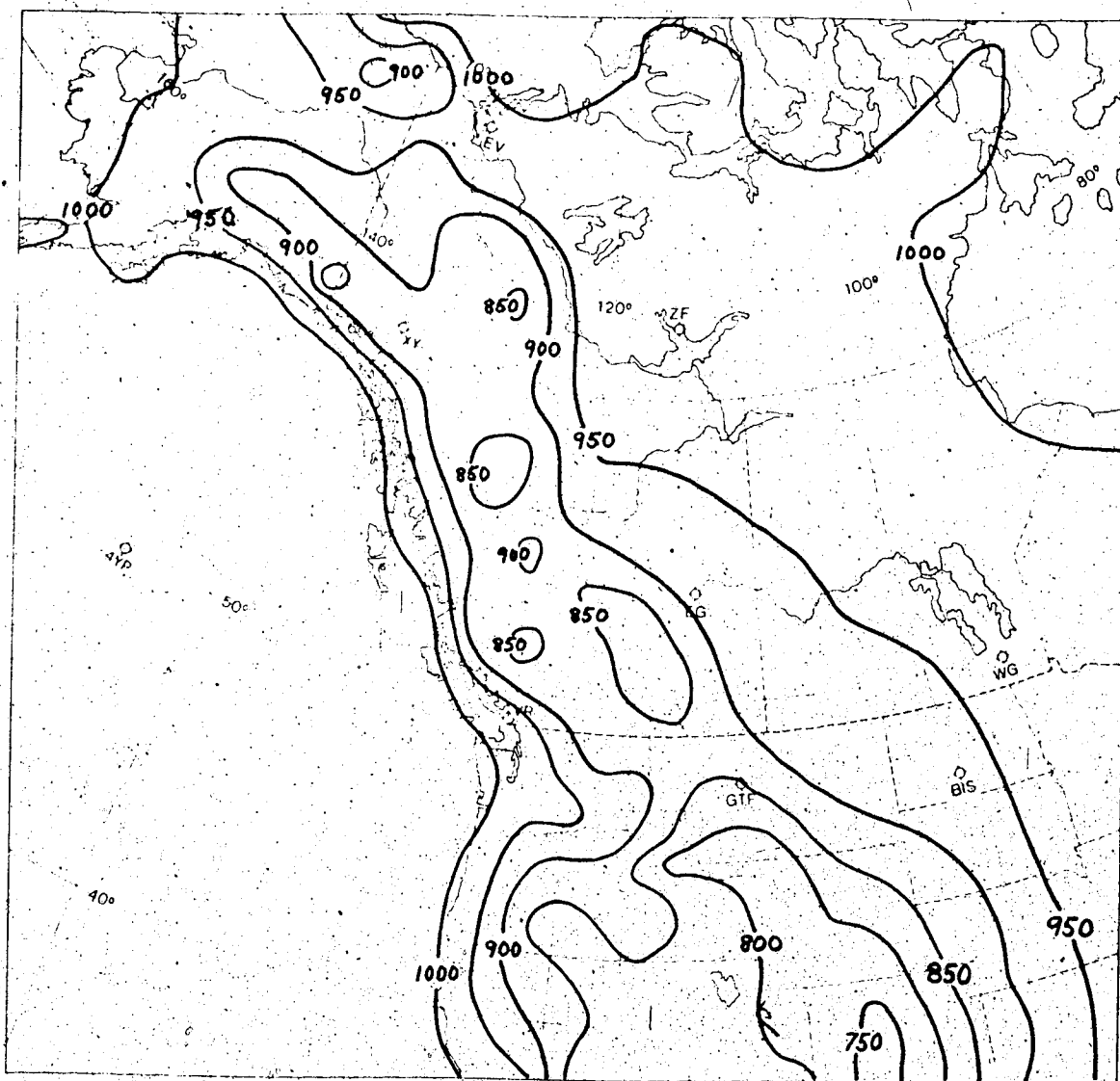


Figure 4. Pressure at terrain height calculated using the United States Standard Atmosphere. The units are millibars.



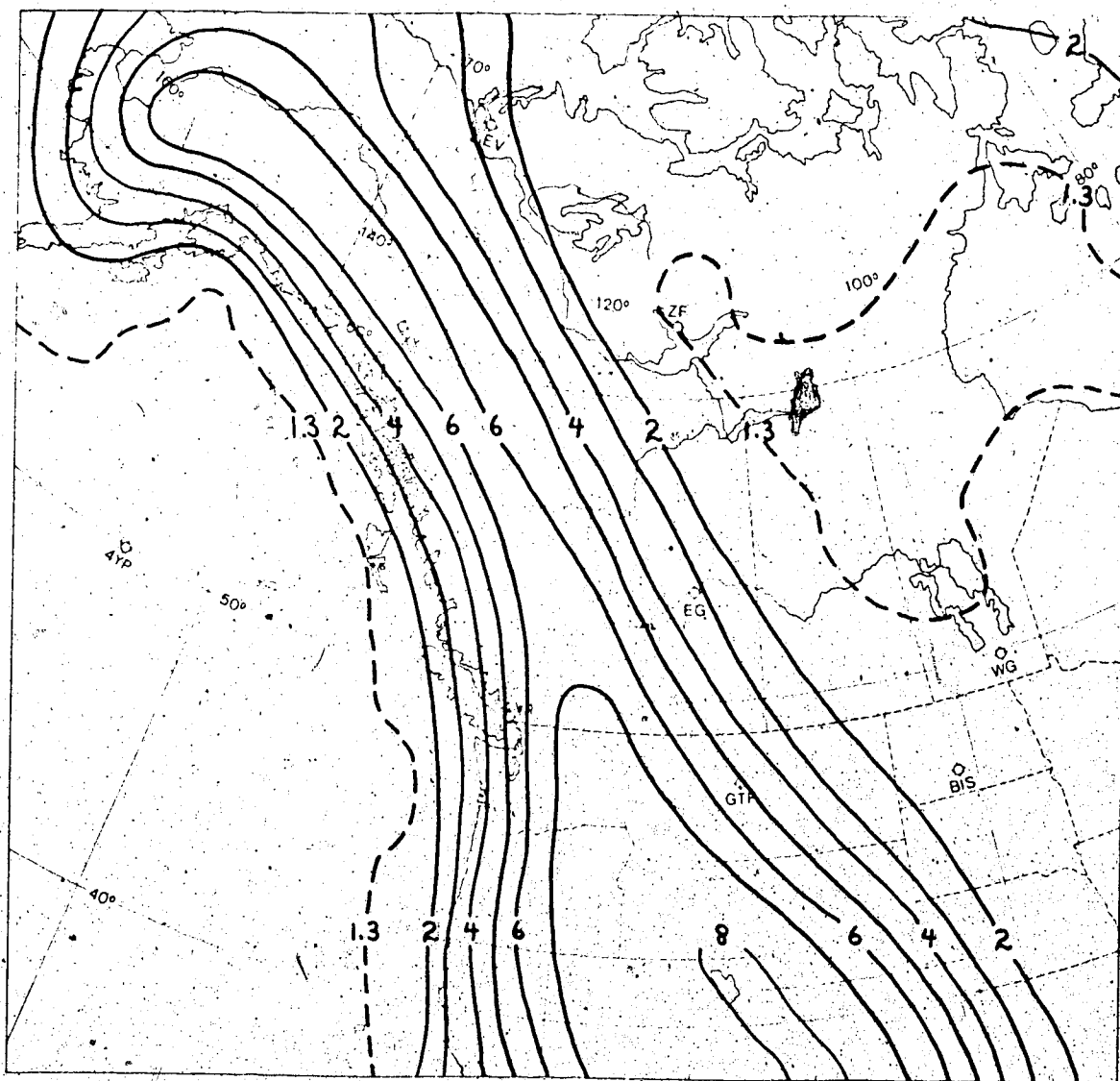


Figure 5. The analysis of the Cressman drag coefficients. The units are  $10^{-3}$  (dimensionless).

the model.

The drag coefficients, which were supplied by Dr. G. Cressman to Mr. G. Schram, have been interpolated to the 200 km grid used in this study. The drag coefficients were in the form of grid point data as discussed by Cressman (1960) in his study with the barotropic model. These coefficients are composed of two components: a constant value of  $1.296 \times 10^{-3}$  (dimensionless) over all surfaces, and an additive quantity which is a function of terrain roughness. Thus the drag coefficient ranges up to slightly

UNDERLYING SURFACE  $10^3 \times$  DRAG COEFFICIENT

WATER	$C_d \leq 1.3$
LAND	$1.3 < C_d \leq 4.0$
MOUNTAINS	$C_d > 4.0$

Table 1. Surface regimes as a function of drag coefficient.

in excess of  $8 \times 10^{-3}$ , the latter over very rough mountains. Figure 5 shows the drag coefficient over the area of this study.

As indicated in the discussion of the lower boundary condition, the turning angle,  $\alpha$ , and the reduction factor,  $r$ , are variable in space depending on the nature of the underlying surface. In this study, three regimes were

chosen, in each of which  $\alpha$  and  $r$  assume constant values. The regimes represent mountainous areas, relatively level land surfaces and extensive water surfaces. The criterion for distinguishing among these areas is based on the magnitude of the Cressman drag coefficients. In this study, the three regimes and the corresponding range of drag coefficients are given in Table 1. The particular values of  $\alpha$  and  $r$  tested are discussed in Chapter V.

### 3.3 The Objective Analysis

An objective analysis program similar to that described by Glahn and Hallenbaugh (1969) is used to interpolate the meteorological fields to the grid points for machine calculation. Studies of a similar type of objective analysis procedure by Stuart (1974) suggest that such a technique compares favorably with the most careful hand analysis. The objective method is essentially one of successive approximation, and is completely described by Glahn and Hallenbaugh as well as by Bergthorssen and Doos (1955) and by Cressman (1959). It is the technique frequently applied in the analysis of spatial fields for numerical weather prediction and analysis.

Since small scale irregularities in the analyzed fields may amplify during time integration of the numerical model, it is desirable to remove such two-grid-interval perturbations from the initial fields. All height fields

were therefore smoothed in the first two cases using the techniques described in Appendix B. The resultant fields appeared reasonably accurate over the continent. When compared with the reported radiosonde data, the analyzed fields had a mean absolute deviation over the entire grid of approximately 20 gpm at all four levels. The accuracy over the data sparse areas is of course difficult to assess and hence only a qualitative judgement could be made. However, with the use of a sufficient density of bogus data points, as suggested above, the analysis was consistent with that of the CMC. At 300 mb no such comparison could be made and, as described in Chapter V, some difficulty with prediction at this level may have been partly due to an incorrect initialization of the geopotential field.

In the third case, the upper air geopotential height data were extracted from a magnetic tape supplied by CMC. A simple program was written to extract the data from a section of the CMC grid which contained the smaller grid used in this study. Since the CMC grid spacing is 381 km, it was necessary to perform an interpolation to the 200 km grid of this study utilizing the objective analysis program. No smoothing or bogussing of the resultant geopotential fields was done, as the original CMC analysis was heavily smoothed.

Since the surface pressure (mean sea level pressure) field is not forecast directly, the actual surface pressure

data does not enter into the model. However, since it is desirable to obtain a forecast surface pressure map for comparison with the actual surface analysis, such a field was obtained, using the Aitken polynomial to extrapolate the surface pressure from the forecast geopotential fields aloft. In order to assess the errors which could be expected from such a procedure, the surface pressure field at the initial time in the first case was objectively analyzed using a program similar to that already described. A comparison of this actual mean sea level pressure field and the extrapolated pressure field appears in Chapter V. Generally there was good agreement between the extrapolated and the actual fields when the broad scale features were compared.

### 3.4 The Static Stability Parameter

The static stability parameter  $\sigma$  used in the model is a function of pressure only, and is computed using the temperatures available in the radiosonde ascents. A simple second-order centered-difference approximation to the static stability equation  $\sigma = -\frac{\alpha}{\theta} \frac{\partial \theta}{\partial p}$  was formulated and, for each of the three intermediate levels,  $\sigma$  was calculated at each radiosonde station in the forecast area. A horizontal average  $\bar{\sigma}$  was then calculated at each level and used in the solution of the omega equation. Since a large station-to-station variability was noted in  $\sigma$ , the standard deviation at each level was also calculated. The numerical

values of the mean stability parameter and the standard deviation are given in Table 2. In general, the largest absolute deviations from the mean occur at high latitudes at the 400 mb level, since the tropopause is approaching this level at these latitudes. At low levels, there are a few stations indicating an unstable stratification ( $\sigma < 0$ ). Thus unfortunately, the mean values used are not representative of any particular region of the grid.

In the current model, some testing of different values of the static stability parameter was performed. A mean stability was calculated for only those radiosonde stations lying in the section of the grid between 45° and 65° north and to the west of the Manitoba-Saskatchewan border. This mean was found to differ from the overall grid average by up to twenty-five percent. However, when these stabilities were employed in the solution of the omega equation, only very small percentage changes (generally less than five percent) in the vertical velocity and height tendency fields were noted. Comparisons of the vertical velocity and forecast height fields as calculated using variable and constant static stabilities by Haltiner et al (1963) and by Cressman (1963) have indicated that only small percentage changes occurred.

Since it appears that the solution to the omega equation is relatively insensitive to the manner in which the static stability is included in numerical models, it

	775 mb		600 mb		400 mb	
CASE	MEAN	SD	MEAN	SD	MEAN	SD
1	2.55	2.84	2.38	2.52	4.93	5.31
2	2.21	2.38	2.32	2.41	4.60	5.11
3	1.79	1.92	2.14	2.17	3.79	4.68

Table 2. Mean and standard deviation (SD) of the static stability over the complete grid ( $10^{-4} \text{ gm}^{-1} \text{ cm}^2 \text{ s}^2$ ) at three levels in the model.

would seem justifiable to use a constant value of the stability at each level. In fact many models have employed a stability based on mean yearly values or on those calculated from a standard atmosphere.

## CHAPTER IV

## NUMERICAL PROCEDURES

4.1 Horizontal Finite-Difference Operators

## a) First Derivatives

The standard centered-difference formulation is used for the horizontal derivatives appearing in equation (2.17), which is the expression for the vertical velocity at the lower boundary. Thus, with reference to Figure 6 which illustrates a nine point section of the interior of the grid, the x-and y-derivatives of the field A at the point i,j are represented by the second-order formulae:

$$\left( \frac{\partial A}{\partial x} \right)_{ij} = (A_{ij+1} - A_{ij-1}) / 2 d_{ij} \quad (4.1)$$



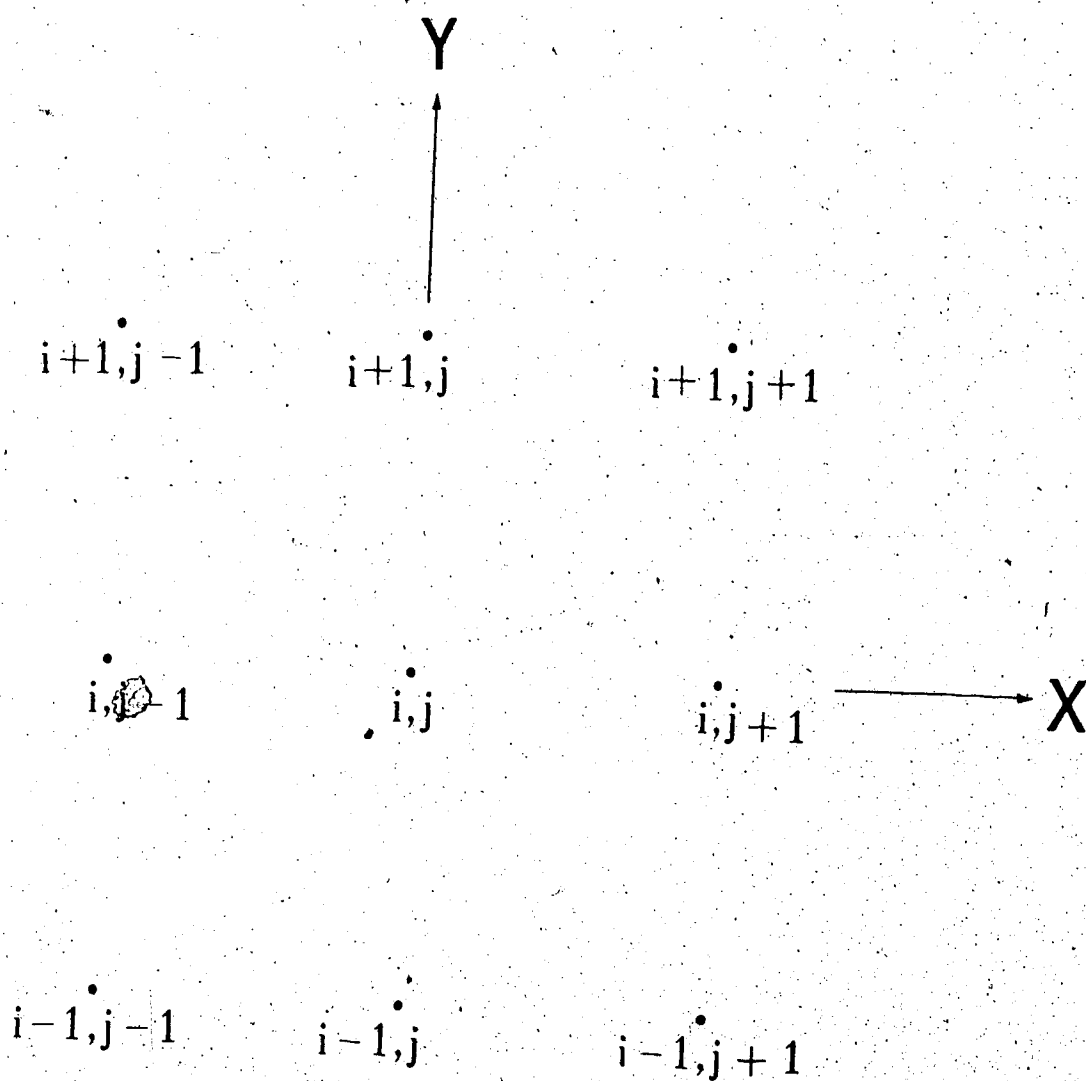


Figure 6. The horizontal grid point structure used in the finite differencing. The  $Y$ -axis corresponds to true north at longitude  $115^\circ$  W.

$$\left(\frac{\partial A}{\partial y}\right)_{ij} \doteq (A_{i+1,j} - A_{i-1,j}) / 2d_{ij} \quad (4.2)$$

At the boundaries of the grid, the horizontal derivatives are approximated by one-sided derivatives. For example if point  $i+1, j$  lay along the northern edge of the grid, then the x-derivative would be calculated in the usual manner, whereas the y-derivative would be approximated by the first-order formula:

$$\left(\frac{\partial A}{\partial y}\right)_{i+1,j} \doteq (A_{i+1,j} - A_{ij}) / d_{i+1,j} \quad (4.3)$$

A similar technique is used to calculate the x-derivative at the eastern and western boundaries and the y-derivative at the southern boundary.

As indicated in Section 2.5, the horizontal wind used in the calculation of the terrain-induced vertical velocity is a function of the geostrophic wind. In the model, this may be either the 850 mb geostrophic wind or a geostrophic wind extrapolated to terrain height. Since the 850 mb level is a forecast level, the calculation of the wind in the first instance is readily performed by taking the horizontal derivatives of the 850 mb height field.

In order to obtain extrapolated winds, the information at the four primary levels in the vertical is extrapolated to terrain height by making use of the Aitken polynomial.

While the geostrophic winds calculated at each of these levels above a grid point  $i,j$  could be extrapolated to terrain height directly, it was found that rather unacceptable winds would be extrapolated if large vertical wind shears occurred. This problem, inherent in the use of the Aitken polynomial, is greatly diminished if the geopotential height is extrapolated, and then the geostrophic wind calculated. Thus with respect to point  $i,j$  of Figure 6, the geopotential height is extrapolated to an isobaric surface which intersects the terrain at pressure  $(p_t)_{ij}$ . The height at each of the four points  $i,j\pm 1$  and  $i\pm 1,j$  on this isobaric surface is then extrapolated from the geopotential height at the primary levels above each of these points. Thus four extrapolations per grid point are required in order to calculate both components of the geostrophic wind vector at point  $i,j$ .

The procedure is repeated for each of the  $19 \times 21$  interior grid points and allows a second-order calculation of the geostrophic wind to be made at terrain height. Along the edges of the grid, extrapolation is made in a similar manner, except that one-sided first-order derivatives are calculated for the wind components parallel to the boundary of the grid. In cases where the terrain height rises above the 850 mb surface, an interpolation is performed making use of the geopotential heights of the four primary levels.

#### b) The Two-dimensional Laplacian

With reference to Figure 6, the standard finite-difference five-point Laplacian operator for variable A may be expressed as:

$$(\nabla^2 A)_{ij} \doteq (A_{i+1,j} + A_{i-1,j} + A_{i,j+1} + A_{i,j-1} - 4A_{ij})/d_{ij}^2 = \frac{\nabla^2 A}{d_{ij}^2} \quad (4.4)$$

This operator is accurate to order  $d_{ij}^2$ .

### c) The Jacobian

With the Jacobian of two variables A and B defined as  $J(A,B) = \frac{\partial A}{\partial x} \frac{\partial B}{\partial y} - \frac{\partial B}{\partial x} \frac{\partial A}{\partial y}$ , the finite-difference equivalent may be written in its five-point form as:

$$J(A,B)_{ij} \doteq [(A_{i,j+1} - A_{i,j-1})(B_{i+1,j} - B_{i-1,j}) - (B_{i,j+1} - B_{i,j-1})(A_{i+1,j} - A_{i-1,j})]/4d_{ij}^2 = J^{++} \quad (4.5)$$

where  $J^{++}$  is the finite-difference representation for J.

In prediction models, non-linear computational instability may arise if the representation of the advective (or Jacobian) terms in the predictive equation is not performed so as to conserve the mean square vorticity and the energy of the system. Arakawa (1966) has shown that a finite-difference Jacobian of the form:

$$J = (J^{++} + J^{x+} + J^{+x})/3 \quad (4.6)$$

will conserve both energy and mean square vorticity. The

various Jacobian operators in this equation are defined as follows:

$$\begin{aligned}
 J(A,B) &= \frac{\partial A}{\partial x} \frac{\partial B}{\partial y} - \frac{\partial A}{\partial y} \frac{\partial B}{\partial x} \doteq J^{++} & a \\
 &= \frac{\partial}{\partial x} \left( A \frac{\partial B}{\partial y} \right) - \frac{\partial}{\partial y} \left( A \frac{\partial B}{\partial x} \right) \doteq J^{+x} & b \quad (4.7) \\
 &= \frac{\partial}{\partial y} \left( B \frac{\partial A}{\partial x} \right) - \frac{\partial}{\partial x} \left( B \frac{\partial A}{\partial y} \right) \doteq J^{x+} & c
 \end{aligned}$$

The finite-difference formulations analagous to equation (4.5) for each of b and c in equation (4.7) may then be combined into the nine-point Arakawa Jacobian for use in the vorticity equation.

#### 4.2 The Vertical Derivatives

Since this model has unequally spaced information levels in the vertical, it is not possible to use a simple centered-difference formulation for the first and second derivatives of  $\omega$  which appear in equations (2.3) and (2.5). Instead a weighted difference scheme is used. Haltiner et al. (1963) calculated these derivatives based on the assumption of a quadratic variation of  $\omega$  with height over three successive levels. In this study, a similar overlapping parabolic profile is assumed with the finite-difference formulation based on the second order Aitken polynomial. The finite-difference approximations for the first and second derivatives of the Aitken polynomial are discussed in Appendix A.

In several portions of the grid, the terrain rises above the 850 mb surface to just below the 700 mb surface. In these areas, special consideration has to be given to the evaluation of the vertical derivatives of the  $\omega$  field. While it may not be physically meaningful to evaluate the forcing functions in the vorticity equation at the 850 mb level if that surface lies below the terrain surface, changes in the vorticity and flow patterns at 850 mb still occur due in part to the influence of the topography. Thus it is desirable to parameterize these changes even if the terrain in places lies slightly above the 850 mb surface. In portions of the grid where the terrain rises above 850 mb, the divergence at 850 mb was extrapolated from that calculated at the terrain height. The 820 mb level was chosen as the cutoff level beyond which no extrapolation was attempted. This surface lies just above the highest mountain ridges in the central and northern portions of the grid. Where the terrain rises above the 820 mb level, the 850 mb divergence was set to zero. Thus at 850 mb, the horizontal divergence was calculated over all of the region of interest even though the terrain rises above the 850 mb surface at several points. Since the terrain does not rise above the 700 mb level, no problems arose in the evaluation of the divergence at that level.

In the omega equation, the second derivative of the  $\omega$  field with respect to pressure is evaluated at the

775 mb level. In regions of high terrain, this term was evaluated in a manner consistent with the calculation of the first derivative of  $\omega$ . Since by the continuity equation, the second derivative of  $\omega$  with respect to  $p$  is equivalent to the rate of change of horizontal divergence with height, the divergence both above and below 775 mb enters into the calculation of  $\frac{\partial^2 \omega}{\partial p^2}$ . In regions where the terrain lay above 820 mb, the evaluation of the rate of change of divergence with height involved only the divergence above 775 mb, the divergence below this level being set equal to zero.

#### 4.3 The Time Step

The vorticity equation used in this study is essentially a non-linear advection equation with a sink or source of vorticity,  $\bar{f} \frac{\partial \omega}{\partial p}$ . Omitting this sink term, a linearized one-dimensional form of the vorticity equation is:

$$\frac{\partial}{\partial t} (\zeta + f) = -C \frac{\partial}{\partial x} (\zeta + f) \quad (4.8)$$

where  $C$  is the advection speed of the vorticity  $\zeta + f$  in the  $x$ -direction. If the advection term on the right-hand-side of this equation is approximated by a centered-difference formulation, and a centered time difference is employed, then the Courant-Friedrichs-Lewy (CFL) condition for linear computational stability of the numerical solution of

equation (4.8) is:

$$\Delta t \leq \frac{\Delta x}{C} \quad (4.9)$$

on a grid with spacing  $\Delta x$  employing a time step of length  $\Delta t$ . The two dimensional analogue of equation (4.9) can be shown to be:

$$\Delta t \leq \frac{\Delta x}{\sqrt{2} C} \quad (4.10)$$

In filtered models, in which rapidly propagating gravity or sound waves cannot occur,  $C$  will be the maximum wind speed in the atmosphere. In the cases chosen, this maximum speed occurs at the 300 mb level, and with the grid spacing of approximately 200 km used in this model, the maximum allowable time step is in the range .5 to .75 hours depending on the 300 mb wind speed.

While the correct choice of the time increment is a sufficient condition to ensure linear computational stability, a non-linear instability may be associated with the finite-difference representation of the advection term. As indicated in Section 4.1, the Arakawa Jacobian, since it conserves both mean square vorticity and mean kinetic energy should eliminate this nonlinear instability. However, as Haltiner (1971) points out, these conservative properties have only been proven for the continuous time derivative case and not for the finite-differencing time step.



The standard centered-time-difference technique used to forecast a new field  $\chi$  is:

$$\chi^{n+1} = \chi^{n-1} + 2\Delta t f^n \quad (4.11)$$

where  $n$  is an integer indicating the number of time steps from the beginning of the forecast, and  $f^n = \left(\frac{\partial \chi}{\partial t}\right)^n$  is the tendency field, which in the current model is calculated by numerical representation of the right-hand-side of the vorticity equation. The procedure is started with a forward time step according to:

$$\chi^1 = \chi^0 + \Delta t f^0 \quad (4.12)$$

As shown by Haltiner (1971), when this forward-then-centered-difference technique is employed, neither the mean square vorticity nor mean energy of the flow are conserved even with the Arakawa formulation of the Jacobian. The result is a non-linear instability, which is initially manifested as a small amplitude temporal oscillation of the numerical solution.

As indicated by Gerrity (1972), this oscillation or separation of the solutions between the even and odd time steps is generally not a serious problem in most numerical models provided that the variation of the vorticity field between successive time steps is small. However, in a

baroclinic model such as that of the current study, the sources of vorticity which arise from the flow of the atmosphere over steep terrain may show large spatial and temporal variations. The resulting separation of the numerical solutions with time then becomes very large, and at some point in time the oscillation reaches such a magnitude that the predicted fields are severely distorted and further prediction is meaningless. This is the manifestation of non-linear instability.

This difficulty has been recognized for some time, and many procedures have been suggested to overcome this so-called 'weak instability'. Gates (1960) used a technique in which the forecast was begun with a short forward time step followed by a sequence of centered time steps of increasing length until the final desired length of time step was achieved. Such a procedure reduces the initial amplitude of the oscillations but does not filter them out completely. Thus the oscillation still increases in time and the procedure has to be re-initiated after several time steps following some temporal smoothing.

An investigation of several time stepping techniques has been undertaken by many authors, especially with reference to the primitive equation models in which some temporal smoothing is generally found to be necessary. In a paper by Lilly (1965), several finite-difference operators were tested in detail for a system of advection equations.

The numerical and analytical solutions to the simplified system of equations were compared, and it was shown that the standard centered-difference formulation in time exhibited extreme instability resulting in time splitting of the numerical solution when certain combinations of initial conditions were specified. Several other time stepping techniques of varying complexity and computational efficiency were also tested, and all appeared to have improved stability. Lilly indicated that the Adams-Bashforth method seemed to be one of the most efficient in terms of computation time required per time-step, and that it exhibited close agreement with the analytical solution to the simplified equations. The difference formulation for this technique is:

$$X^{n+1} = X^n + \left[ \frac{3}{2} f^n - \frac{1}{2} f^{n-1} \right] \Delta t \quad (4.13)$$

where again  $n$  indicates the time level,  $X$  is the predicted field and  $f$  the tendency field.

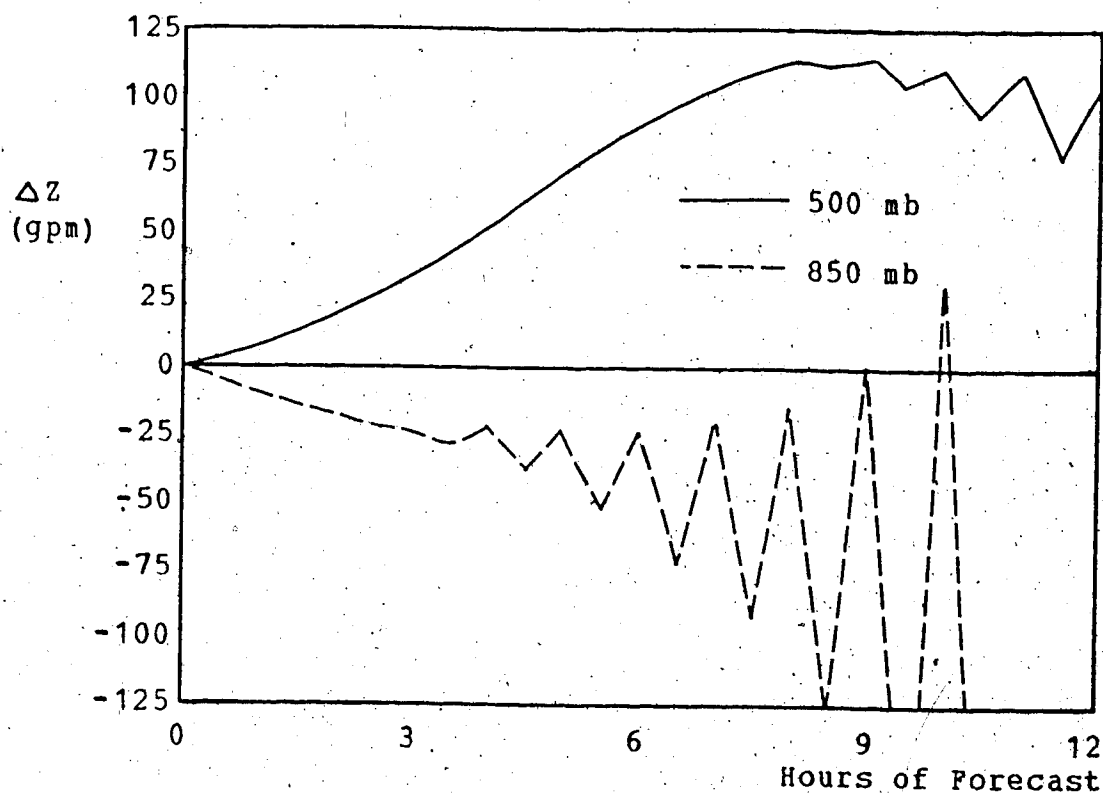
Further tests on the accuracy of various time stepping techniques were undertaken by Molenkamp (1968) again using a simple advection model. A comparison of several time stepping procedures suggested that the Adams-Bashforth technique was of comparable accuracy to the centered-difference formulation when both were used to predict the advection of simple patterns. As well, the Adams-Bashforth technique showed a smaller tendency towards damping of the

advected fields than did the centered-difference formulation.

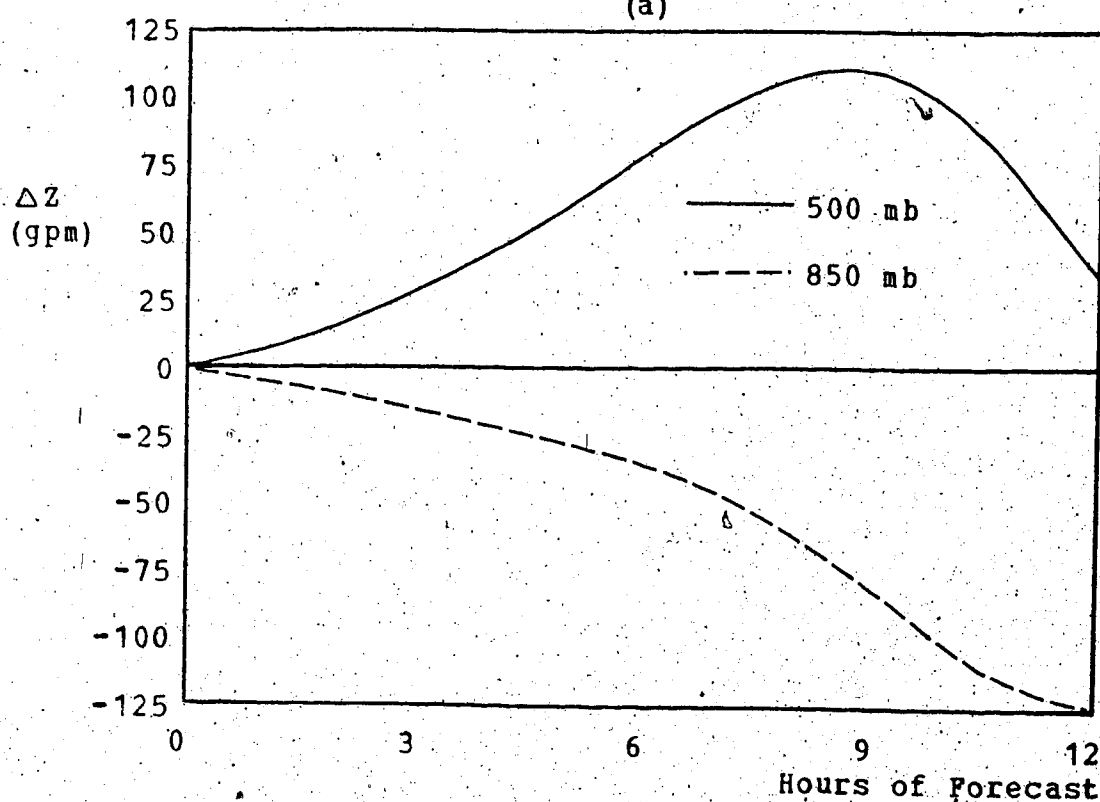
In the present study, forecasts were first computed with the first-forward-then-centered-difference technique, but it became evident that a tendency toward separation of the solutions at alternate time steps increased with certain lower-boundary conditions. In Figure 7, the differences forecast from the initial value of the 850 and 500 mb geopotential height at grid point (12,14) are plotted as a function of time. The grid point chosen is the closest one to Edmonton, Alberta as shown in Figure 1. The oscillatory nature of the solution is most apparent at 850 mb where the lower boundary condition is most influential and the amplitude of the oscillation rapidly increases with time. By about nine hours (or 18 time steps), the oscillations have commenced at higher levels and the forecast has long since become meaningless. When the Adams-Bashforth time step is used and all other initial conditions are unchanged, the forecast shows no tendency towards oscillation. Thus the Adams-Bashforth time step yields a computationally stable solution to the time-dependent equations for this case and no further problems attributable to the time stepping procedure were encountered.

#### 4.4 Solution of the Differential Equations

The right hand sides of the vorticity and omega



(a)



(b)

Figure 7. Forecast height differences from the initial condition as a function of time at 850 mb and at 500 mb: (a) forward then centered time step, (b) a single forward followed by Adams-Bashforth time step. Both were calculated at grid point 12,14 which is indicated in Figure 1.

equations consist of forcing functions composed of differential operators acting on other differential operators; for example, the Jacobian operating on the Laplacian of the height field. Because of the manner in which the operators are formulated in the finite-difference scheme, these forcing functions can be evaluated only over a portion of the grid which excludes a strip two grid points wide all around the lateral boundary. The solution to the omega equation then consists of finding a simultaneous solution to a set of 969 finite-difference equations - one equation for each of  $17 \times 19 \times 3$  points in the three dimensional grid. The vorticity equation is solved at each of four levels independently, and therefore a solution to four sets of 323 ( $17 \times 19$ ) finite-difference equations is required.

The solutions to the finite-difference forms of the vorticity and omega equations are achieved by means of an iterative process known as Liebmann over-relaxation. This procedure is frequently used in numerical weather prediction, and the technique is described in texts by Thompson (1961) and Haltiner (1971). A brief description of the technique, and the parameters used to achieve the numerical solution follows.

The vorticity and omega equations may be written in the form of a Helmholtz equation as follows:

$$\nabla^2 T + F(T) = G(x, y, p, t) \quad (4.14)$$

where  $T=T(x,y,p,t)$  is the  $\omega$  or the height tendency field and the forcing function is  $G$ .  $F$  is a function which involves the second derivative of  $\omega$  in the omega equation, while  $F$  is zero in the vorticity equation. When equation (4.14) is represented in finite-difference form, the following relation is obtained:

$$\nabla^2 T_{ijk}^m + K F_{ijk} - K' G_{ijk} = R_{ijk}^m \quad (4.15)$$

where  $T_{ijk}^m$  is the  $m$ 'th approximation to the field  $T$  at point  $(i,j,k)$  and  $\nabla^2$  is the five-point Laplacian operator defined in equation (4.4). The functions  $K$  and  $K'$  involve the grid spacing and the static stability, and  $R$  is the residual which is to be made as small as possible. A new estimate for the  $T$  field may be derived from the previous estimate using the equation:

$$T_{ijk}^{m+1} = T_{ijk}^m + \beta R_{ijk}^m \quad (4.16)$$

In this equation  $\beta$  is the relaxation parameter, which should be chosen so as to maximize the rate of convergence of the iteration technique. Through experimentation it was found that in the solution of the vorticity equation, a value of 0.45 for  $\beta$  allowed a convergent solution to be achieved in 25 to 35 iterations at each time step. The same value of  $\beta$  was used in all three cases tested.

In the solution of the omega equation, it was found necessary to use a value of  $\beta$  in Case 3 different from that used in Cases 1 and 2. A numerical solution to the omega equation was achieved in 15 to 25 iterations if a value of  $\beta = 0.285$  was used in Cases 1 and 2 while in Case 3, a value of  $\beta = 0.245$  was the optimum value used to achieve rapid solution. The rate of convergence in the solution to the omega equation was very sensitive to the relaxation parameter. An increase of only 8% in  $\beta$  resulted in a doubling of the number of iterations required to solve the omega equation in Case 3. Both the  $\omega$  and the height tendency fields were calculated to an accuracy such that the largest residual was about 1% of the synoptic scale value to be expected from a scale analysis of the vorticities and omega equations. This corresponds to an error of about  $10^{-2}$  microbars  $s^{-1}$  for the  $\omega$  field and  $10^{-5}$  gpm  $s^{-1}$  for the height tendency field.

The numerical solution described above is essentially the solution to a boundary value problem at each time step. In general, the values of the function  $T$  in equation (4.14) are unknown along the lateral and vertical boundary and must be specified as a function of time. In the omega equation, the upper and lower boundary conditions have already been described. Along the lateral boundaries,  $\omega$  is set to zero at each grid point in the outermost two rows of points around the grid.



/ In the vorticity equation, the lateral boundary condition for the height tendency field may be specified in a number of ways. As in the omega equation, the specification is made in the outermost two rows of points. In many filtered equation models, a clamped lateral boundary condition or  $\frac{\partial Z}{\partial t} = 0$  is assumed. This condition is reasonable if the area of solution for the vorticity equation covers a hemisphere so that the lateral boundary extends into subtropical regions. Synoptic scale changes in the flow patterns, and hence in the geopotential field, vary very slowly with time in these regions compared to the changes observed in middle to high latitudes. Thus for integration periods of from one to three days over a hemisphere, the clamped boundary condition does not result in serious errors.

If the integration area is small however, the assumption of a clamped lateral boundary condition will result in more serious error, especially if the integration period is more than a few hours. In order to minimize this problem, the grid is made large enough that the region of interest at the center of the grid is far removed from the lateral boundaries. For example in the models of Petterssen et al (1962), Pedersen (1962), Greystone (1962) and Danard (1966), the lateral boundaries are approximately 4000 to 5000 km from the interior region of interest, with the result that the clamped boundary condition has only a small

effect on the behavior of synoptic scale motions at the center of the grid. In the current model however, the boundaries are located in regions where the atmosphere is undergoing rapid circulation changes and the clamped boundary condition would be erroneous.

Many regional models have been formulated in which a small area grid of short grid length is meshed into a portion of a large scale grid. The lateral boundary condition on the meshed grid is specified by the interior solution of the large scale model, which may itself cover a hemisphere. In fact, several meshings have been employed going down to a grid size as small as  $1/8$  of that of the hemispheric grid. The filtered equation models of Hill (1968) and Shapiro and O'Brien (1970) are two examples in which such a procedure has been employed.

In the current study, since it was not feasible to develop a hemispheric four-level model to provide the lateral boundary condition, it had to be specified in a different way. In an early baroclinic model run by Thompson and Gates (1956), the lateral boundary condition for the tendency field was specified to be the observed 24 hour height tendency averaged over a period centered at the time of initialization of the forecast. In the current study, a height tendency field was calculated based on the height difference between the initial height field and that observed 12 hours after the initial time. This tendency was

used as a lateral boundary condition for the solution of the vorticity equation at each time step. The lateral boundary condition for the tendency field was therefore constant with time.

With such a specification of the lateral boundary condition, the model is a simulation model rather than a true forecast model. However, the solution in the interior of the grid should now be able to reflect variations in the lower boundary condition which is the purpose of this study. Information gained on the importance of the lower boundary condition could then be included in a meshed prediction model.

#### 4.5 The Forecast

With the initial and boundary conditions specified in the manner described above, a forecast is achieved following a straightforward marching procedure. At each time step, the omega equation is solved subject to the lateral and vertical boundary conditions indicated in previous sections. At this point the vorticity field is explicitly smoothed using the smoothing operator described in Appendix B. This smoothing should help to control linear computational instability. The vorticity and omega fields are then used in the vorticity equation which is solved subject to its lateral boundary conditions. The above cycle (solution of the omega then vorticity equation) is repeated, after

generation of a new geopotential height field at each time step, until the desired length of forecast is achieved. The vorticity, height and  $\omega$  fields at any time step can be stored or printed out for later analysis.

All programs were written in the Fortran language and compiled using the Fortran H compiler. The compilation and running were done on the University of Alberta IBM 360/67 computer and required about 1 minute of processing time per hour of forecast. Because of the large number of logical tests written into the program, the program is rather inefficient, and it is expected that a large saving in processor time could be achieved were the programs rewritten in a streamlined form.

## CHAPTER V.

## RESULTS AND DISCUSSION

5.1 Preliminary Comments

Although three cases were chosen to demonstrate the influence of the lower boundary condition in the numerical prediction, most of the experimentation was conducted on the January 5, 1972 case, hereafter referred to as Case 1. This was a case of major cyclogenesis in the lee of the Canadian Rocky Mountains, most of the activity occurring in the 12 hour period following the initial time of the forecast. In Case 2 (Mar. 5, 1972) and Case 3 (Apr. 27, 1974), actual lee cyclogenesis did not occur but it appeared that the Rocky Mountains had an effect on the movement and intensity of the existing synoptic features. The synoptic situations for Cases 1 to 3 are described fully below.

In the following discussions, most of the emphasis will

be on the 850 mb geopotential field although a discussion of the surface pressure fields is presented in the Case 1 forecasts. In Cases 2 and 3, since the surface pressure patterns were very similar to the 850 mb patterns, little additional insight into the validity of different lower boundary conditions could be gained from examination of the surface pressure forecasts.

## 5.2 Testing of the Numerical Procedures

In the initial testing on Case 1, numerous forecasts of length 1 to 3 hours were run to test the numerical procedures employed in the model. The response of the model to the reduction factor and turning angle used to obtain the boundary layer wind was tested. To evaluate the influence of different combinations of  $\alpha$  and  $r$ , three hour forecasts of the surface pressure field were computed. The forecast pressure change pattern was then subjectively compared with the actual 3 hour pressure change (isallobaric) fields which were analyzed from surface maps. The terrain-induced vertical velocity fields were also subjectively compared with the observed low level cloud patterns. The assumption is made that the presence of low cloud indicates the presence of moderately strong ascent. Therefore, a qualitative comparison of the areal extent of observed cloud patterns and vertical velocity fields as computed at the lower boundary of the model is an indication that the lower boundary condition is performing reasonably well.

In the preliminary testing, it was found that the turning angles had only a small apparent effect in modifying the vertical velocity field and hence the resultant height tendency fields. It was therefore decided to use a fixed set of turning angles in all subsequent testing. The choice of these angles was based partially on the findings of Sawyer (1959), and Greystone (1962), and on the summary provided in Petterssen (1956), and partially on the subjective comparisons of the terrain induced vertical velocity fields with the observed low level cloud patterns. The angles chosen were  $10^\circ$ ,  $20^\circ$  and  $40^\circ$  (to be abbreviated in further discussions as  $\alpha : 10, 20, 40$ ) over sea, land and mountains respectively. An exhaustive testing of the effect of variation of the turning angles, employing many 12 hour forecasts, was beyond the scope of this work.

The reduction factor  $r$  was also tested in the same manner as  $\alpha$  and a great variation in the accuracy of the forecast was observed when  $r$  was varied. As a result of this testing, the best reduction factors for use in determining the boundary layer wind were 1.0 over the sea, 0.9 over land and 0.8 over mountains (abbreviated  $r: 1.0, .9, .8$ ). Since the frictionally-induced vertical velocity is proportional to the square of the boundary layer wind, and hence to the square of the reduction factors, the vertical velocity is very sensitive to small changes in  $r$ . Limitations on available computer time did not permit the

complete testing of the reduction factor in 12 hour forecasts. A few runs with different sets of  $r$  are compared in the following sections to illustrate the effect of the reduction factor on the predicted flow patterns.

Using the above set of turning angles and reduction factors, other variations in the lower boundary condition were then tested. Twelve hour forecasts were run to test the effects of smoothing of the terrain, the use of extrapolated versus 850 mb. geostrophic winds in calculation of  $\omega_g$ , and the level at which  $\omega_g$  originates, either terrain height or 1000 mb. The results of these tests are illustrated in Section 5.3.

In order to obtain a quantitative comparison of the forecasts, root mean square (RMS) errors between the forecast and observed (verification) geopotential height fields were calculated at the four primary forecast levels in the model. The standard formula for this quantity (Panofsky and Brier, 1968) is

$$RMS = \sqrt{\frac{1}{n} \sum_k (F_k - O_k)^2} \quad (5.1)$$

where  $F$  is the forecast geopotential height at point  $k$  and  $O$  is the observed value. This statistic was calculated for the entire grid and on the subsection of the grid centered over Alberta as indicated in Figure 1. Over the whole grid, the number of points was 483 while over the Alberta section



it was 35. The forecast geopotential height and surface pressure field changes at the grid point closest to Edmonton were also compared with the 12 hour changes in those fields observed at Edmonton. In the following discussions of the different runs made for Case 1, these statistical measures will be compared along with the forecast height and pressure patterns.

### 5.3 Case 1: January 5, 1972

Figure 8 shows the objective analysis of the 850 and 500 mb geopotential height fields at the initial time in Case 1. An 850 mb low and 500 mb trough were initially moving eastwards across the Gulf of Alaska toward Whitehorse (XY). A trough at 850 mb and also at 700 mb (not shown) extended south from the low to just west of Vancouver Island. A large area of warm air advection extended ahead of the low into the southern Yukon, central British Columbia and into western Alberta.

In Figure 9, the initial objective analysis of the surface pressure field is compared with the surface pressure field which was extrapolated from the objective analyses aloft. The actual analysis (top) indicated that a deep (968 mb) surface low was initially present slightly south of the position of the low at the 850 mb level. In the extrapolated field, this feature is shifted northward but it is of approximately the same depth as the analyzed cyclone.

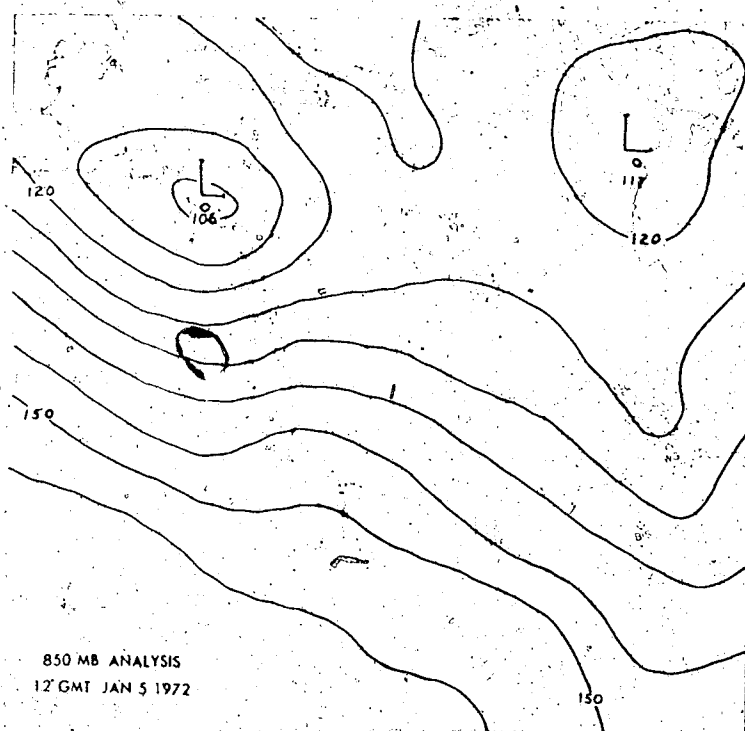
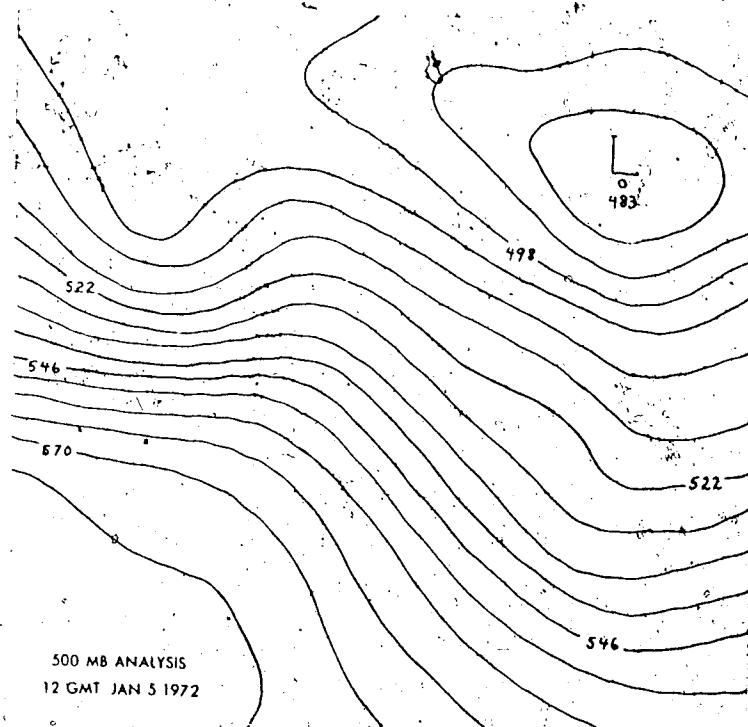


Figure 8. Initial isobaric analysis at 850 and 500 mb in Case 1. Geopotential heights are in decameters. Contour interval is 6 decameters.

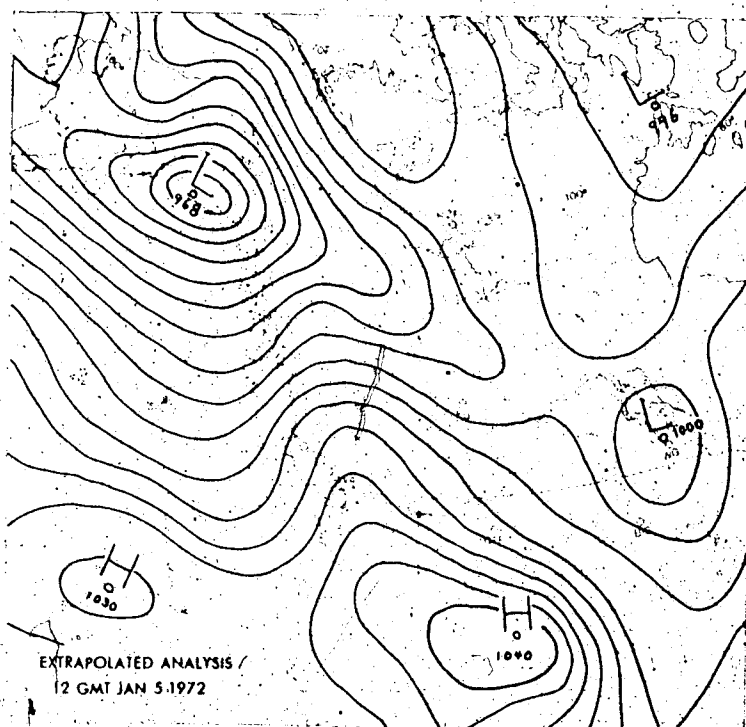
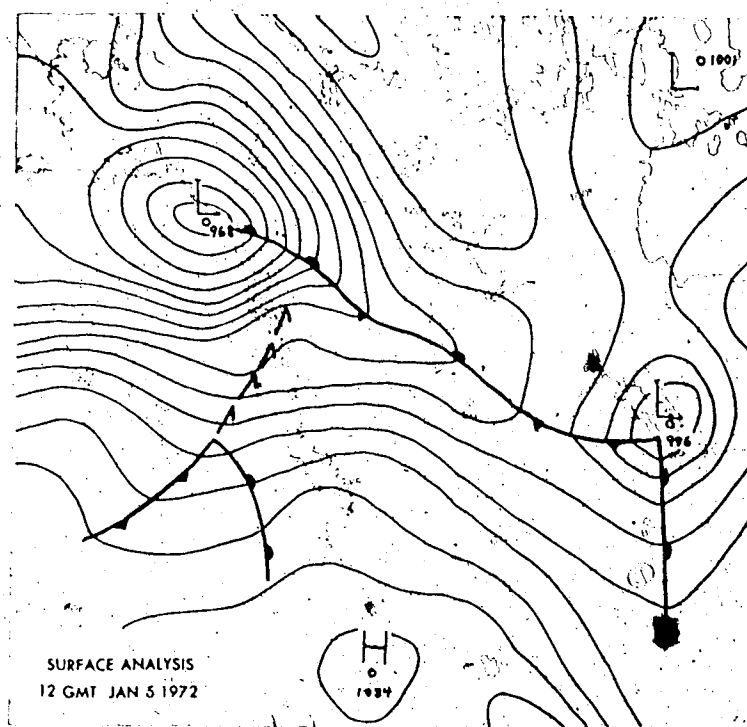


Figure 9. Initial surface analysis and the initial surface pressure field extrapolated to mean sea level in Case 1. Pressures are in mb. Contour interval is 4 mb.

The lee trough extending into Alberta is in much the same position as that of the actual analysis. The trough off the British Columbia coast, however is a much more significant feature in the extrapolated analysis, probably because it reflects the trough analyzed at higher levels. The overemphasis of this trough in the extrapolated analysis indicates that perhaps the bogussing aloft over the Eastern Pacific may not have been quite correct. In spite of the obvious differences in the two surface pressure fields in the data sparse areas, the extrapolation technique appears to give a reasonable representation of the mean sea level pressure field at the initial time.

The RMS error between the analyzed and extrapolated pressure fields was calculated using equation (5.1). Over Alberta, this error was 3.6 mb while over the whole map, the error increased to 5.0 mb. These errors are in part due to the bogussing problems discussed in Chapter III, and in part due to errors inherent in the extrapolation technique. An estimate of the magnitude of the latter errors is given in Appendix A.

The analyses of the geopotential and surface pressure fields for 0000 GMT January 6, 1972 (the verification fields for the 12 hour forecasts) are shown in figures 10 and 11. The 850 mb analysis indicates that a significant change in the low level circulation pattern had occurred over Alberta. A sharp trough has been formed, the axis of which lies

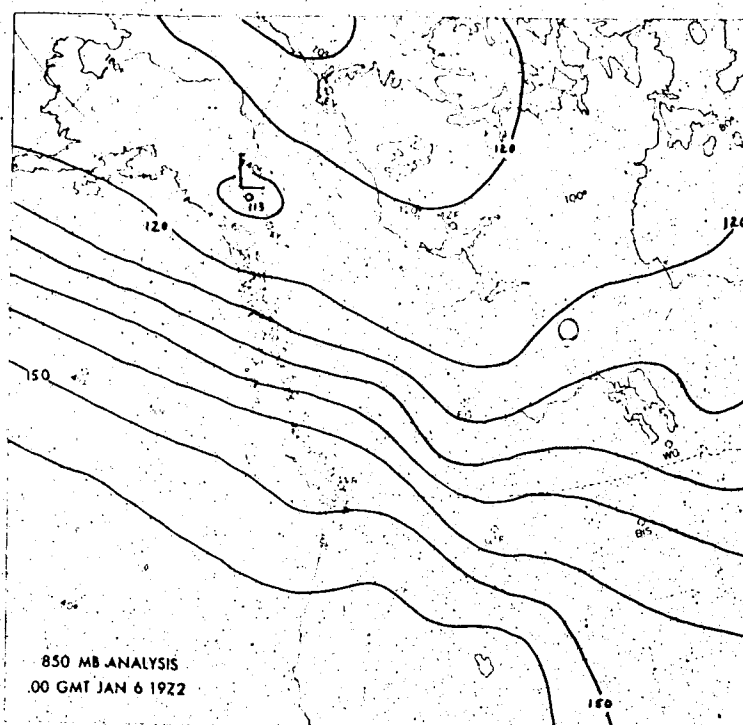
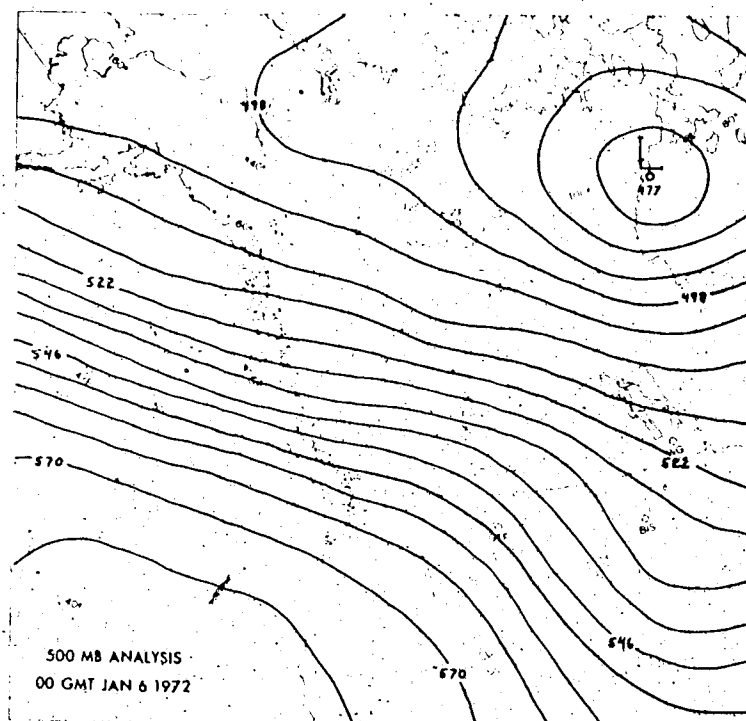


Figure 10. Verification analysis at 850 and 500 mb in Case 1. Heights in decameters.

through north central Alberta. In the 12 hour period, the 850 mb height fall at Edmonton (EG) was 100 gpm. The closed low initially in the Gulf of Alaska had moved slowly inland and filled by 70 gpm while the trough through central Manitoba had shifted eastward. At 500 mb, the flow over Alberta shifted from northwesterly to west-northwesterly with the approach and broadening of the ridge initially present through central British Columbia. The trough initially in the Gulf of Alaska is no longer present and a strong, essentially zonal flow is evident all across the west-central portion of the grid.

The extrapolated surface pressure field is presented in Figure 11 along with the surface analysis which is a subjective hand analysis of the observed surface pressure field. No objective analysis of this surface pressure field was attempted. Again it is evident that the extrapolation technique performs well with a twin-centered surface low in Alberta lying only slightly to the northwest of its correct position. The depth of this feature has been correctly extrapolated, as has the strong pressure gradient lying along the Rocky Mountains from west-central Alberta to southern Montana. The extrapolated analysis also indicates the presence of a secondary low south of Vancouver Island. This weak feature is apparently associated with the occluding frontal wave on the actual surface analysis, the apex of which was analyzed to be in that area.

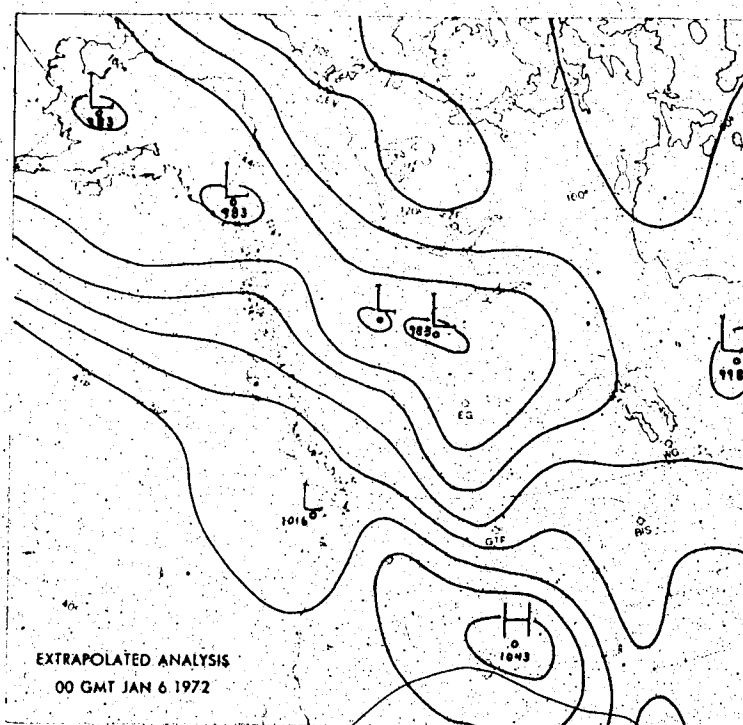
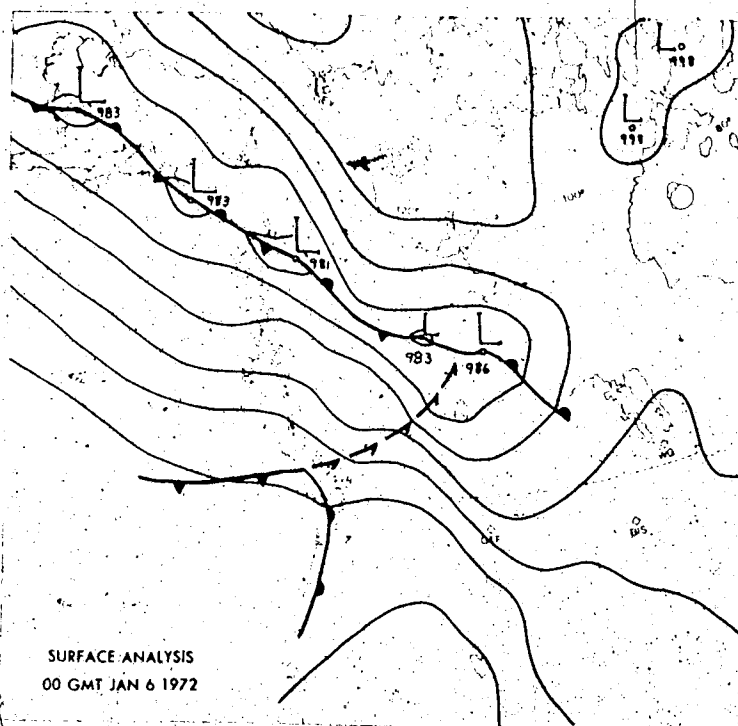


Figure 11. Verification analysis at the surface and the surface pressure field extrapolated to mean sea level from the upper level verification fields. The contour interval is 8 mb.

#### 5.4 Comparison of Several Forecast Runs Case 1

##### 5.4.1 Smoothing of the Topography: Runs 1A, 1B, 1C

The topographical field used in this study was that extracted by Schram (1974) from aerological charts. While a great deal of smoothing is inherent in the extraction technique used, the topography is quite steep in many places and slopes as large as  $8 \times 10^{-3}$  (dimensionless) exist. From a scale analysis of quasi-geostrophic motions, Haltiner (1971) indicates that the maximum permissible slope should be of the order of  $1 \times 10^{-3}$ . On the other hand, a similar calculation by Sawyer (1959) of the ratio of vertical to horizontal dimensions in orographically induced disturbances, suggested that slopes as large as  $8 \times 10^{-3}$  are reasonable. In the model used by Greystone (1962), the maximum slopes of his smoothed terrain were as large as  $7 \times 10^{-3}$ . With these conflicting ideas, it then seems desirable to test the sensitivity of the model to the steepness of the underlying terrain.

In this section, a comparison is made of the influence of two different topographical fields on the forecast. One forecast uses the original topography, (Run 1A), and a second (Run 1B) uses a topographical field which is obtained by means of a single application of the spatial smoothing operator described in Appendix B, to the original topography. In a third run, (1C), the boundary layer



vertical velocity was calculated using the smoothed topography but  $\omega_g$  originates at 1000 mb. In Runs 1A and 1B,  $\omega_g$  originates at the particular topographical surface used. These three runs demonstrate the importance of the topography in the calculation of the divergence fields at the lowest levels in the model.

Figure 12 shows the smoothed terrain field (converted to pressure in the U.S. Standard Atmosphere) in which the maximum terrain slope has been reduced to about  $2.5 \times 10^{-3}$ . A comparison of Figure 12 with the original topographical field of Figure 4 shows that the heights of some 'peaks' in mountainous areas were reduced by up to 50 mb by the smoothing operator.

In Runs 1A to 1C, the boundary layer winds were all calculated through extrapolation as described in Section 4.1. The turning angles  $\alpha$ : 10, 20, 40 and reduction factors  $r$ : 1.0, .9, .8 were used to calculate the frictional component of  $\omega_g$ . The peak values of the total vertical velocity at the lower boundary at the initial time were reduced by up to 20% when the smoothed boundary was used, but the shapes of the  $\omega_g$  fields were not noticeably altered.

Quite significant differences in the forecast geopotential height and surface pressure fields are apparent when Runs 1A and 1B are compared in Figures 13 to 15. A comparison of the 850 mb forecast fields in Figure 13 indicates that both runs tend to fill the Gulf of Alaska low

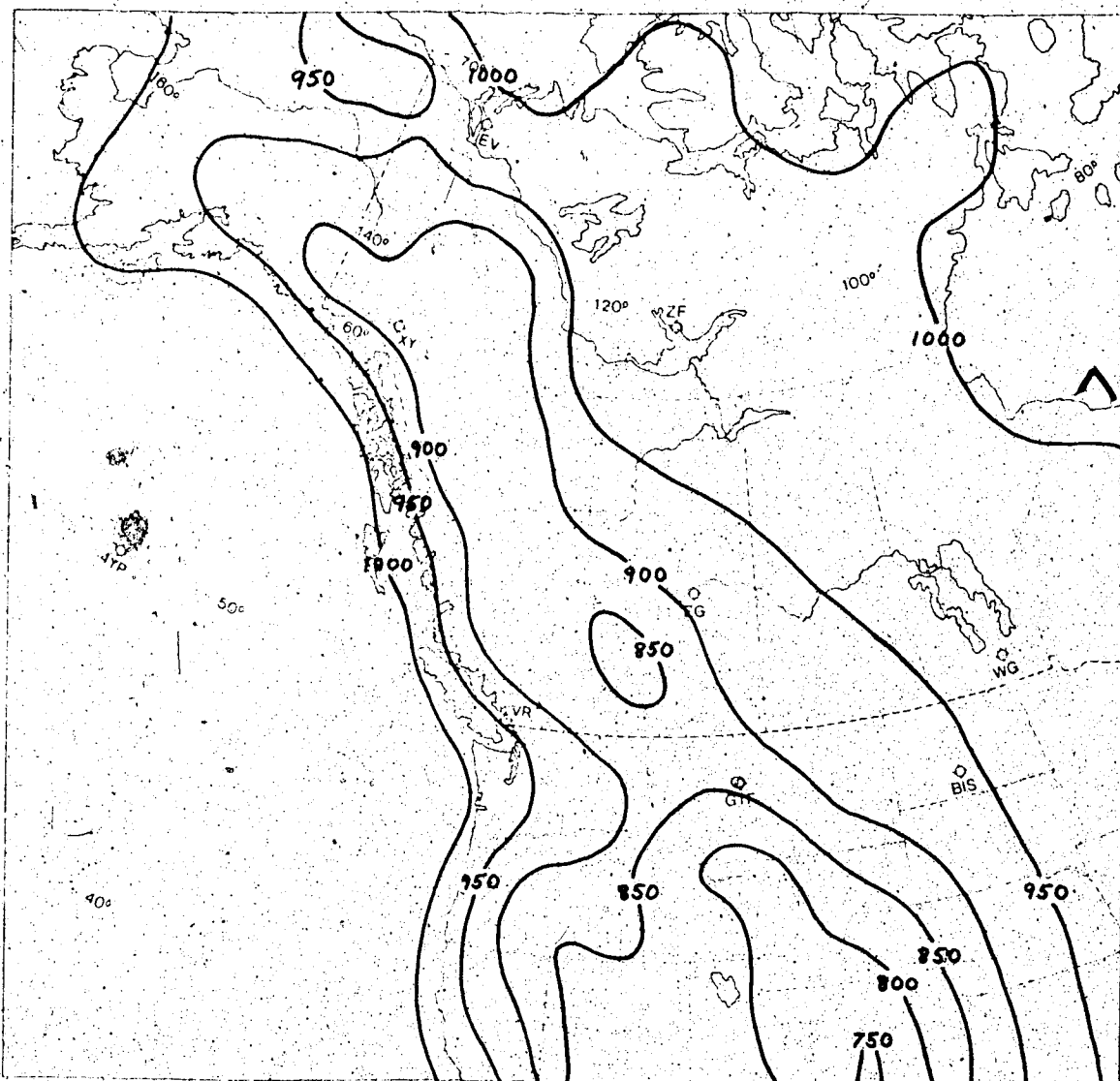


Figure 12. Smoothed terrain pressure field labelled in mb.

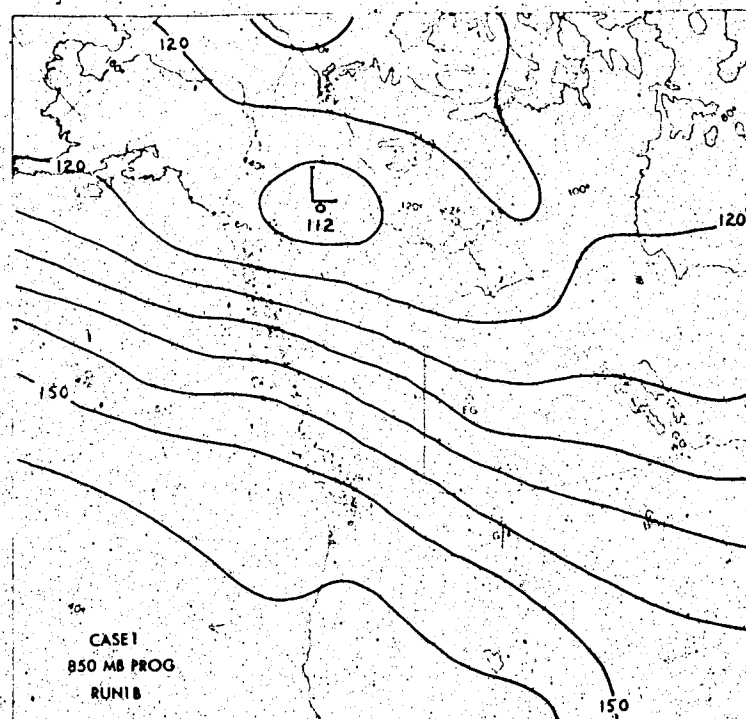
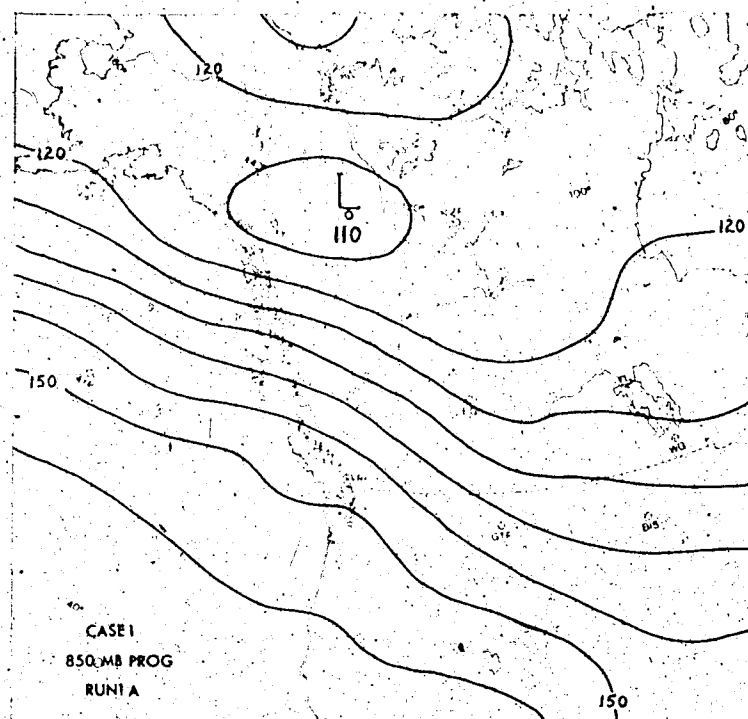


Figure 13. 12 hour forecast (PROG) at 850 mb for Runs 1A and 1B. Heights are in decameters.

and generate a lee trough at 850 mb through east-central Alberta. However in both cases, these tendencies are underforecast in 12 hours (C.f. Figure 10). A significant difference in the RMS errors for the 850 mb forecasts over Alberta is indicated in Table 3 and the most accurate forecast is obtained with the unsmoothed terrain. Figure 14

CASE 1	RMS ERRORS		FIELD CHANGES		
	MAP/ALBERTA		FORECAST/ACTUAL		
RUN	850 mb (gpm)	500 mb (gpm)	850 mb (gpm)	500 mb (gpm)	MSL (mb)
1 A	20/16	31/58	-83/-100	80/35	-26/-14
1 B	19/36	32/53	-44/-100	52/35	-9/-14
1 C	25/58	29/47	-36/-100	56/35	-6/-14

Table 3. Root-mean-square (RMS) errors for Run 1 calculated for the whole grid (MAP) and over the 35 point Alberta subsection (ALBERTA). Field changes at grid point 12,14 are compared with the observed changes at Edmonton, Alberta.

compares the 500 mb forecasts of Runs 1A and 1B. While the differences between the two are small, there is a tendency for both forecasts to overintensify the 500 mb trough as it moves inland from the Gulf of Alaska. As a result of this spurious intensification, the upper-level height gradient over western Alberta was forecast to be somewhat in excess of its actual value. The incorrectly forecast

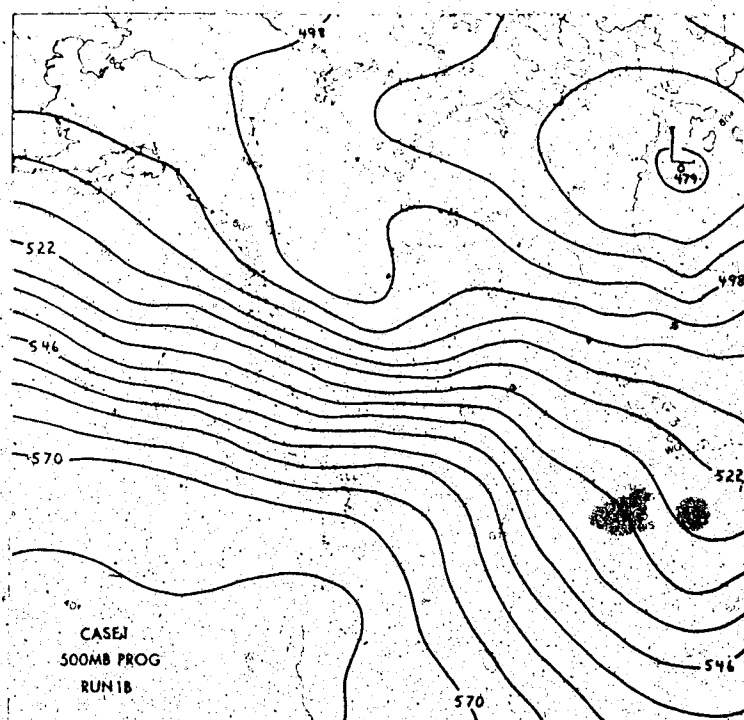
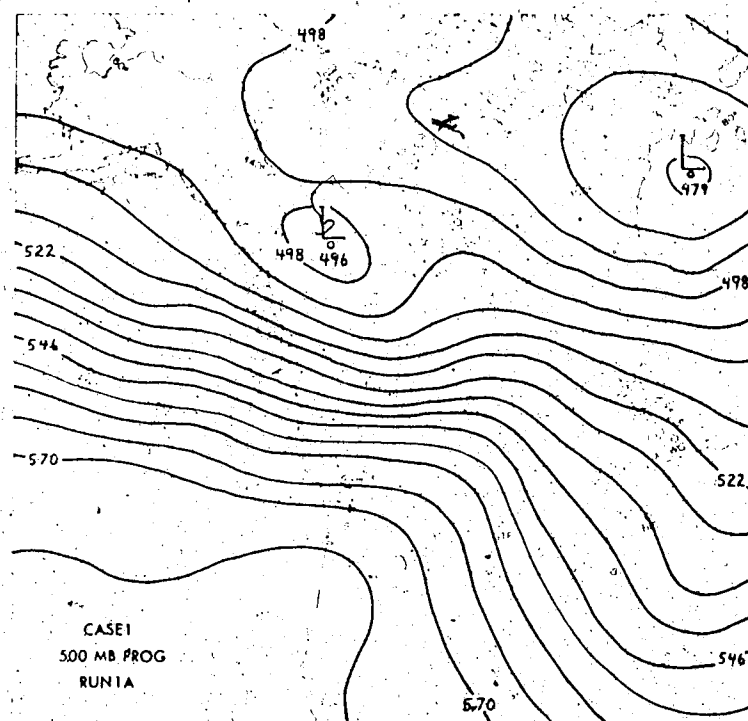


Figure 14. 12 hour forecast at 500 mb for Runs 1A and 1B. Heights are in decameters.

intensification in the middle to high troposphere was observed in all runs performed with Case 1. The sources of this error will be discussed below.

At the surface, both Runs 1A and 1B forecast the development of a lee cyclone in north-central Alberta, as illustrated in Figure 15. This feature is much better defined in Run 1A, and the forecast position of the low center was within about one grid length (200 km) of the actual position indicated in Figure 11. The major difference between the two runs was in the pressure change forecast in the lee of the mountains. This difference is illustrated in Table 3, where the 12 hour pressure change forecast with the original terrain (1A) was almost double the observed value, while with the smoothed topography, (1B), the pressure change was about one-half of that observed.

From a comparison of Run 1A and Run 1B, it is apparent that the smoothness of the topographic surface has a significant effect on the formation and rate of intensification of the lee cyclone in this numerical model. The reason for this effect becomes apparent when the nature of the divergence term at 850 mb in the vorticity equation is examined. The finite-difference analogue for this term at 850 mb is approximately  $\bar{f} \frac{\omega_{775} - \omega_g}{775 - P_t}$  and smoothing of the terrain will result in a decrease of  $\omega_g$  and an increase in  $P_t$ . Thus, this term will generally tend to

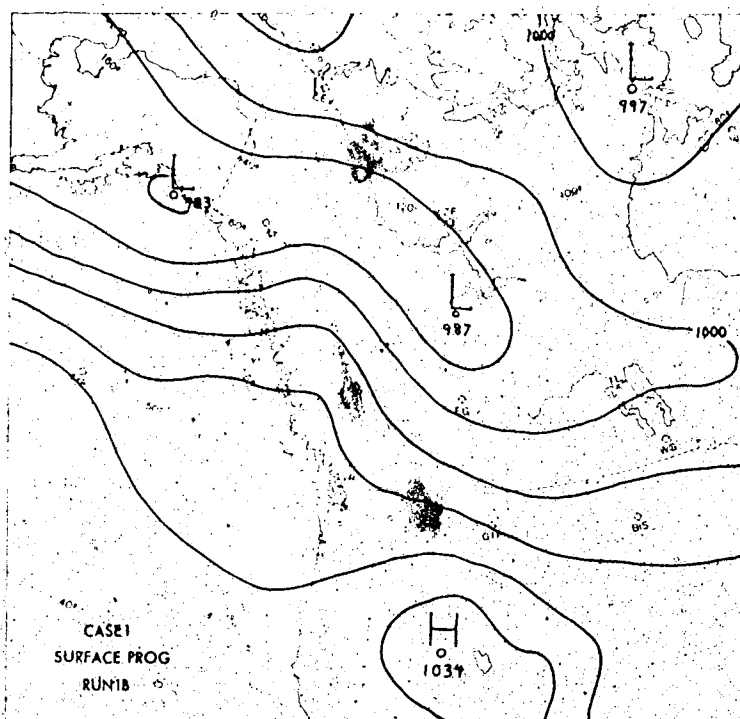
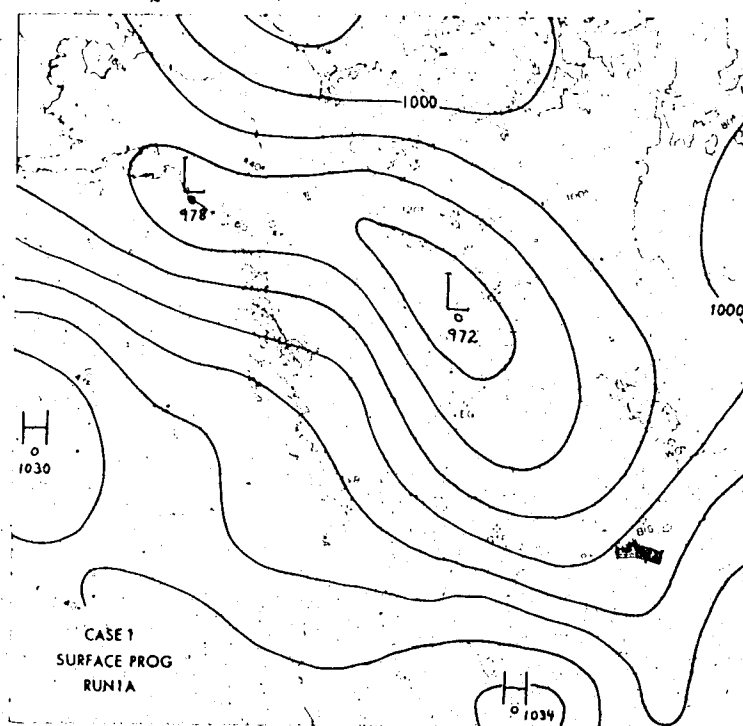


Figure 15. 12 hour extrapolated surface pressure forecasts for Runs 1A and 1B. Pressures are in mb and the contour interval is 8 mb.

decrease in the lee of the mountains due to both effects and vorticity production will be reduced. If  $P_t$  is set equal to 1000 mb, i.e.  $\omega_g$  originates at the 1000 mb surface, the vorticity production is further reduced.

The twelve hour forecast 850 mb and surface pressure fields for Run 1C are shown in Figure 16. The most apparent features of the 850 mb field are the underprediction of the deepening of the Alberta trough and the small amount of filling of the Gulf of Alaska low as it moved inland. The surface pressure field shows no formation of a closed cyclone in Alberta and the slightly intensified lee trough was shifted to the north of the position predicted in Runs 1A and 1B. The statistics in Table 3 verify the inaccuracy of this forecast at low levels over Alberta. It is of interest, however, to note that the RMS error at 500 mb was lower in Run 1C than in either of the other two runs.

Cressman (1963) observed only small changes in the hemispheric prediction pattern when comparisons were made of 500 mb forecasts, with  $\omega_g$  at 1000 mb or at  $P_t$ . A similar trend is noted in the current study at 500 mb (Table 3) but at 850 mb, and at the surface, the forecast is quite inferior when the crude approximation of  $\omega_g$  at 1000 mb is employed. In the cases tested by Danard (1966) using a similar multilevel quasi-geostrophic model, poor forecasts were obtained in mountainous areas; a result that is apparently due in part to the fact that in his model,  $\omega_g$



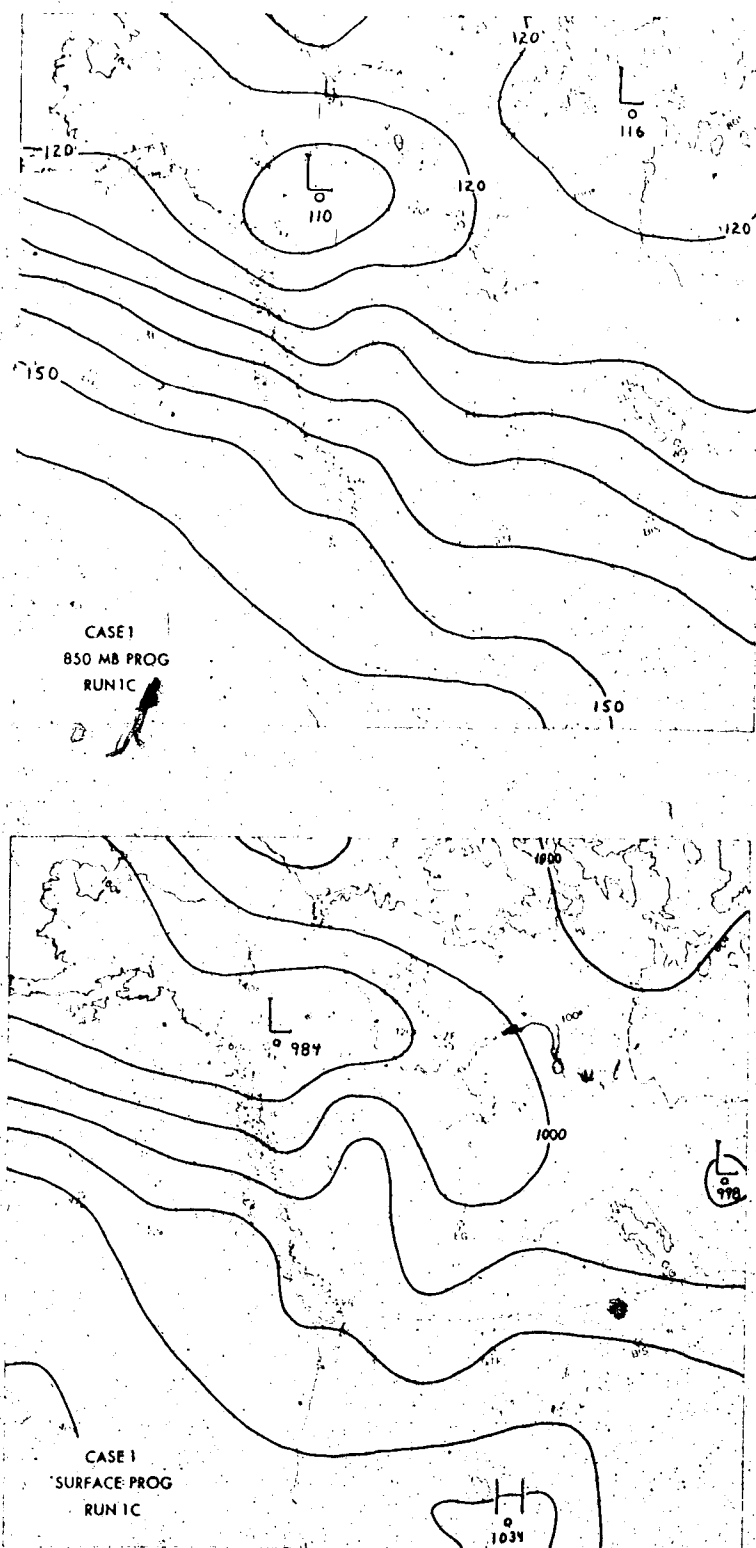


Figure 16. 12 hour forecast at 850 mb and the extrapolated surface forecast for Run 1C.

originated at 1000 mb.

#### 5.4.2 Friction and Topography: Runs 2A, 2B and 2C

In order to determine the relative importance of frictional convergence and orographic lift in the 12 hour forecasts, three runs were made. Run 2A was a forecast with a completely smooth and flat lower boundary. The boundary layer vertical velocity  $\omega_g$  was set to zero everywhere over the grid, and the lower boundary pressure was set to 1000 mb. Run 2B illustrates the effect of the orographic component of vertical velocity only.  $\omega_g$  was calculated using an extrapolated horizontal wind and the smoothed topography described in the previous section. In Run 2C, the full frictional effect was included in addition to the orographic influence. The frictional vertical velocity was calculated using the extrapolated wind in its unreduced form  $(r:1.0,1.0,1.0)$  and the standard set of turning angles  $\alpha:10,20,40$  as well as the smoothed topography used in Run 2B.

In all three of these runs, the vorticity field was explicitly smoothed every two iterations using the smoothing operator described in Appendix B, as compared to Runs 1A, 1B and 1C where the smoothing was done every 12 iterations. This was done to see whether more frequent smoothing significantly altered the forecast fields or RMS errors. The resulting forecast fields are shown in Figures 17

through 20, and the statistical computations are summarized

CASE 1	RMS ERRORS		FIELD CHANGES		
	MAP/ALBERTA		FORECAST/ACTUAL		
RUN	850 mb (gpm)	500 mb (gpm)	850 mb (gpm)	500 mb (gpm)	MSL (mb)
2 A	42/51	45/73	-63/-100	53/35	-9/-14
2 B	36/59	39/70	-28/-100	51/35	-5/-14
2 C	20/44	26/47	-37/-100	60/35	-7/-14

Table 4. RMS errors and field changes at Edmonton for Run 2.

in Table 4. Discussion will again center on the low level development, and a brief discussion of some of the initial  $\omega$  fields will be presented. For the sake of brevity, a comparison of only the 500 mb statistics will be attempted, the forecast flow patterns at this level being visually little different from those of Runs 1A and 1B.

The 850 mb and surface pressure forecasts for the flat frictionless boundary condition of Run 2A are illustrated in Figure 17. As is to be expected with such a poor boundary condition, no lee cyclogenesis is predicted and the steady deepening of the 850 mb and surface low centers is apparent. The inland propagation of the 850 mb and surface troughs is clearly indicated. Both move eastward a distance of 1000 km

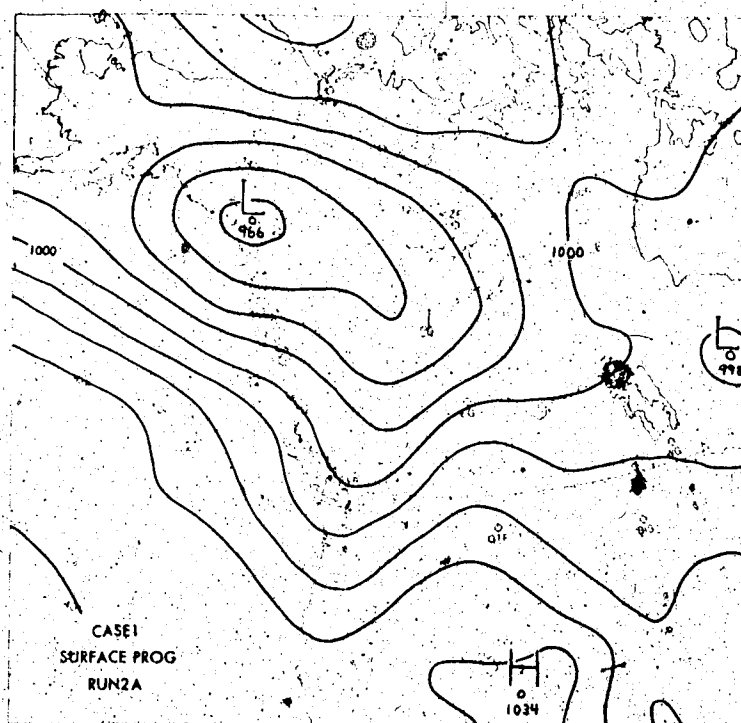
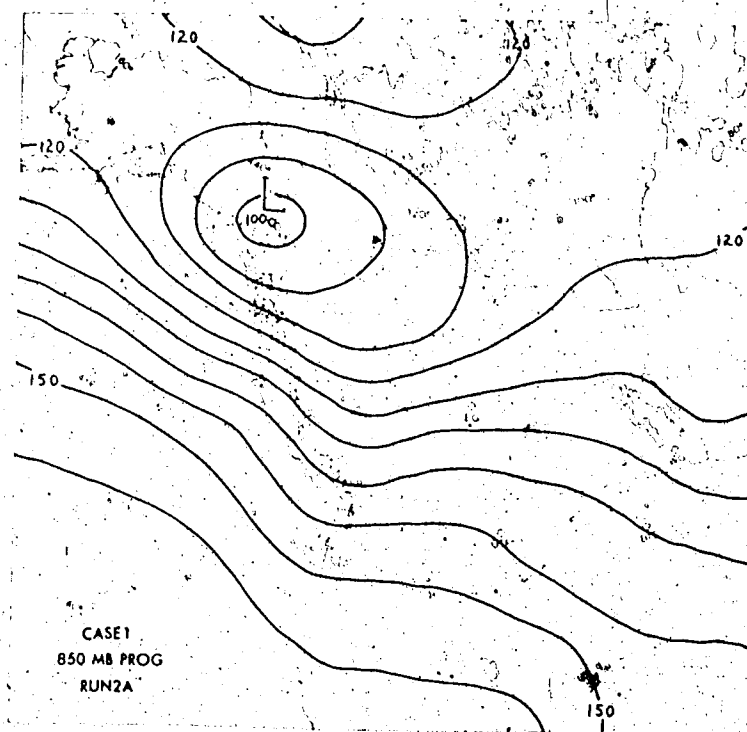


Figure 17. 12 hour forecast at 850 mb and at the surface for a flat frictionless boundary condition.

in the 12 hour period while the low in the Gulf of Alaska moves very slowly eastward. The forecast surface pressure change at Edmonton reflects the approach of the trough at the surface and aloft. The RMS errors for this run are large and further indicates that in Case 1, the lower boundary has a major influence in the development of the low level features.

Figure 18 shows the orographic component of the terrain-induced vertical velocity field at the initial time in Run 2B, as well as the  $\omega$  field at 600 mb. At the lower boundary, the orographic lift is strongest along the west coast of British Columbia, while several areas of subsidence are evident to the lee of the Rocky Mountains through northeastern British Columbia, southern Alberta and on the Montana-Wyoming border. The maximum ascent computed at the southern tip of the Alaskan Panhandle was about  $12 \text{ cm s}^{-1}$ . The subsidence in northeastern British Columbia had a maximum value near  $3.5 \text{ cm s}^{-1}$  while a more intense area of subsidence associated with the flow off the south coast of Alaska had a peak value of nearly  $8 \text{ cm s}^{-1}$ .

At 600 mb, the  $\omega$  pattern is typical of that observed with all combinations of the lower boundary condition at the initial time in the Case 1 forecasts. The maximum area of ascent over the Alaskan Panhandle is associated with the 500 mb trough in the Gulf of Alaska. Although not indicated in Figure 18, an area of very weak subsidence was initially

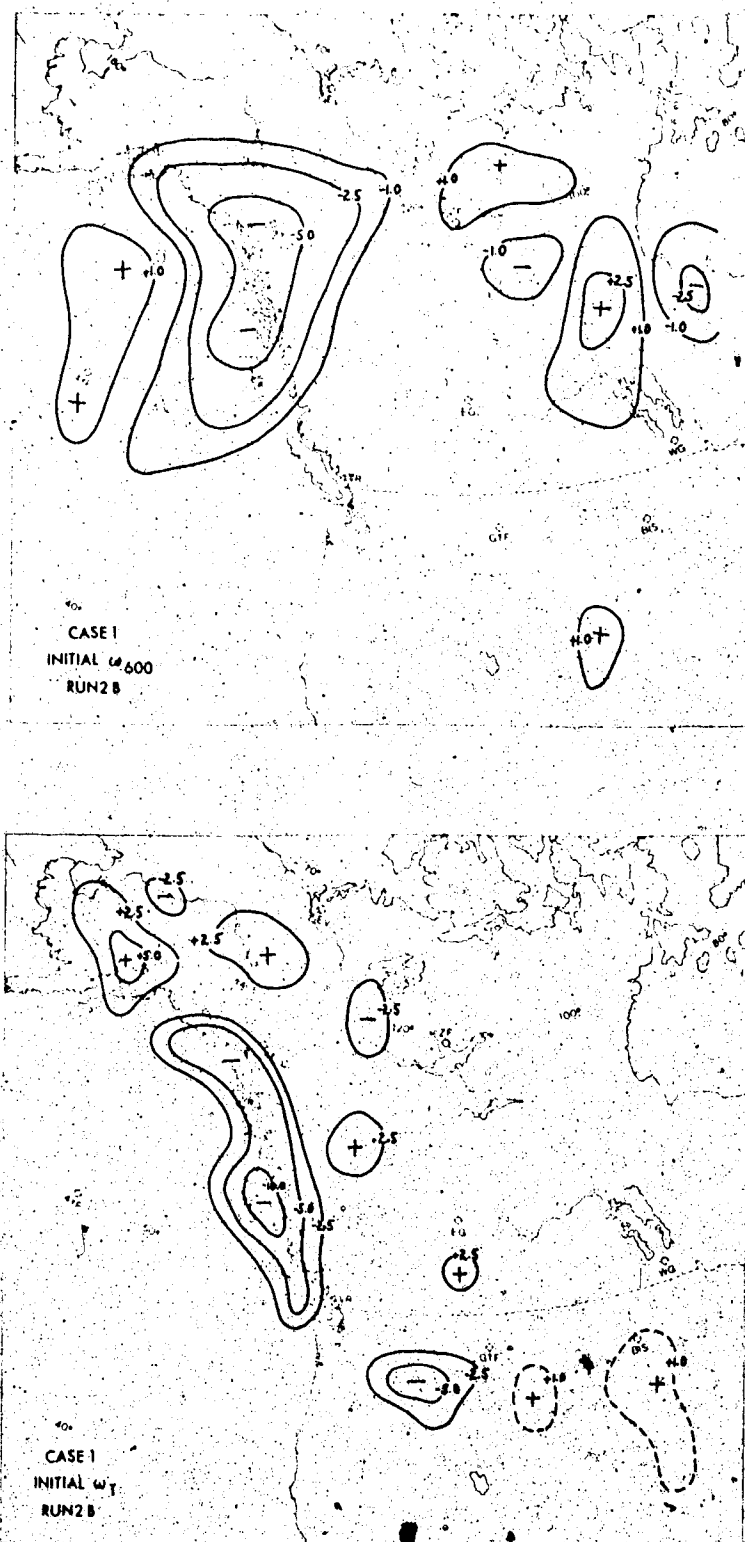


Figure 18. Orographically induced omega field at the surface (bottom) and the omega field at 600 mb (top) for the initial time in Run 2B. At the surface,  $w = -0.9\omega$  where  $w$  is the vertical velocity in  $\text{cm s}^{-1}$  and  $\omega$  is the 'vertical velocity' in microbars  $\text{s}^{-1}$ . At 600 mb,  $w = -1.27\omega$ . Negative values of  $\omega$  denote ascent while positive values denote subsidence.

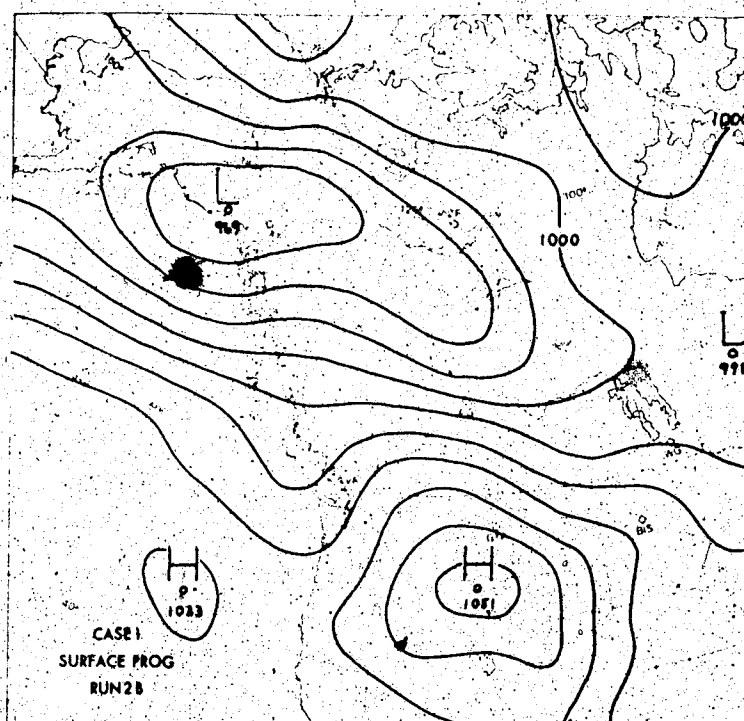
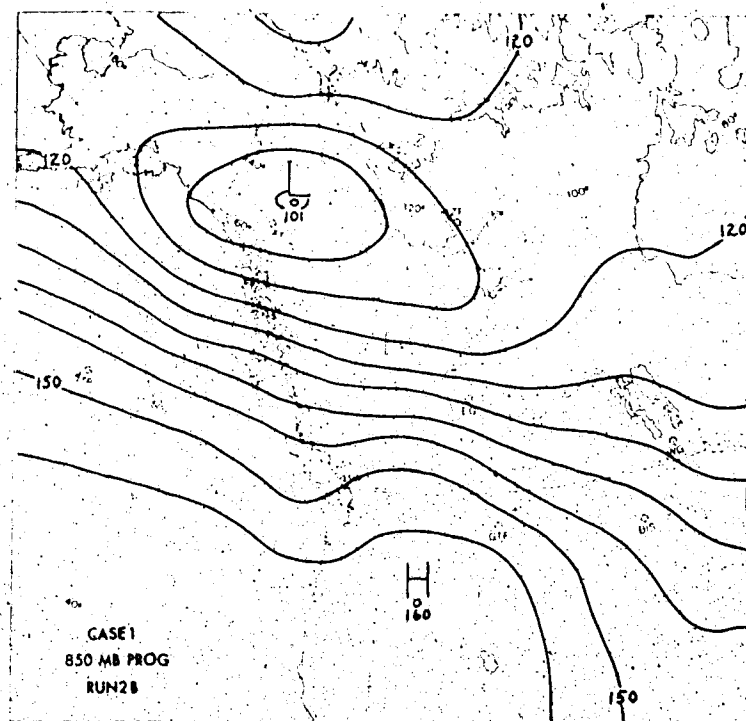


Figure 19. 12 hour forecast at 850 mb and at the surface with the orographic component of  $\omega_g$  only (Run 28).

present over Alberta at this time.

In Figure 19, the low level forecasts of Run 2B are shown, and there is some indication of an improvement over the fields forecast in Run 2A. The 850 mb trough which was observed to be moving through British Columbia in Run 2B is now considerably weakened and a lee trough is generated in northern Alberta. The rate of deepening of the 850 mb low is reduced, but the tendency is still of the wrong sign. The forecast surface pattern shows some evidence of the generation of a weak cyclone in northern Alberta, but the surface cyclone center in the southwestern Yukon is the dominant feature. Strong anticyclogenesis is also occurring in eastern Idaho. It is associated with the extensive area of strong ascent induced in that region at the lower boundary of the model (see Figure 18). This ascent results in the calculation of a large negative vorticity tendency at 850 mb through the term  $\int \frac{\partial \omega}{\partial p}$ .

When the frictional component of vertical velocity is included in Run 2C, a much more reasonable forecast is achieved. Figure 20 shows the full vertical velocity  $\omega_t + \omega_f$  at the initial time. Several features are of particular importance. The term  $\omega_f$  is quite large, as is evident from a comparison of Figures 18 and 20. Along the west coast of British Columbia,  $\omega_f$  is of the same sign as  $\omega_t$  and very strong ascent is induced in this area. Particularly noteworthy is the strong band of ascent





extending into the Pacific Ocean south of ship 4YP. This band is associated with the surface trough and frontal system indicated in Figure 9. The vertical velocities are quite large within this band, attaining peak values of about  $11 \text{ cm s}^{-1}$ . West of Edmonton, subsidence has been enhanced by the inclusion of friction. In many other areas,  $\omega_f$  is larger than and opposite in sign to  $\omega_t$ . This is most apparent in central Idaho where the orographic lift indicated in Figure 18 has been masked by the large frictionally-induced subsidence.

At 600 mb, the shape of the  $\omega$  pattern at the initial time is quite similar to that of Figure 18. A notable increase<sup>0</sup> in the middle level  $\omega$  field is evident however. At the center of the ascent area over Whitehorse (XY), the peak value was increased by about 30% owing to the enhanced low level ascent.

The forecast 850 mb and surface pressure fields for Run 2C are shown in Figure 21 where the effects of the frictional convergence are clearly indicated. At 850 mb the low in the Gulf of Alaska has been completely filled. In spite of the nearly correct height tendency forecast in this area, the formation of the lee trough in Alberta is still not very well handled. The forecast 850 mb height change at Edmonton was much less than the observed value (see Table 4). The RMS errors over Alberta were reduced from those of Runs 2A and 2B while over the whole map, this reduction was

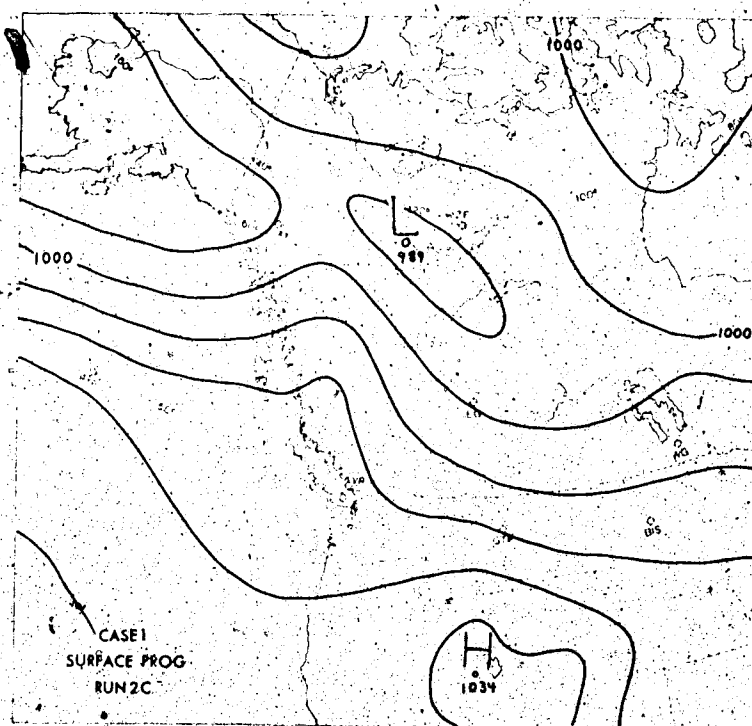
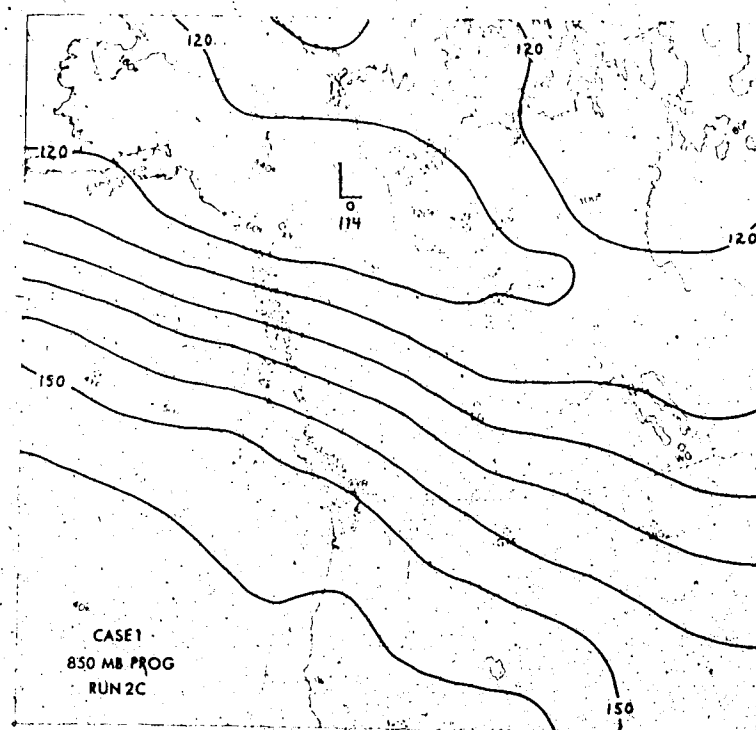


Figure 21. 12 hour forecast at 850 mb and the surface with full friction and orography at the lower boundary.

quite large at both 850 and 500 mb.

The surface pressure pattern also shows some improvement. A closed lee cyclone is clearly indicated although the depth and location of this feature are not quite correct. The effect of the change in sign of the field over Idaho is also quite evident, and the strong anticyclogenesis which was predicted there in Run 2B has been greatly reduced. As well the horizontal pressure gradients over the Pacific near ship 4YP compare quite favorably with those of the actual analysis for the forecast verification time (Figure 11) and they are an improvement over the strong gradients forecast in Runs 2A and 2B.

In the three runs described in this section, the importance of friction in the development of weather systems near the mountains is apparent. In the model, strong frictionally-induced ascent along the west coast of British Columbia combined with weaker ascent aloft results in the generation of anticyclonic vorticity at 850 mb and the approaching cyclone fills. There is however, a detrimental effect at 850 mb in the lee of the mountains. In Run 2C, the generation of anticyclonic vorticity due to frictional ascent at the lower boundary prevents the proper deepening of the 850 mb trough and surface cyclone in northern Alberta. Thus a slight adjustment to the frictionally-induced  $\omega$  field is necessary, and this is accomplished by modifying the manner in which the horizontal wind in the

boundary layer is parameterized.

#### 5.4.3 Small Frictional Vertical Velocity: Run 3

In this run, the importance of the magnitude of the frictional convergence in the numerical model is further demonstrated. In the calculation of  $\omega_f$ , the turning angles  $\alpha:10,20,40$  and the reduction factors  $r:.5,.2,.2$  were used with an extrapolated horizontal wind at the lower boundary. In addition, the unsmoothed terrain was used and the vertical velocity at the lower boundary originated at this terrain surface.

The forecast 850 mb and surface pressure fields for this run are shown in Figure 22 and the statistics are listed in Table 5. These statistics are compared with those of Run 1A since the two runs are similar in the sense that they both employ an unsmoothed topographical field and differ only in the amount of frictional convergence at the lower boundary. Run 3 is of interest because it is the worst low level forecast of any of the runs attempted and it is one of the worst at upper levels.

At 850 mb, the low in the Gulf of Alaska has rapidly deepened in the 12 hour period. While an 850 mb trough was formed over Alberta, the rate of intensification of this feature was too rapid as is evident in the field change forecast at Edmonton. The surface pressure forecast is a reflection of the inaccuracy at 850 mb. The lee cyclone was

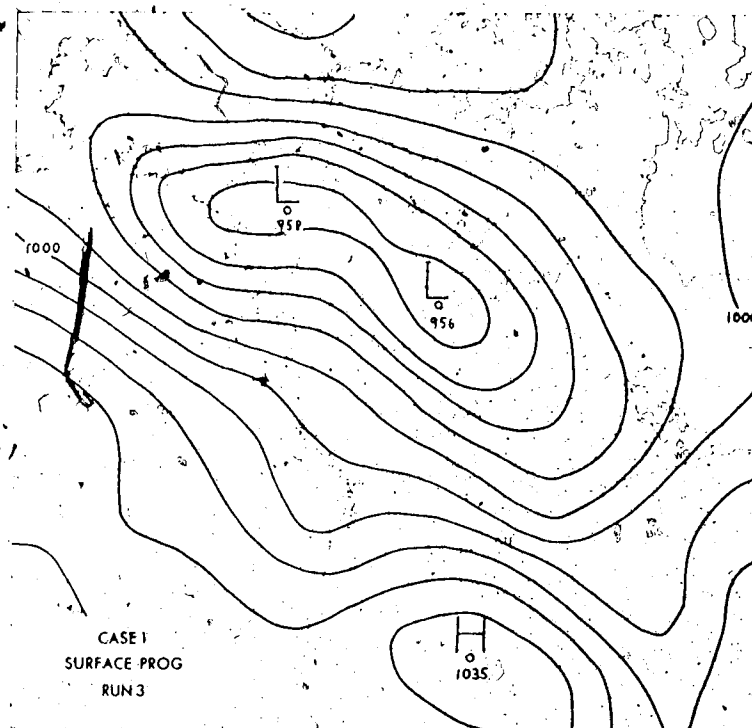
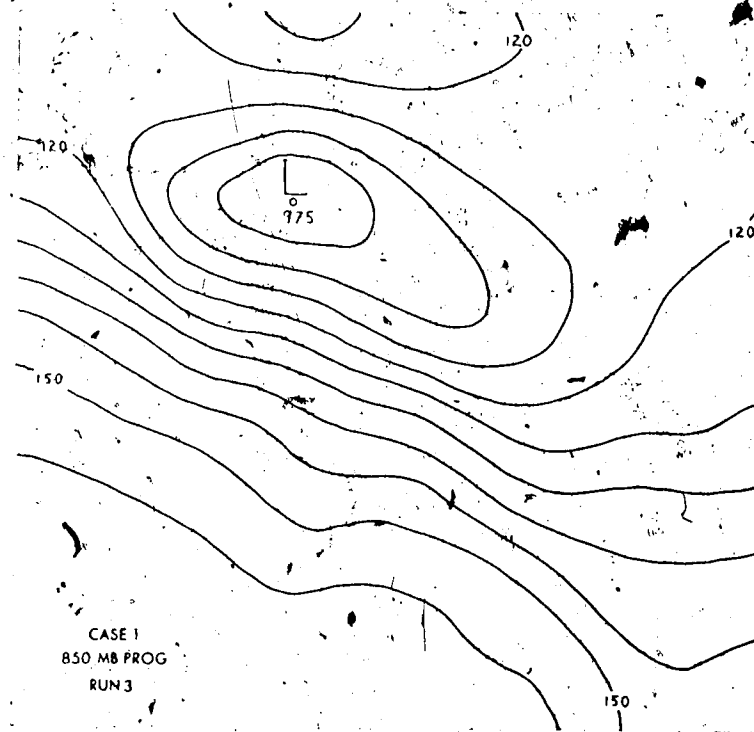


Figure 22. 12 hour forecast at 850 mb and at the surface with a small frictionally-induced  $\omega$  field at the lower boundary.

generated in approximately the correct position but it was forecast approximately 27 mb too deep. A similar error in the forecast of the pressure change at Edmonton is indicated in Table 5. When these statistics are compared with those of Run 1A, the differences are quite significant. Thus it

RMS ERRORS			FIELD CHANGES		
CASE 1	MAP/ALBERTA		FORECAST/ACTUAL		
RUN	850 mb (gpm)	500 mb (gpm)	850 mb (gpm)	500 mb (gpm)	MSL (mb)
3	47/70	37/66	-124/-100	55/35	-35/-14
1 A	20/16	31/58	-83/-100	80/35	-26/-14

Table 5. RMS errors and field changes at Edmonton for Run 3 compared with those of Run 1A.

is apparent that frictionally-induced ascent plays an important role in the rate of intensification of cyclones. If this ascent is not large enough to oppose the orographic subsidence in the lee of the mountains, which in this run is quite large with the unsmoothed terrain, there is generally strong vorticity production in the lee of the mountains resulting in the intense cyclogenesis observed.

#### 5.4.4 The 850 mb Wind in PBL Computations: Run 4

In all of the forecasts described to this point, the horizontal wind used in the lower boundary layer calculations was obtained by extrapolation from the upper level height fields. In this section, the results of an experiment are described in which the 850 mb geostrophic wind was used in the PBL. In Run 4, the turning angles and reduction factors were identical to those of Run 1B, and since the smoothed topography was also employed, Run 4 will be compared with Run 1B to illustrate the differences which occur in the numerical prediction when two different boundary layer winds are used.

Figure 23 shows the 850 mb and surface pressure fields forecast in Run 4. The low at 850 mb was moved inland in a correct manner but the rate of filling was quite slow. The troughing over Alberta was well defined at this level, but it was slightly underforecast both in terms of the magnitude of the height changes at Edmonton as well as the sharpness of the Alberta trough. At the surface, the lee cyclone is well-organized and it is forecast within 3 or 4 mb of its observed depth. However, the position of the center is about five hundred km northwest of the correct position.

When the statistics are compared with those of previous runs, it is seen that overall, Run 4 produced the best forecast with one notable exception at 850 mb over Alberta. At both 850 and 700 mb (not shown), Run 4 exhibited the



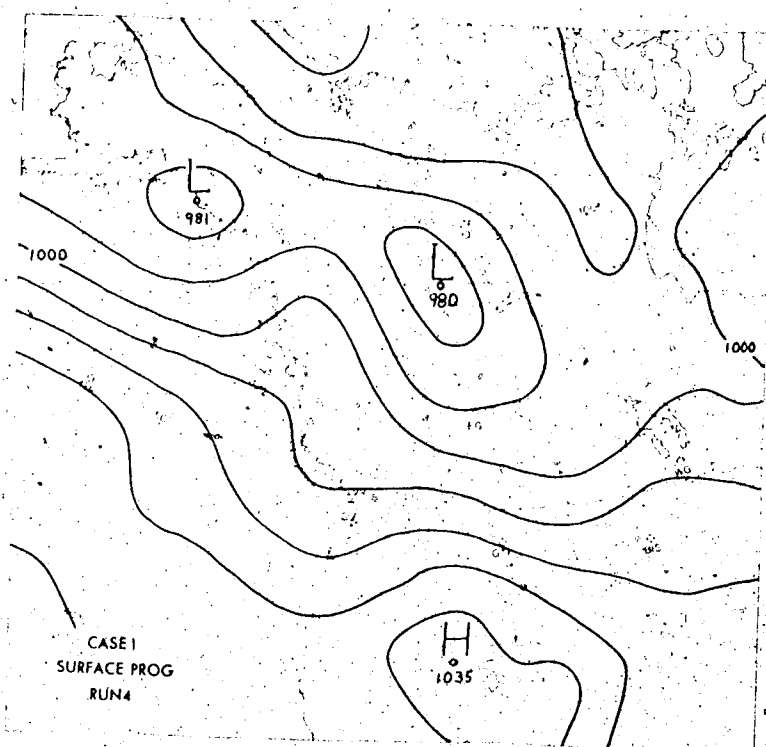
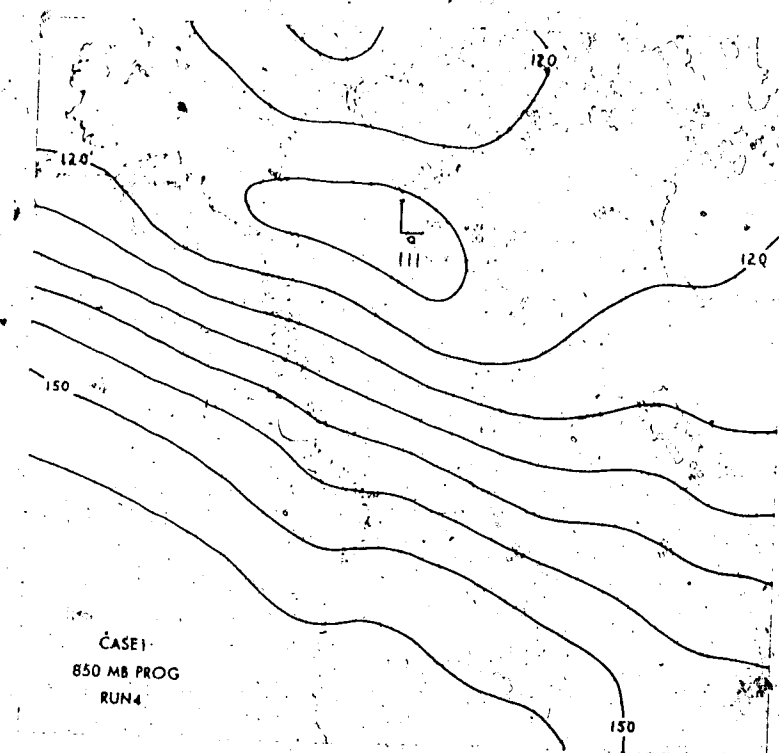


Figure 23. 12 hour forecast at 850 mb and at the surface with the 850 mb geostrophic wind used in boundary layer calculations.

CASE 1	RMS ERRORS		FIELD CHANGES		
	MAP/ALBERTA		FORECAST/ACTUAL		
RUN	850 mb (gpm)	500 mb (gpm)	850 mb (gpm)	500 mb (gpm)	MSL (mb)
4	15/24	29/54	-63/-100	55/35	-12/-14
1 B	19/36	32/53	-44/-100	52/35	-9/-14

Table 6. RMS errors and field changes at Edmonton for Run 4 compared with those of Run 1B.

lowest RMS errors over the whole map while at 500 mb the error was the second lowest over both Alberta and the whole map. The best agreement with the observed pressure change at Edmonton was also achieved with this run. These statistics are somewhat surprising because it was not expected that an 850 mb wind would provide a good approximation to the PBL wind, except perhaps in the higher mountainous areas. However the difference in the forecasts is likely due to the fact that the extrapolation was to terrain height since the thickness of the PBL is assumed to be zero in this model. A model formulated with a boundary layer of some finite thickness might be expected to yield a better forecast.

Since this run appears to generate the best set of statistics and gives a low level forecast which is reasonable, the lower boundary condition used in Run 4 is

tested in Cases 2 and 3 and the results are described below.

In all the runs done on Case 1, systematic errors were apparent as the model over-intensified the 500 mb trough and tended to displace the low level features somewhat to the north of the correct positions which are indicated in Figures 10 and 11. Similar errors were noted in the forecasts done on Cases 2 and 3 and the sources of these errors are discussed in Section 5.7.

#### 5.5 Case 2: March 5, 1972

The analysis of the initial and final conditions for this case are shown in Figures 24 and 25, and the results of two forecast runs are shown in Figures 26 and 27. The statistics generated from these forecasts are tabulated in Table 7. Two runs were attempted for each of Cases 2 and 3 to show the difference between two distinct sets of lower boundary conditions. (Run 1 is a forecast with the full lower boundary condition as tested in Run 4 of Case 1 and Run 2 has the flat and frictionless (simple) boundary of Run 2A.

Figure 24 shows the 850 and 500 mb analyses at the initial time in Case 2 (1200 GMT March 5, 1972). The prominent feature at 850 mb was the closed low near the Queen Charlotte Islands which was moving rapidly northeastward at that time. This feature was associated

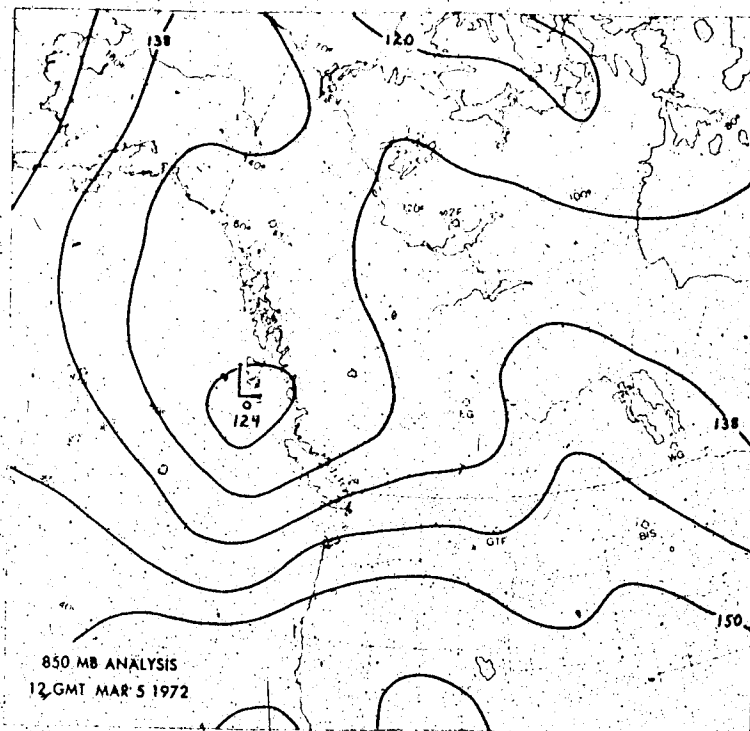
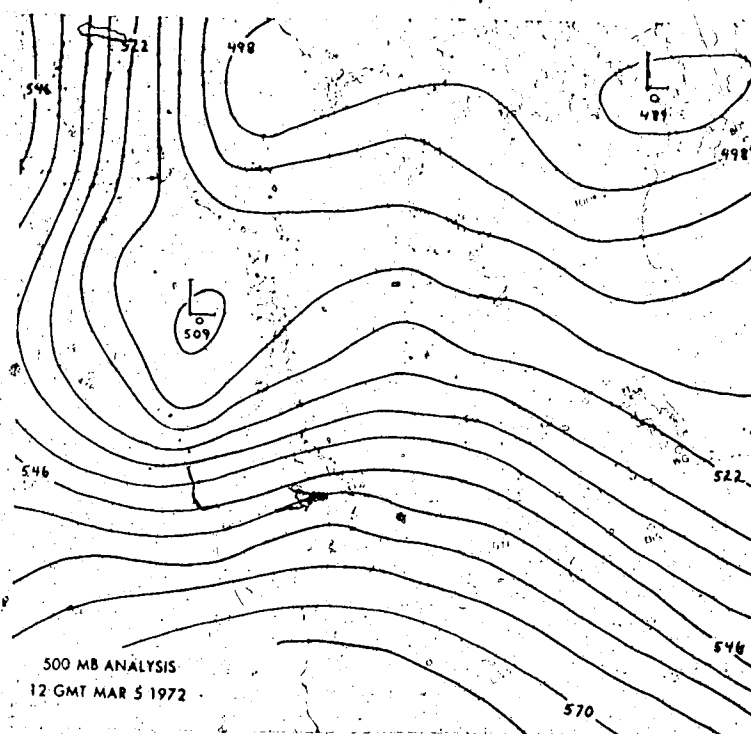


Figure 24. Analysis at the initial time at 850 mb and at 500 mb for Case 2.

with a 500 mb trough and low initially oriented along longitude  $140^{\circ}$  W. With the westerly flow present over the Rocky Mountains, there is some indication of the presence of a lee trough at 850 mb, extending from Edmonton to east of Great Falls (GTF) and thence southeastward through central Wyoming.

In the following twelve hour period, the 850 mb low continued moving east-northeast to lie on the Alberta British Columbia border as shown in Figure 25. The shape of this low and the associated trough became elongated with the major axis of the trough extending from southern Alaska through west-central Alberta, and thence essentially along the lee of the mountains through eastern Wyoming and Colorado. The position of a trough which had extended south of the initial 850 mb low, remained fixed during the period when the low moved inland. At 500 mb, the southern section of the trough swung eastward through about  $8^{\circ}$  of longitude while the northern portion of the trough remained fixed. Both the 850 and 500 mb lows deepened slightly in the 12 hour period.

The 12 hour forecasts of the 850 mb fields for the full and simple lower boundary conditions are shown in Figure 26. In Run 1, the overall appearance of the forecast pattern is quite similar to the actual verification field of Figure 24. The position of the low center was about 200 km north of its observed position, but the orientation of the trough was

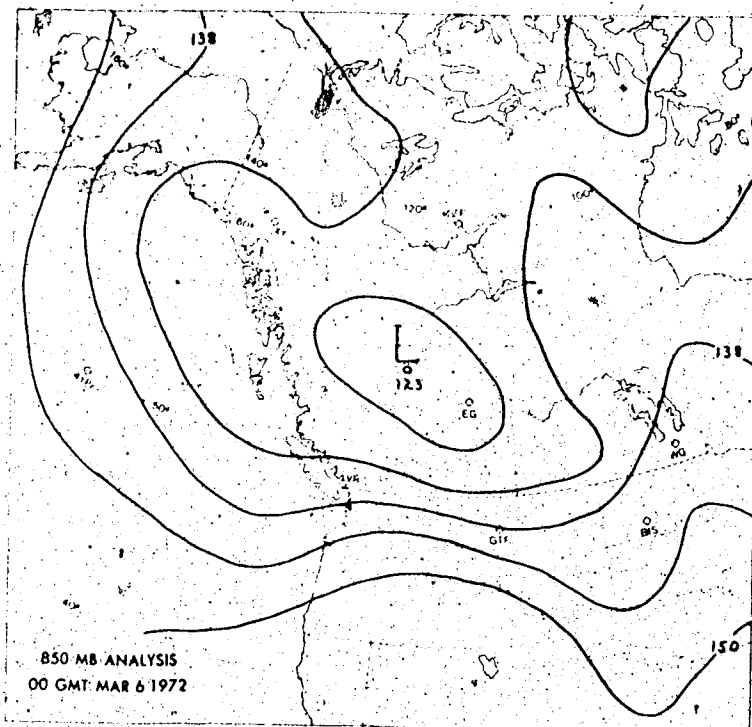
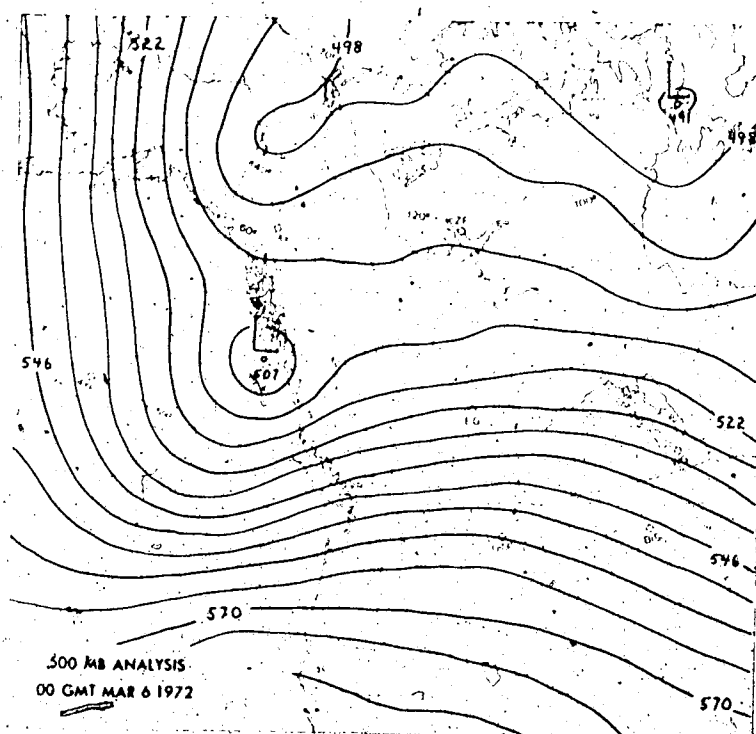


Figure 25. Analysis at verification time at 850 mb and at 500 mb.

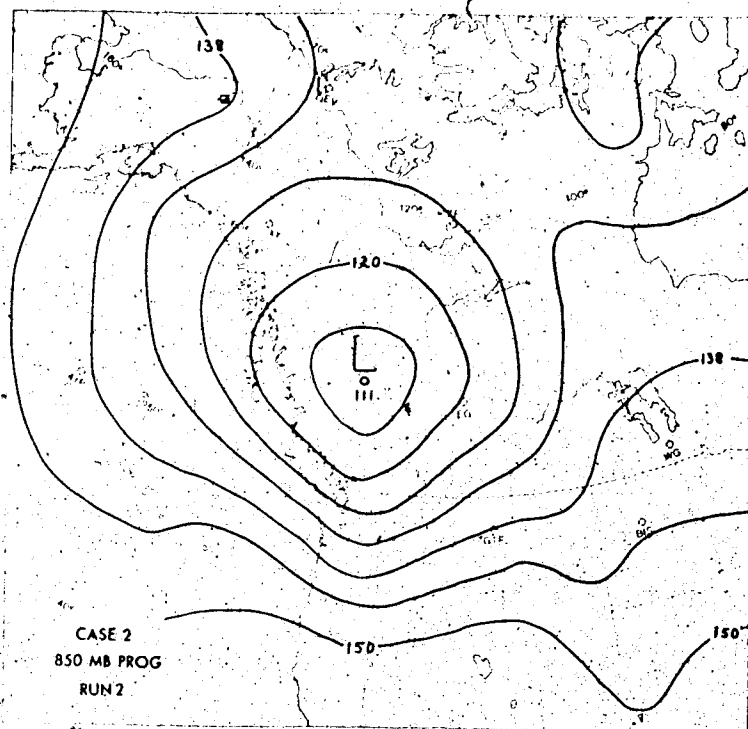
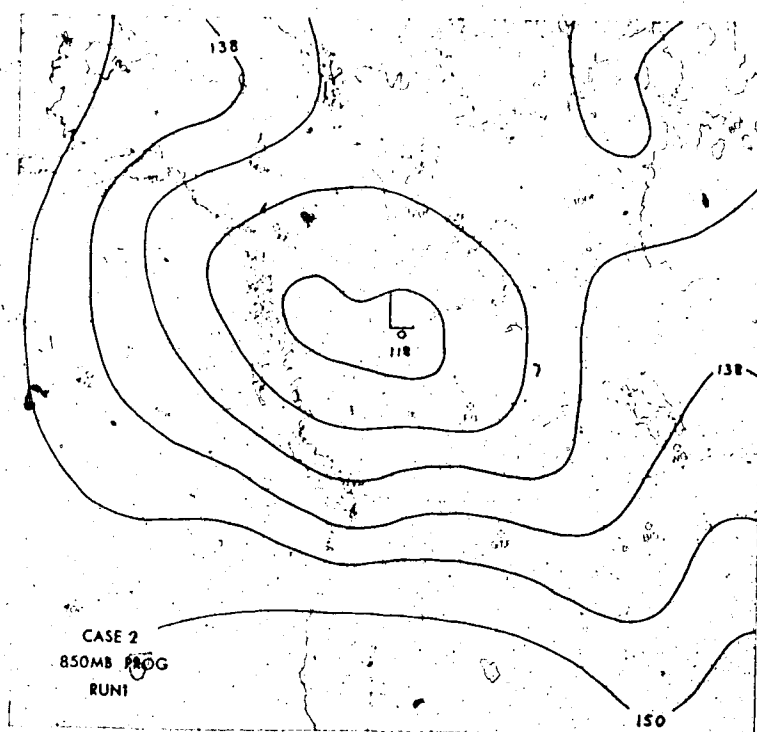


Figure 26. 850 mb forecasts with full lower boundary condition (Run 1) and flat frictionless boundary condition (Run 2).

quite similar to that of Figure 25. This is in contrast to the pattern forecast in Run 2 with the flat frictionless boundary condition discussed in Run 2A of Case 1. With no orographic or frictional influence present, an essentially circular low was forecast to move inland at a much slower speed than that observed. As well, the trough south of the low was forecast to move inland with the low in Run 2. In Run 1, frictional and orographic ascent combined to weaken and slow this feature in its passage through Washington. A weak ridge was maintained along a line through the Alberta-British Columbia border and south through western Montana.

The forecast depth of the 850 mb low and the intensity of the circulation were quite different in Runs 1 and 2. While the 850 mb low was deepened in both runs, the rate was not as large in Run 1 as in Run 2. The observed deepening of the center was only 10 gpm whereas in Run 1 a fall of 60 gpm was forecast. Without the presence of lower boundary effects to provide a control on the deepening rate, a change in depth of -140 gpm was forecast in Run 2.

The 500 mb forecast of Run 1 is shown in Figure 27 and the statistics pertaining to this case are given in Table 7. The error in the 500 mb geopotential pattern reflects the fact that the speed of the trough and 500 mb low were forecast to be too great. When Figures 27 and 25 are compared, it is seen that the southern portion of the major 500 mb trough was moved a distance of  $12^\circ$  longitude in 12



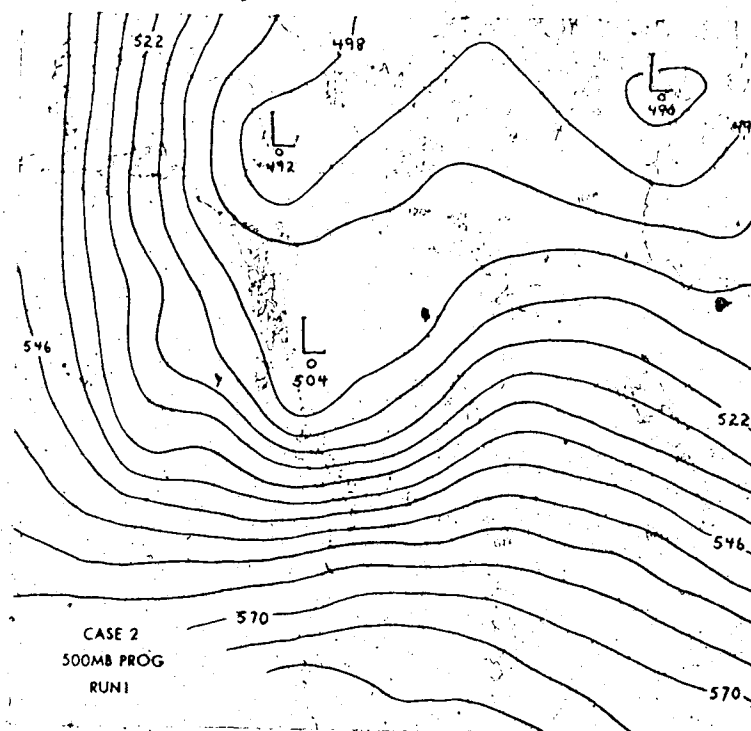


Figure 27. 500 mb forecast with full lower boundary condition.

CASE 2	RMS ERRORS		FIELD CHANGES		
	MAP/ALBERTA		FORECAST/ACTUAL		
RUN	850 mb (gpm)	500 mb (gpm)	850 mb (gpm)	500 mb (gpm)	MSL (mb)
1	24/43	27/53	-121/-117	-59/-31	-16/-15
2	40/78	39/74	-171/-117	-64/-31	-27/-15

Table 7. RMS errors and field changes at Edmonton for the full and simple lower boundary conditions of Case 2.

hours or 50% faster than the actual speed. As well, the low was forecast to deepen by 50 gpm instead of the observed 10 gpm. A similar error in the 500 mb field over Edmonton is indicated in Table 7 where the forecast change was approximately twice the observed. When the statistics for Runs 1 and 2 are compared at low levels, it is seen that a much better forecast was achieved with the full lower boundary condition. In fact the large 850 mb height and surface pressure changes were almost perfectly forecast in Run 1. With this lower boundary condition, significant skill is demonstrated.

#### 5.6 Case 3: April 27, 1974

The synoptic situation in this case differs significantly from that of the other two cases, and in contrast to Cases 1 and 2, only slight changes in the weather patterns occurred in the 12 hour forecast test period. The analyses at the initial time (0000 GMT April 27, 1974), are shown in Figure 28. Over the central portion of the map, the circulation at 500 mb was dominated by a closed low, the center of which was moving slowly eastward across Oregon and Idaho through a distance of approximately 300 km in 12 hours. As this feature began to cross the Rocky Mountain chain at the time of the analysis of Figure 28, the center appeared to accelerate and by the end of the 12 hour period it was located 500 km to the northeast, as

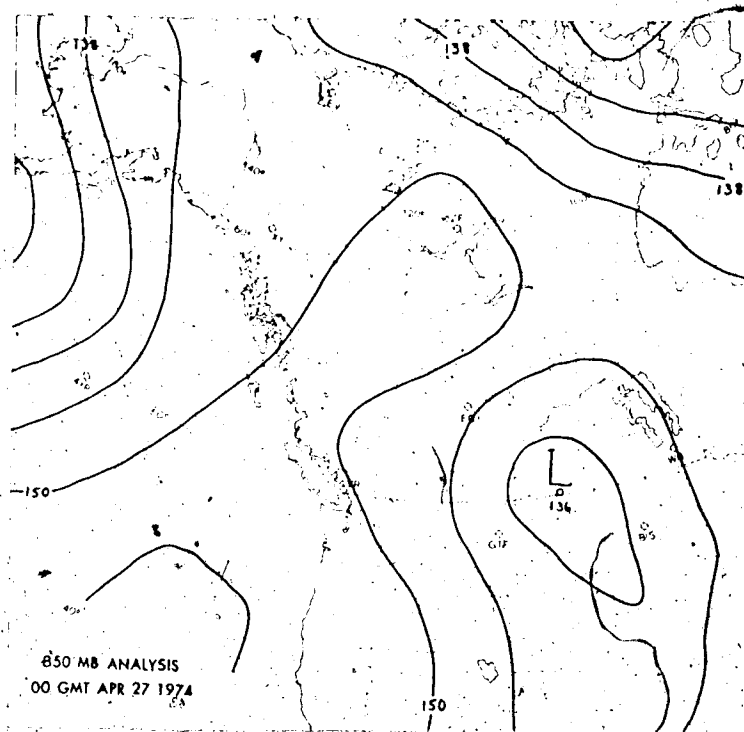
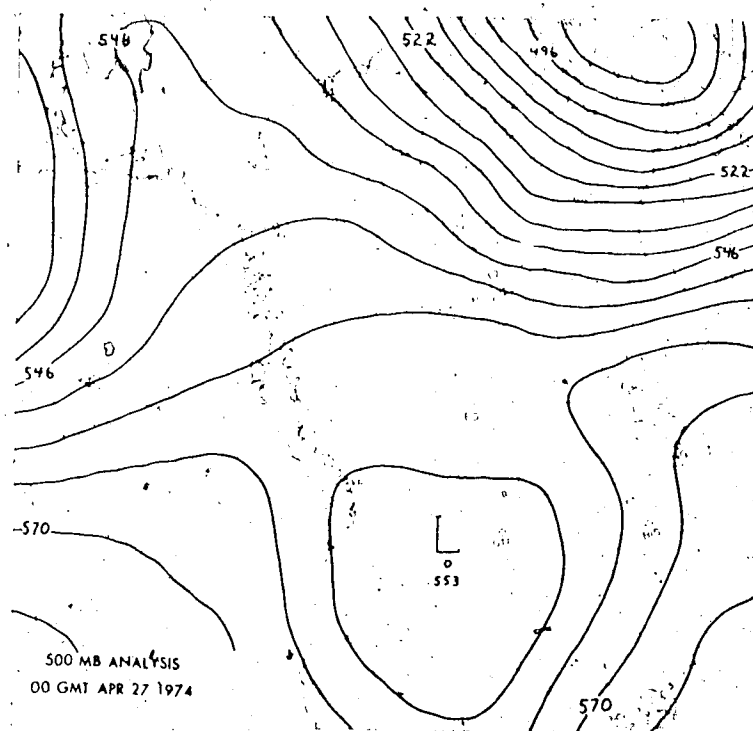


Figure 28. Geopotential analysis at the initial time at 850 mb and 500 mb for Case 3.

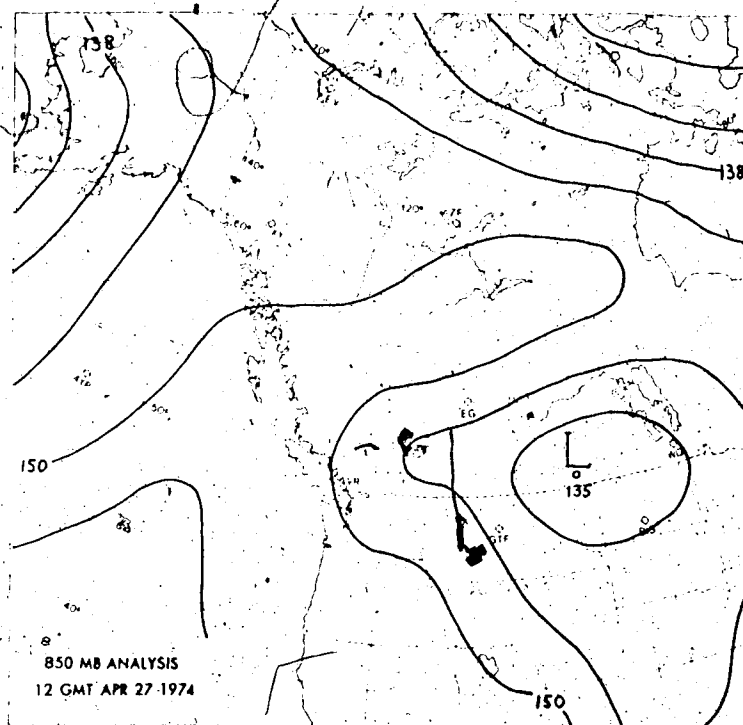
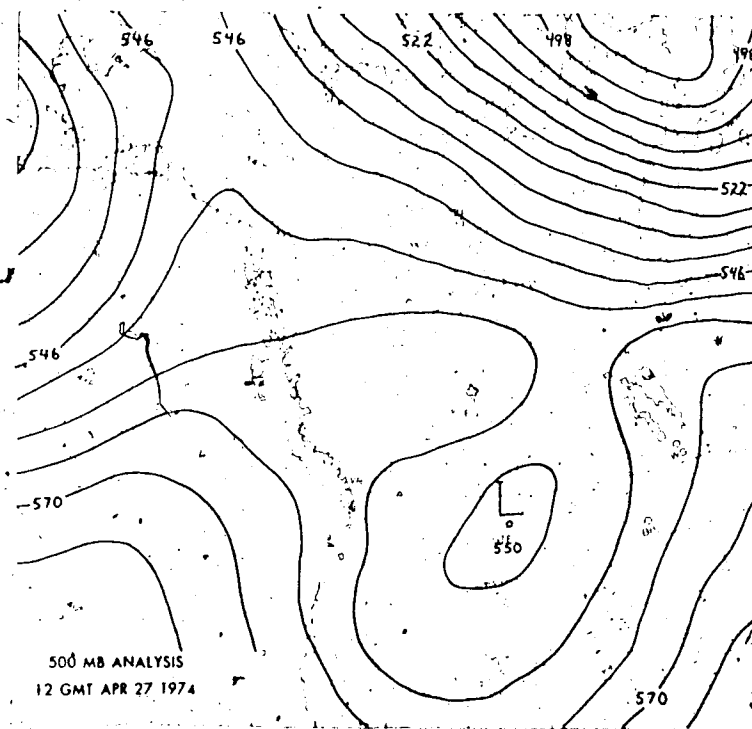


Figure 29. Geopotential analysis at the verification time at 850 mb and 500 mb for Case 3.

shown in Figure 29.

At low levels, southern Alberta was experiencing heavy snow and strong winds which may be partially attributable to the presence of the trough at 850 mb in that area. The low center shown at 850 mb in Figures 28 and 29 had formed several hours prior to this analysis time, and it did not move appreciably in the 12 hour period of this study. With the approach of the 500 mb low however, the weak trough analyzed to the west of the 850 mb low became quite sharp in 12 hours. This intensification, combined with the strong upslope gradient through southern Alberta at all levels, was largely responsible for the severe weather experienced.

The results of two forecast runs are shown in Figures 30 and 31 and the statistics are summarized in Table 8. The same sets of lower boundary conditions were tested in Case 3 as in Case 2. In Figure 30, the two 850 mb forecasts are compared. Run 1 with the full lower boundary condition shows a slight filling by 30 gpm of the 850 mb low. The sharpening trend of the southern Alberta trough is indicated, and this is slightly more pronounced than that forecast by Run 2. In Run 2, the 850 mb low was deepened by 30 gpm and the center of the low was shifted westward, closer to the 500 mb low center.

The results of Run 1 are shown in Figure 31. At 500 mb the motion of the low center was forecast well. Although the speed of movement of the low was slightly less than that

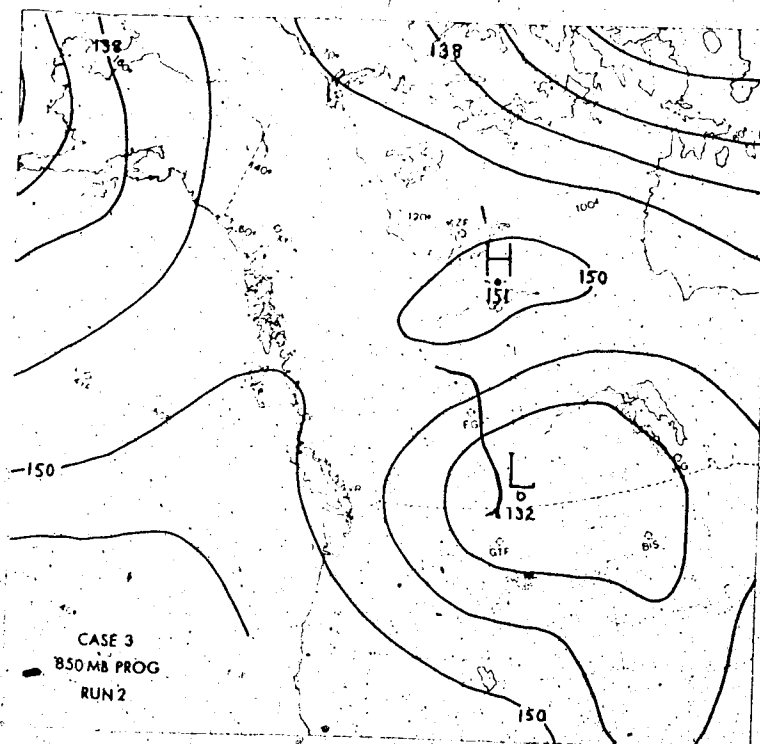
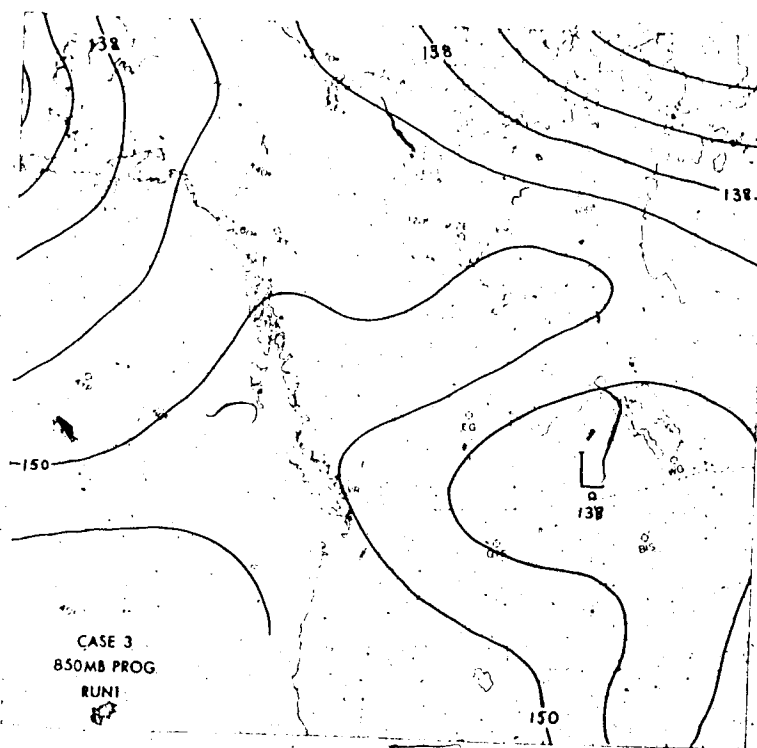


Figure 30. 850 mb forecasts with full lower boundary condition (Run 1) and the flat frictionless boundary condition (Run 2).

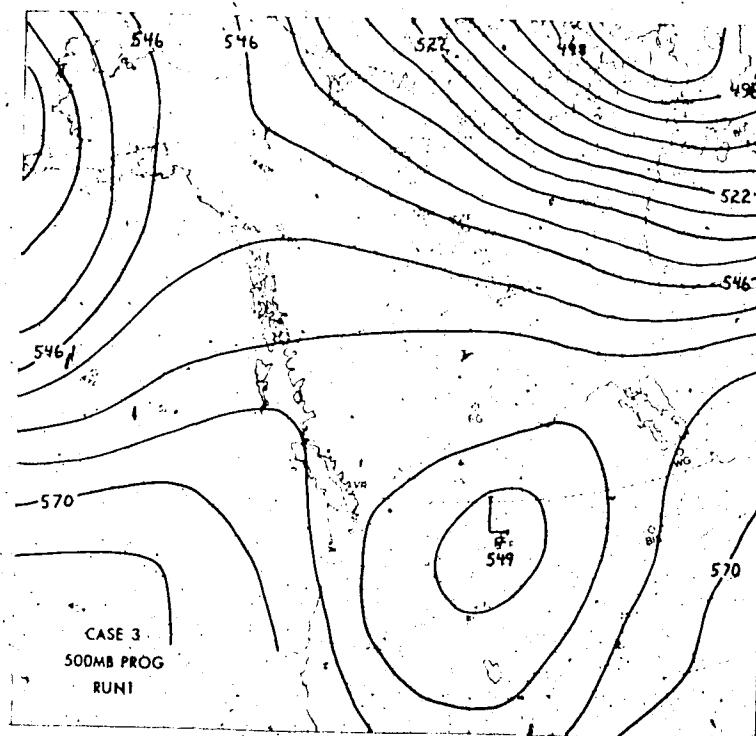


Figure 31. 500 mb forecast with the full lower boundary condition.

RMS ERRORS			FIELD CHANGES		
CASE 3	MAP/ALBERTA		FORECAST/ACTUAL		
RUN	850 mb (gpm)	500 mb (gpm)	850 mb (gpm)	500 mb (gpm)	MSL (mb)
1	14/13	17/12	20/19	-16/-10	7/5
2	19/35	15/22	-39/19	-39/-10	-5/5

Table 8. RMS errors and field changes at Edmonton for the full and simple boundary conditions of Case 3.

observed, the deepening of 40 gpm compares well with the observed deepening of 30 gpm. In Run 2 (not shown) the only major difference was that the low was forecast to deepen by over 70 gpm during the same period.

A comparison of the statistics in Table 8 shows much the same trend as that of the other two cases. With the full lower boundary condition, actual intensification is somewhat reduced at all levels. At 850 mb over Alberta, this resulted in a reduction of RMS errors by over 60% when compared to Run 2. At 500 mb, Run 1 again gave a better forecast over Alberta than did Run 2, although over the whole map, the flat frictionless lower boundary condition gave a marginally better forecast. The field changes at Edmonton were handled extremely well with the full lower boundary condition (Run 1) but quite poorly in Run 2 where the wrong trend was forecast at low levels.

In these statistics, one of the most apparent features is the fact that the RMS errors are generally much smaller than those of Cases 1 or 2. This may be partly due to the better analysis of the initial condition of Case 3 provided by the CMC objective analysis. However the major reason for the small error was that only a small 12 hour change in the weather systems occurred and no rapid movement or intensification of the weather systems was observed.

The results of this case verify the results noted above in the testing of Case 1. It is again evident that the



lower boundary condition has a major influence on numerical prediction. The particular boundary condition used in Run 1, with 850 mb geostrophic winds employed in the boundary layer computations, is a parameterization which provides an accurate 12 hour forecast.

### 5.7 Systematic Errors in the Model

One of the most serious errors in the model was the inaccurate forecast of the upper level isobaric fields. This error was largest at 300 mb but in Case 1 the 500 mb error was also of some significance. While these fields themselves were not of interest in this study, errors at these levels appeared to be the cause of systematic errors at lower levels. When the 300 mb forecast fields were analyzed, the presence of a small amplitude wave pattern of short wave length (2 or 3 grid lengths) was noted. This pattern was most evident in Case 1 but was also present with reduced amplitude in Cases 2 and 3. There was a very slight indication of a similar occurrence at 500 mb in all cases. The amplification of the wave pattern with time indicates that some form of computational instability may have been present in the model.

When RMS errors at 300 mb were computed, they were observed to be much larger than the error calculated at lower levels. In the runs of Case 1, the RMS error over the whole map ranged between 70 and 90 gpm, while over Alberta

this error increased to 200 gpm or higher in many of the runs. For Cases 2 and 3 the RMS errors were much smaller at 300 mb, dropping to around 80 gpm over Alberta in Case 2 and to 30 to 40 gpm in Case 3.

To estimate the effect of large errors at 300 mb in the extrapolated surface pressure field, the extrapolation program was tested on real data. It was observed that the direct effect was essentially below detection and that changes in the 300 mb height of 200 gpm resulted in a change in the extrapolated pressure of only 0.5 mb. Thus even though the 300 mb field may be in serious error, the surface pressure field is not directly affected by this.

Errors in the geopotential fields at lower levels are induced by the errors aloft because all levels of the model are related through the omega field. Because of the intense spurious wave pattern induced at 300 mb, large vertical velocities are generated at 400 mb through the solution of the omega equation. Since this field is influential in baroclinic development at 500 mb through the divergence term of the vorticity equation, the error at 300 mb eventually propagates to 500 mb and perhaps even lower with time. In Case 1 for example, the 500 mb trough overintensifies as it moves inland. This occurs because of an incorrect forecast of the high level  $\omega$  fields, apparently caused by errors at 300 mb. Since the major region of 500 mb error was over the southern Yukon, there is a tendency for the

extrapolation of an area of artificially low pressure in the northern portions of the grid. Hence the surface lee cyclone and trough tended to be systematically shifted northward in Case 1, in spite of a quite accurate forecast at 850 mb.

There are two possible reasons for the instability at 300 mb. A careful examination of the initial 300 mb field generated by the objective analysis program in Case 1 showed that a strong wind jet of  $78 \text{ m s}^{-1}$  was located directly above the 500 mb trough in the Gulf of Alaska. From a consideration of the radiosonde station reports of the 300 mb wind as well as the CMC 500 mb analysis in that area, a wind of this magnitude appeared to be about two times too large. This difficulty with the analysis is believed to have been caused by the inability to provide good 300 mb bogus data in that region. With the CFL condition (equation 4.10) barely satisfied at the initial time, the jet may strengthen to the point that the stability criterion is violated. Thus, analysis errors at the initial time, causing instability to be initiated, may be one reason for the large error at 300 mb and thereby the contamination of the forecast at lower levels.

A second reason for the errors at 300 mb is the specification of the lateral boundary condition for the vorticity equation. As Charney et al (1950) originally indicated, a sufficient condition for the solution of the

vorticity equation is that the height field be specified on all lateral boundaries and the vorticity field on the inflow boundary. In the model used in this study, the vorticity is specified on all lateral boundaries, including the outflow boundary, by means of the observed vorticity change (as obtained from the observed height change) over a 12 hour period. This change is assumed to be linear with time and on the outflow boundary, an inconsistency results which can be described in terms of a mismatch between the vorticity being advected towards the boundary and the vorticity being carried through the boundary by the boundary condition. The result of this mismatch is that the vorticity not carried through the boundary is reflected back into the grid at the outflow boundary. This phenomenon is described by Shapiro and O'Brien (1970) who give an example in which such a mismatch causes the formation of large amplitude noise in the vorticity field at the outflow boundary. In a paper by Rennick (1973), several experiments were described in which such a reflection caused the generation of two grid length oscillations in the height and vorticity fields.

Thus it appears that the oscillations observed in the 300 mb field in the forecasts of this study may have been caused by an incorrect specification of the outflow boundary condition. At 300 mb the vorticity advection is large because of the strong gradients present at that level with the result that the reflection problems are most pronounced at that level.

There are several methods whereby these problems are eliminated, the best being a Lagrangian advection scheme described by Shapiro and O'Brien (1970) in which the vorticity on the outflow boundary is specified to be that advected by the model. The alternative in most models is the use of spatial smoothing to eliminate the reflected noise. Although smoothing was used in the current study, it did not appear to be sufficient to remove the noise completely. The smoothing was applied to the vorticity field rather than the geopotential field and this also may have been a mistake. However further testing of solutions to this problem were beyond the scope of this study. Certainly if this type of model were to be used for extended length forecasts, an improvement in the specification of the lateral boundary condition would be necessary. It appears that an advection scheme for the outflow boundary could suffice.

## CHAPTER VI

## SUMMARY AND CONCLUSIONS

A four-level model of the atmosphere was formulated, in which the quasi-geostrophic vorticity and omega equations were solved to obtain short term prediction of atmospheric motions over Western Canada. These equations, with pressure as the vertical coordinate, were solved numerically on a grid encompassing Western Canada, the Yukon, parts of the Northwest Territories, Alaska, the Eastern Pacific Ocean and the northwestern United States. The grid point spacing was 200 km. To ensure non-linear computational stability, it was found necessary to employ the Adams-Bashforth time stepping procedure with a step length of one-half hour. Three synoptic situations were chosen in which some degree of cyclogenesis in the lee of the Rocky Mountains had occurred. Using an objective analysis scheme, the data were analyzed at 850, 700, 500 and 300 mb for input in the model.

The data were obtained from the Northern Hemispheric Data Tabulation summaries for the first two cases, bogus data being introduced into the objective analysis program in the data sparse regions of the Eastern Pacific. In the third case, the initial data consisted of the output of the objective analysis program used by the Canadian Meteorological Center in Dorval, Quebec. This data was interpolated to the grid used in this study from the hemispheric grid data employed at CMC.

Twelve hour forecasts were computed for each of the three cases in order to test different parameterizations of the lower boundary condition. Extensive testing of several types of lower boundary condition was carried out on Case 1 while in Cases 2 and 3, only limited testing was done to verify the results observed in the forecasts of Case 1. The vertical velocity at the lower boundary,  $\omega_g$ , consisted of orographic and frictional components, calculated using the geostrophic wind within the model. In the calculation of the frictional component of  $\omega_g$ , the geostrophic wind was modified to simulate the wind near the bottom of the planetary boundary layer. For purposes of comparison, forecasts were also computed with a flat, frictionless lower boundary where the vertical velocity was zero.

Vertical velocities in the boundary layer were calculated using two different idealized terrain surfaces with different amounts of smoothing. The vertical velocity

was assumed to originate at the terrain surface but for comparison, a forecast was computed in which the vertical velocity was assumed to originate at the 1000 mb surface. In order to obtain a quantitative assessment of the many forecasts, a root-mean-square error between the forecast and the verification fields was calculated. As well, the forecast changes of the geopotential height and surface pressure fields near Edmonton, Alberta were compared with the observed changes at Edmonton.

It was found that the pressure level at which the boundary layer vertical velocity is assumed to originate is important in the numerical model. Differences in the smoothness of the terrain field resulted in slightly different forecasts. A more accurate result was achieved if the maximum slope of the terrain was reduced and small scale irregularities in the terrain were removed by spatial smoothing. If the boundary layer vertical velocity originated at the 1000 mb surface, the forecast over Alberta deteriorated noticeably.

A forecast run with only orographically-induced vertical velocity at the lower boundary was shown to exhibit comparatively little skill while if friction was introduced, a much more accurate prognosis was achieved. Frictional vertical velocities had to be quite large to obtain an accurate forecast. Thus it appears that frictional effects are at least as important as large scale orographic lift and



subsidence, in governing the behavior of weather systems near the Canadian Rocky Mountains. This is in broad agreement with the results of Newton (1956), who found that friction is the dominant factor in the first few hours of lee cyclogenesis. In the current model, the absence of any frictional or orographic effects results in a poor forecast.

It appeared that the use of an 850 mb geostrophic wind, rather than a wind extrapolated to the lower boundary, resulted in a slightly more accurate forecast. It is probable however, that more extensive testing of the extrapolation technique, and improved parameterization of the frictionally-induced vertical velocities should result in the attainment of yet more accurate forecasts.

This study has demonstrated that some aspects of the lee cyclogenesis process can be successfully duplicated with a multi-level quasi-geostrophic model. In forecasting the lee cyclone, it is of utmost importance to formulate a lower boundary condition in which frictional effects are properly parameterized. Middle to upper tropospheric flow as well as that at lowest levels is modified if boundary layer effects are properly taken into account.

## BIBLIOGRAPHY

- Arakawa, A., 1966: Computational design for the long term numerical integrations of the equations of atmospheric motion. J. Computational Phys., 1, 119-143.
- Asselin, R.A., 1966: A technique for designing smoothing operators. Dept. Of Transport, Meteorological Branch, CIR-4417, TEC-615, 30 pp.
- Bergthorsen, P. and B. Doos, 1955: Numerical weather map analysis. Tellus, 7, 329-340.
- Berkofsky, L. and E.A. Bertoni, 1955: Mean topographic charts for the entire earth. Bull. Amer. Meteor. Soc., 36, 350-354.
- Cressman, G.P., 1959: An operational objective analysis program. Mon. Wea. Rev., 87, 367-374.
- \_\_\_\_\_, 1960: Improved terrain effects in barotropic forecasts. Mon. Wea. Rev., 88, 327-342.
- \_\_\_\_\_, 1963: A three level model suitable for daily numerical forecasting. National Meteorological Center Technical Memorandum No. 22, U.S. Department of Commerce Weather Bureau, Washington, D.C., 22 pp.
- Danard, M.B., 1966: A quasi-geostrophic numerical model incorporating effects of release of latent heat. J. Appl. Meteor., 5, 85-93.
- \_\_\_\_\_, 1971: A numerical study of the effects of long wave radiation and surface friction on cyclone development. Mon. Wea. Rev., 99, 831-839.
- Egger, J., 1972: Incorporation of steep mountains into numerical forecasting models. Tellus, 24, 324-335.

-----, 1974: Numerical experiments on lee cyclogenesis. Mon. Wea. Rev., 102, 847-860.

Gates, W.L., 1960: Notes on the suppression of the oscillation (weak instability) of first-forward-then-centered time differences in numerical integration. J. Meteor., 17, 572-574.

Gerrity, J.P., 1972: A note on the computational stability of the two step Lax-Wendroff form of the advection equation. Mon. Wea. Rev., 100, 72-73.

Glahn, H.R. and G.W. Hollenbaugh, 1969: An operationally oriented small scale 500 millibar height analysis program. U.S. Department of Commerce, Essa Technical Memorandum WBTM TDL 19, 18 pp.

Greystone, P., 1962: The introduction of topographic and frictional effects into a baroclinic model. Quart. J. Roy. Meteor. Soc., 88, 256-270.

Haltiner, G.J., 1971: Numerical weather prediction. John Wiley and Sons, Inc., New York and Toronto, 317 pp.

-----, L.C. Clarke and G.E. Lawniczak, 1963: Computation of large scale vertical velocity. J. Appl. Meteor., 2, 242-259.

Hess, S.L., 1959: Introduction to theoretical meteorology, Holt, Rinehart and Winston, New York., 362 pp.

Hill, G.E., 1968: Grid telescoping in numerical weather prediction. J. Appl. Meteor., 7, 29-38.

Lilly, D.K., 1965: On the computational stability of numerical solutions of time-dependent non-linear geophysical fluid dynamics problems. Mon. Wea. Rev., 93, 11-26.

Lorenz, E.N., 1955: Available potential energy and the maintenance of the general circulation. Tellus, 7, 157-167.

- Molenkamp, C.R., 1968: Accuracy of finite-difference methods applied to the advection equation. J. Appl. Meteor., 7, 160-167.
- Newton, C.W., 1956: Mechanisms of circulation change during a lee cyclogenesis. J. Meteor., 13, 528-539.
- Panofsky, H.A. and G.W. Brier, 1968: Some applications of statistics to meteorology. Pennsylvania State University, University Park, Pennsylvania, 224 pp.
- Pedersen, K., 1963: On quantitative precipitation forecasting with a quasi-geostrophic model. Geofys. Publ., 25, 25 pp.
- Petterssen, S., 1956: Weather analysis and forecasting, Vol 1. McGraw-Hill Book Company, New York, 428 pp.
- \_\_\_\_\_, D.L. Bradbury and K. Pedersen, 1962: The Norwegian cyclone model in relation to heat and cold sources. Geofys. Publ., 24, 243-280.
- Rennick, M.A., 1973: Boundary conditions for a barotropic forecast model. Summary Reports-Fellowship in Scientific Computing, NCAR Tech. Note TN/PROC-90 109-129.
- Sawyer, J.S., 1959: The introduction of the effects of topography into methods of numerical forecasting. Quart. J. Roy. Meteor. Soc., 85, 31-43.
- Schram, G.R., 1974: The influence of orography and surface friction on synoptic scale vertical motions over western Canada. M.Sc. Thesis, Univ. Of Alberta.
- Shapiro, M.A. and J.J. O'Brien, 1970: Boundary conditions for fine mesh limited-area forecasts. J. Appl. Meteor., 9, 345-349.
- Stuart, D.W., 1964: A diagnostic study of the synoptic scale vertical velocity motion and its contribution to mid-tropospheric development. J. Appl. Meteor., 3, 669-684.

\_\_\_\_\_, 1974: A comparison of quasi-geostrophic vertical motions using various analyses. Mon. Wea. Rev., 102, 363-374.

Thompson, P.D., 1961: Numerical weather analysis and prediction. MacMillan and Co., New York, 166 pp.

\_\_\_\_\_, and W.L. Gates, 1965: A test of numerical prediction methods based on the barotropic and two parameter baroclinic models. J. Meteor., 13, 127-141.

Wiin-Nielsen, A., 1959: On certain integral constraints for the time-integration of baroclinic models. Tellus, 11, 45-59.

## APPENDIX A

## THE AITKEN POLYNOMIAL

Given the set of  $n+1$  points  $\{x_0, f(x_0)\}, \{x_1, f(x_1)\}, \dots, \{x_n, f(x_n)\}$ , the  $n$ 'th order Aitken polynomial which interpolates this set is defined by:

$$P_{0, \dots, m, n} = \frac{1}{x_n - x_m} \text{DET} \begin{pmatrix} P_{0, \dots, m} & x_m - x \\ P_{0, \dots, m-1, n} & x_n - x \end{pmatrix} \quad (\text{A.1})$$

Using this result, a second-order parabolic interpolation of the function,  $f(x)$  is:

$$P_{0,1,2} = \frac{1}{x_2 - x_0} \left[ (x_2 - x) P_{0,1} - (x_1 - x) P_{0,2} \right] \quad (\text{A.2})$$

where

$$P_{0,1} = \frac{1}{x_1 - x_0} \left[ (x_1 - x) f(x_0) - (x_0 - x) f(x_1) \right] \quad (\text{A.3})$$

and

$$P_{02} = \frac{1}{x_2 - x_0} [(x_2 - x) f(x_0) - (x_0 - x) f(x_2)] \quad (A.4)$$

The first derivative of  $P_{012}$  with respect to  $x$  is simply:

$$P'_{012} = \frac{1}{x_2 - x_1} [(x_2 - x) P'_{01} - (x_1 - x) P'_{02} - P_{01} + P_{02}] \quad (A.5)$$

where  $P'_{01} = \frac{1}{x_1 - x_0} [f(x_1) - f(x_0)]$

and  $P'_{02} = \frac{1}{x_2 - x_0} [f(x_2) - f(x_0)]$

The second derivative  $P''_{012}$  reduces to:

$$P''_{012} = 2 \left( \frac{P'_{02} - P'_{01}}{x_2 - x_1} \right) \quad (A.6)$$

In the numerical model, the  $\omega$  field is assumed to have a parabolic profile with respect to pressure and the first and second derivatives of  $\omega$  are obtained from equations (A.3) to (A.6) where  $p_i = x_i$  and  $\omega_i = f(x_i)$ . Then given the omega field ( $\omega_0, \omega_1, \omega_2$ ) at three levels ( $P_0, P_1, P_2$ ), the first derivative of  $\omega$  at level  $P$  can be shown to be of the finite-difference form:

$$\begin{aligned} \frac{\partial \omega}{\partial P} = \frac{1}{P_2 - P_1} & \left[ \frac{1}{P_1 - P_0} \{ \omega_1 (P_0 + P_2 - 2P) - \omega_0 (P_1 + P_2 - 2P) \} \right. \\ & \left. - \frac{1}{P_2 - P_1} \{ \omega_2 (P_0 + P_1 - 2P) - \omega_0 (P_1 + P_2 - 2P) \} \right] \end{aligned} \quad (A.7)$$

while the second derivative is simply:

$$\frac{\partial^2 \omega}{\partial p^2} = \frac{2}{p_2 - p_1} \left( \frac{\omega_2 - \omega_0}{p_2 - p_0} - \frac{\omega_1 - \omega_0}{p_1 - p_0} \right) \quad (\text{A.8})$$

It may be readily verified that if these derivatives are evaluated at pressure  $p_1$  and if the differences  $p_2 - p_1$  and  $p_1 - p_0$  are equal, the standard centered-difference forms for the first and second derivatives are obtained.

As well as using the Aitken polynomial to interpolate the  $\omega$  field, a third-order form  $P_{0123}$  is used to approximate the logarithmic variation of geopotential height with pressure in the vertical. This third-order polynomial is then used to extrapolate the mean sea level pressure to zero geopotential height. For this case the dependent variable is the pressure and the independent variable is the height of the four isobaric surfaces: 850, 700, 500 and 300 mb above each point in the horizontal grid.

In order to obtain an estimate of the error associated with the use of the interpolating polynomial to extrapolate surface pressures, the technique was tested on a randomly chosen set of 18 radiosonde ascent reports. The geopotential heights of the four isobaric surfaces were used in the program and the pressure at the height above mean sea level of the radiosonde station was extrapolated. This pressure was then compared with the actual station pressure reported at the radiosonde station. The deviations from the



observed pressure were in the range of zero to six mb and the standard deviation for the 18 soundings (at 10 different stations) was calculated to be 2.6 mb. This error is assumed to be the approximate error existing in the extrapolation of the mean sea level pressure maps in the discussions in Case 1.

## APPENDIX B

## SPATIAL SMOOTHING

Small scale irregularities are introduced into meteorological fields by the numerical techniques used in the objective analysis programs. These irregularities are often described as noise, which is superimposed upon the meteorologically significant wave patterns. Noise of wave length two-grid-lengths or less is a particular problem since such noise is aliased into the longer wave patterns. When numerical prediction of the meteorological waves is attempted, these aliased short waves will often tend to amplify with time, thereby distorting or obscuring the meteorological phenomena.

Even if this noise is not initially present, it may be introduced into the prediction because of the truncation errors associated with the finite-difference representation

of the partial derivatives in the meteorological equations. Thus it is desirable to remove the noise initially and perhaps periodically from the fields. This is accomplished by means of spatial smoothing.

The theory of smoothing techniques will not be described here. The reader is referred to discussions in Haltiner (1971) and Asselin (1966). A two-dimensional smoothing operator may be written in finite-difference form as:

$$\bar{f}_{ij} = f_{ij} + S/4 \nabla^2 f_{ij} \quad (B.1)$$

where  $\bar{f}_{ij}$  is the smoothed value of the field  $f$  at point  $(i,j)$ ,  $\nabla^2$  is the five-point Laplacian operator defined in equation (4.4) and  $S$  is a smoothing parameter which may be negative. In the current study,  $S=1/2$  was used in all smoothing. It may be shown that this value of the smoothing parameter completely filters out the two-grid-length noise and damps out waves shorter than two-grid-lengths. Waves longer than two-grid-lengths are also damped somewhat, but this damping is not very severe for the meteorologically significant waves of the quasi-geostrophic system.

Smoothing was applied to the vorticity field and was done both at the initial time and at regularly spaced intervals in the forecast period. The frequency with which smoothing was performed seemed to have little effect on the

magnitude of the RMS errors in the forecasts.

The same smoothing operator was also applied to the pressure and density fields at terrain height (obtained using the U. S. Standard Atmosphere).